Second-Day Road Log: From Bernalillo to San Ysidro, around Southern Nacimiento Mountains, to San Luis and Guadalupe in the Middle Rio Puerco Valley

Daniel J. Koning, Larry S. Crumpler, Maya Elrick, Karl E. Karlstrom, Stephen G. Wells, Spencer G. Lucas, and Stephanie M. Jeffries

2024, pp. 25-78. https://doi.org/10.56577/FFC-74.25

in:

Geology of the Nacimiento Mountains and Rio Puerco Valley, Karlstrom, Karl E.;Koning, Daniel J.;Lucas, Spencer G.;Iverson, Nels A.;Crumpler, Larry S.;Aubele, Jayne C.;Blake, Johanna M.;Goff, Fraser;Kelley, Shari A., New Mexico Geological Society 74 th Annual Fall Field Conference Guidebook, 334 p.

This page is intentionally left blank to maintain order of facing pages.

SECOND-DAY ROAD LOG:

RIO PUERCO VALLEY FROM BERNALILLO TO SAN YSIDRO, AROUND SOUTHERN NACIMIENTO MOUNTAINS, TO SAN LUIS AND GUADALUPE IN THE MIDDLE RIO PUERCO VALLEY

DANIEL J. KONING[1], LARRY S. CRUMPLER[2], MAYA ELRICK[3], KARL E. KARLSTROM[3], STEPHEN G. WELLS[1], SPENCER G. LUCAS[2], AND STEPHANIE M. JEFFRIES[4]

[1] New Mexico Bureau of Geology and Mineral Resources, 801 Leroy Place, Socorro, NM 87801; dan.koning@nmt.edu
[2] New Mexico Museum of Natural History and Science, 1801 Mountain Road, NM, Albuquerque, NM 87108
[3] Department of Earth and Planetary Sciences, University of New Mexico, Albuquerque, NM 87131
[4] Bureau of Land Management, Rio Puerco Field Office, 100 Sun Avenue, Suite 330, Albuquerque, NM 87109

Assembly Point: Southwestern parking lot, Santa Ana Star Casino
Departure Time: 7:30 AM
Distance: 154 miles
Stops: 3 (2 optional)

Views, landmarks, and outcrops are given using the clock system. For example, 12:00 is straight ahead, 9:00 is to the left, and 3:00 is to the right. Waypoints are given in decimal degrees [latitude, longitude] and are listed in the waypoint table on page 103 of this guidebook (also available digitally).

SUMMARY

Today we travel northwestward from Bernalillo to the middle Rio Puerco Valley. Goals are to discuss: (1) transgressions and regressions of the North American Interior Seaway (Late Cretaceous), (2) late Quaternary slope and alluvial geomorphic processes, (3) incision of the Rio Puerco, and (4) late Pliocene–early Pleistocene basaltic volcanism of the Puerco necks part of the Jemez lineament. We cross the geologic nexus that is the focus of the 2024 Fall Field Conference, which includes the Nacimiento Mountains (southern extension of the Rocky Mountains), Rio Grande rift, and Colorado Plateau physiographic provinces. Trending northeast-southwest through this nexus is the Jemez lineament, where notable volcanism and surface uplift occurred during the late Neogene.

The drive from Bernalillo to San Ysidro crosses the Ziana horst and north-striking faults of the Rio Grande rift. Near the Todilto-capped White Mesa, we cross the Jemez-San Ysidro fault zone which marks the western extent of Santa Fe Group rift fill and hence the traditional boundary between the rift and the adjoining Colorado Plateau, although some extensional strain clearly "bleeds over" into the adjoining plateau.

From San Ysidro, we follow the Rio Salado around the southern end of the Nacimiento Mountains. The drainage cuts across two anticlines on the immediate footwalls of the San Ysidro and Nacimiento faults. The Nacimiento fault is an important structure in north-central New Mexico that had 3–19 mi (5–30 km) of right-lateral slip in the Laramide and ~0.6 mi (~1 km) of east-up throw (Baltz, 1967; Woodward, 1987; Woodward et al., 1997; Cather, 1999; Pollock et al., 2004). Paleogene–Neogene exhumation of the up-thrown block created the Nacimiento Mountains we see today, which are cored by Proterozoic crystalline rocks locally overlain by late Paleozoic strata. Along the west side of the Nacimiento fault, there are great exposures of the entire Mesozoic section, from reddish Triassic terrestrial strata to the yellowish Cretaceous marine strata.

We turn left off U.S. Route 550 and drive State Road 279 westward to the town of San Luis and then southward down the middle Rio Puerco Valley. The relatively smooth topography developed on easily erodible, marine Cretaceous strata is punctuated to the south by numerous resistant, black, steep-sided peaks, like small skyscrapers silhouetted on the skyline. These are the Rio Puerco necks, representing hardened magma and lapilli that filled the lower crater and upper throat of 3.7–2.5 Ma volcanoes (Hallett et al., 1997). Flanking the Rio Puerco Valley to the east and west are the lava-capped Mesa Prieta and Mesa Chivato. Stop 1 examines marine strata in an outcrop of the Cretaceous Point Lookout Sandstone overlying the Satan Tongue of the Mancos Shale, where small transgressions occurred during a major ca. 84–81 Ma regression. We also discuss geomorphic and alluvial processes that shape the landscape of the southeastern Colorado Plateau. Afterward, we cross the Rio Puerco at the ghost town (now ranch headquarters) of Cabezon and travel dirt roads southward to Cerro Guadalupe (Stop 2), where we have lunch. Cerro de Guadalupe and adjoining Cerro de Santa Clara (Optional Stop 1) offer great illustrations of the stratigraphy and "plumbing" that immediately underlie a basaltic cinder cone or phreatomagmatic crater.

After backtracking to Cabezon, we continue traveling down the middle Rio Puerco Valley. At the mouth of Chico Arroyo, we descend into a beautiful, secluded part of the Rio Puerco and pass through the ghost town of Guadalupe. Here, the Cretaceous story of sea level rises and falls intermeshes with a human story of two groups of people: Ancestral Puebloans (900–1300 CE) and Hispanic farmers and ranchers (1870s to 1950s). Modern Puebloan peoples preserve a history of their ancestors

in their verbal and ceremonial traditions. The Anglo-European history of ghost towns of the American Southwest can be sleuthed by examining artifacts and other remnants (Sagstetter and Sagstetter, 1998), to which one may add some information provided by historic big-city newspaper articles or government documents. In the Guadalupe area, however, the lives and struggles of the resident Hispanic population in the late 19th and early 20th centuries are richly narrated by the published stories of author Nasario García, who was raised here and whose family has deep roots here. That hundreds of people could live in this relatively arid environment is amazing. We ponder how climate change and land use in the late Holocene impacted the landscape, the river, and the two groups of people (Ancestral Puebloan and Hispanic) whose lifestyles were so intertwined with their environment.

[Waypoint]
Mileage Description *Distance between stops*

0.0 Assemble in the parking lot on the southwestern side of Santa Ana Star Casino. The first segment of the road log is an abbreviated version of miles 0 through 19.2 of the First-Day Road Log. Here, we just give mileages to important road intersections so you can continue the road log from where we turned off of U.S. Route 550 on Day 1.

Proceed south from the parking lot and turn right (west) on U.S. Route 550. **ZERO ODOMETER at this intersection.** *0.5*

Waypoint 1 [35.325601°, -106.564426°]

0.5 Intersection with State Road 528 (Pat D'Arco Highway). *0.8*

1.3 Intersection of U.S. Route 550 and State Road 347 (Paseo de Volcan). *3.7*

5.0 Intersection with the northern extension of Unser Boulevard. *10.8*

15.8 Entrance road to Zia Pueblo on the right and buildings associated with southern Zia Pueblo. *3.4*

19.2 Cabezon graded dirt road to left. This leads to White Ridge and the Ojito Wilderness as well as Stop 1 of Day 1. The road eventually leads to Cabezon Peak and the Rio Puerco. *0.6*

19.8 To left, yellowish Mancos Shale on the hanging wall of the east-down San Ysidro fault. The pinkish sand and sandy muds on the west side (footwall) of the fault are called lower Morrison Formation on the San Ysidro geologic map (Woodward and Ruetschilling, 1976), but are more properly assigned to the Middle-Late Jurassic Summerville Formation (Anderson and Lucas, 1996; Lucas, 2021). *0.3*

20.1 Cross the San Ysidro fault. Strata on the north tip of the butte at 9:00 are on the immediate footwall of the fault. This particular stratigraphic sequence continues north-northwestward around the slopes of White Mesa (listed from top to bottom): Todilto Formation (Jurassic), Entrada Sandstone (Jurassic), and upper Triassic red beds of the Petrified Forest Formation. The Todilto is composed of a basal brownish, kerogenic, thinly laminated, limestone bed (~4–5 ft, ~1–1.5 m thick) overlain by ~100 ft (~30 m) of white gypsum. The Entrada Sandstone is white to pale yellow to orangish tan, fine- to medium-grained sandstone that is 100–120 ft (30–36 m) thick. Thicknesses and descriptions are from the San Ysidro quadrangle geologic map (Woodward and Ruetschilling, 1976) and Lucas (2024). *0.1*

20.2 Road bends to north and travels on Holocene alluvium. Straight ahead (to north) lies the scenic Jemez River valley. *0.5*

20.7 Cross the Rio Salado, a major tributary to the Jemez River. U.S. Route 550 follows the lower part of this drainage. *0.3*

21.0 Road bends to left. *0.2*

21.2 Slow down as we enter the village of San Ysidro. This area was settled in 1699 by Juan Trujillo and others. In 1786, a land grant was given to Antonio Armenta and Salvador Sandoval (Julyan, 1998). San Ysidro is a common New Mexico place name typically honoring Saint Isidore, the patron saint of farmers, gardeners, and sheepherders. His intercession is invoked for good crops, and he is widely honored in New Mexico during May, when a statue of the saint is carried through the farm fields (Julyan, 1998). *0.4*

21.6 Junction with State Road 4. **RE-ZERO ODOMETER.** *0.2*

FIGURE 2.1. Gravely terrace deposit overlying reddish mudstones of the Petrified Forest Formation (Trpf) and greenish Morrison Formation strata (Jm), the two Mesozoic units being separated by the east-down San Ysidro fault (Woodward and Ruetschilling, 1976). The terrace deposits consists of 10–15 ft (3–5 m) of cemented sandy gravel. This terrace of the Rio Salado correlates with Qt4 of Pazzaglia et al. (1997, 1998) and has an estimated age of 150 ka (see Reed et al., 2024).

Waypoint 2 [35.555284°, -106.779638°]

0.2 Road bends to left and travels due west. *0.1*

0.3 At 3:00 is 10–15 ft (3–5 m) of cemented sandy gravel that overlies the Petrified Forest Formation (Fig. 2.1). *0.4*

FIGURE 2.2. View to southwest of White Mesa. The cliff-forming, white stratigraphic unit on top is the Todilto Formation, consisting mainly of gypsum that is currently being mined just south of the rim. Below lies 50 ft (15 m) of yellowish-orangish Entrada Sandstone, which in turn overlies reddish Triassic strata (Petrified Forest Formation of the Chinle Group).

0.7 View to southwest of White Mesa, underlain by gypsum of the Todilto Formation (Fig. 2.2). *0.3*

1.0 Cross a small wash. *0.5*

1.5 San Ysidro Trials Area to the right. This network of trails (and dirt roads) allows access to beautiful slot canyons carved in sandstones of the Agua Zarca Formation of the Chinle Group (which correlates to the Shinarump Formation). *0.5*

2.0 View straight ahead of Triassic strata on the right (north side) of the Rio Salado, where reddish-brown mudstones (Petrified Forest Formation) overlie white to brown sandstones of the Agua Zarca Formation on the south-plunging dip slope of the Nacimiento uplift. A conceptual model of how Rio Salado incision has progressed since the early Pleistocene is presented in Figure 2.3. *0.3*

2.3 Road bends left. *0.3*

2.6 On left, notable salt precipitation on Holocene deposits. Across the Rio Salado, a nice view straight ahead of Jurassic strata (Todilto and Entrada) overlying Triassic strata (Petrified Forest Formation). *0.2*

2.8 View to right of travertine spring-mound deposits. These are modern analogues of the processes that have cemented the Pleistocene terrace gravels we discussed on Day 1 and which were seen just west of San Ysidro (e.g., Fig. 2.1). *0.5*

3.3 Road bends to right and wraps around the nose of a southward-plunging, west-dipping monocline developed on the immediate footwall of the Nacimiento fault. The monocline is cored by Agua Zarca Sandstone draped locally with a veneer of reddish-brown mudstones of the Petrified Forest Formation. Springs present at the foot of the slope are called North Highway Springs (McGibbon et al., 2018). These are geochemically distinct from the Tierra Amarilla anticline springs and intermediate in composition between them and Soda Dam and Jemez Pueblo springs (see Day 3). Based on a variety of geochemical tracers, McGibbon et al. (2018) interpreted the entire Tierra Amarilla spring system to be in a nexus of groundwater mixing that includes local meteoric recharge, waters from the Aqua Zarca and Paleozoic aquifers, and waters from the Nacimiento and Jemez mountains, including Valles Caldera geothermal waters. Semiconfined fault conduits, especially the Nacimiento, Jemez, and northeast-trending faults that cross the mountain blocks, provide the connectivity for this mixing. *0.7*

4.0 Cross the Nacimiento fault. At 2:00, well-cemented sandstone of the Agua Zarca Formation (right) is juxtaposed across the fault with reddish Summerville Formation (left). View to left of spring mounds visited in Stop 2 of Day 1.

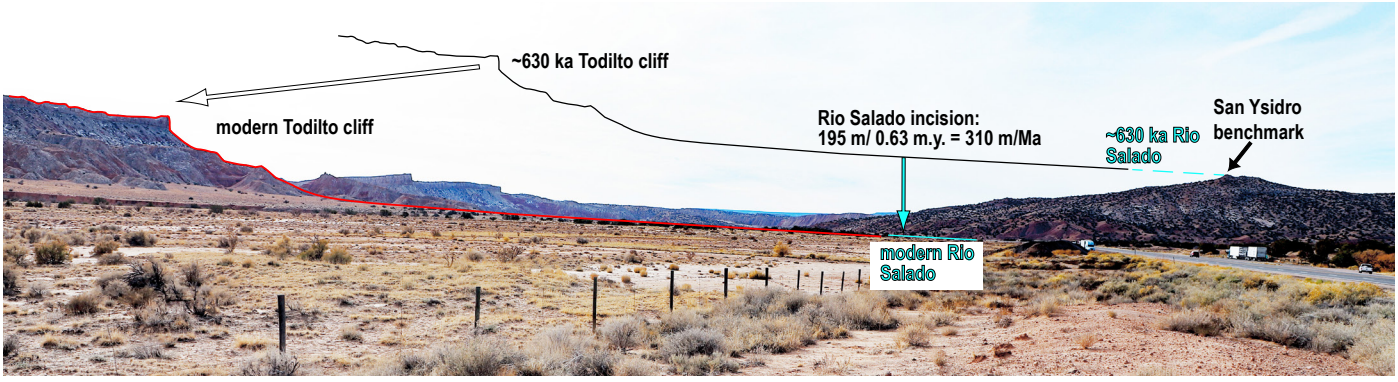

FIGURE 2.3. The skyline illustrates a conceptual model of river incision of the Rio Salado over the past 630 ka, from the high gravels at the San Ysidro Benchmark (correlated with Qt1 of Pazzaglia et al., 1997, 1998; Reed et al., 2024) to the modern river bed. During this time, self-similar cliff retreat of the Todilto cliff can be envisioned to have "slid down" the 10–15° dip slope of south-plunging Nacimiento uplift, concurrent with progressive vertical incision by the Rio Salado.

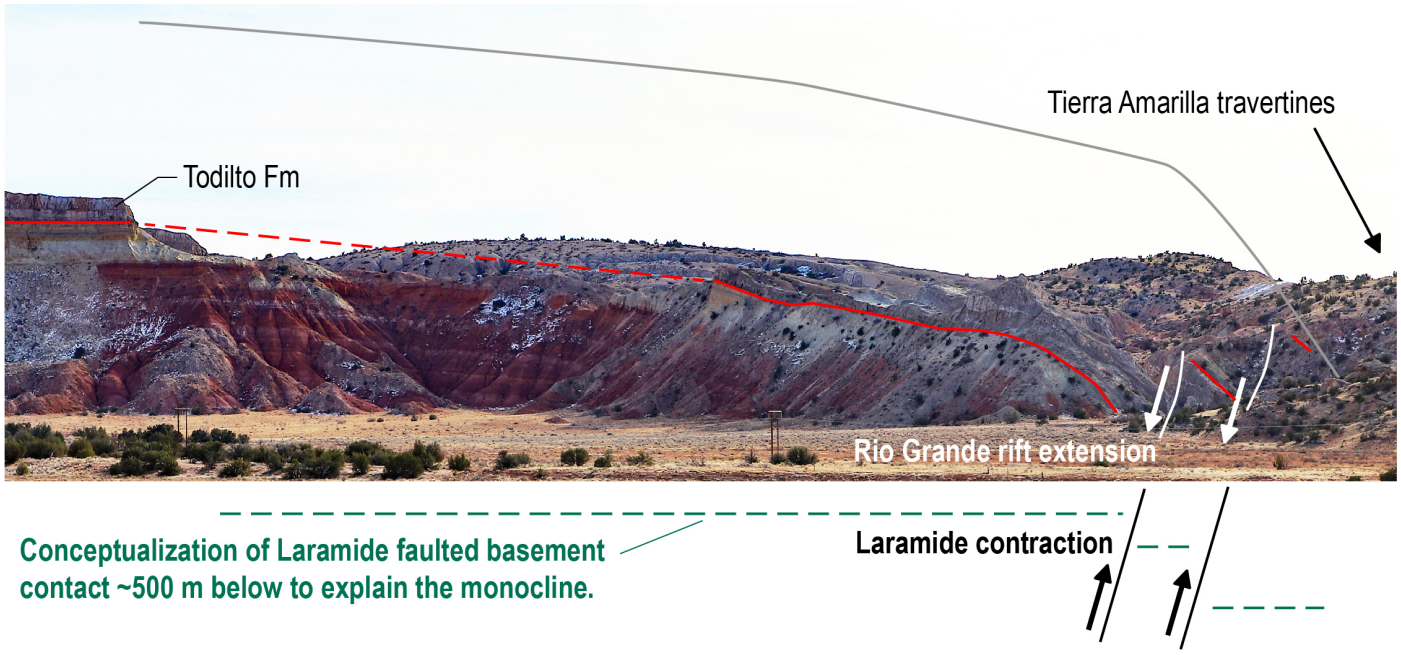

FIGURE 2.4. Southward view of the Tierra Amarilla anticline from the southern edge of the Rio Salado. Gray and red lines (red representing the base of the Todilto Formation) illustrate stratigraphic contacts deformed into a monocline by initial east-up motion along the Nacimiento fault. The base of the Todilto Formation has been downthrown to the east by normal reactivation of the Nacimiento fault.

Directly south is a view of the inverted monoclinal structure along the eastern fault that helps form the core of the Tierra Amarilla anticline (Fig. 2.4). *0.3*

4.3 At 9:00, the Todilto and Entrada formations overlie reddish strata of the Petrified Forest Formation. *0.5*

4.8 Road cut to left, exposing mangled, whitish Todilto-Entrada formations overlying reddish strata of the Petrified Forest Formation. *0.1*

4.9 Enter Zia Pueblo. *0.5*

5.4 Road bends to right and follows the Arroyo Peñasco, a south-flowing tributary to the Rio Salado. In the upper Arroyo Peñasco drainage are Mississippian marine strata that serve as the type section of the Arroyo Peñasco Formation (Group) of Armstrong (1955). The main Rio Salado drainage continues northwestward on the left side of the Todilto-capped ridge. Up the Arroyo Peñasco drainage and for about 7 mi north along the frontal Nacimiento fault zone are the Peñasco travertine mounds and cemented gravel terraces. The terraces can be correlated "around the corner" to Rio Salado and Jemez terraces (Formento-Trigilio and Pazzaglia, 1998; Reed et al., 2024). Waters in these springs are similar to those at Twin Mounds (Day 1, Stop 2) and are inferred to contain distal manifestations of fluids derived from the Valles Caldera geothermal system (McGibbon et al., 2018) that have found their way across

FIGURE 2.5. View to north of strata on the west side of the Nacimiento fault. The location of the fault is demarcated by a thick, black line. To left (west) of the fault are the Todilto (Jt), Summerville (Js), and Morrison (Jm) formations (oldest to youngest). On the right (east) of the Nacimiento fault lie relatively horizontal Permian-Triassic strata (listed in ascending order): reddish Yeso Group (Py), tannish Glorieta Sandstone (Pg), Moenkopi Formation (Trm, forming a ribbed slope), and resistant sandstones of the Agua Zarca Formation (Traz).

the mountain block along northeast-trending faults. *0.3*

5.7 View straight ahead of structure and strata along the north-striking Nacimiento fault zone. The fault lies at the base of the steep cliff underlain by the following stratigraphic sequence (listed in ascending stratigraphic order): Yeso, Glorieta, Moenkopi, and Agua Zarca formations (Fig 2.5). Left (west) of the fault, strata dip 16–34° eastward and consist of the following formations (listed in ascending stratigraphic order): reddish Petrified Forest Formation, Entrada and Todilto couplet (straight ahead), Summerville Formation (reddish strata in north-trending drainage), and slightly greenish-yellow Morrison Formation (Fig. 2.5). *0.4*

6.1 Road bends left and crosses the Arroyo Peñasco, which has incised about 30 ft (10 m) into weakly consolidated Holocene valley fill. Todilto Formation seen to left (west), where dissolution has formed caves. **Permission from Zia Pueblo is needed prior to visiting these caves.** *0.3*

6.4 Entering into a broad valley bordered on the southwest and northeast by ridges ~250–300 ft (75–90 m) tall that are capped by the Todilto-Entrada couplet, which overlies reddish strata of the Petrified Forest Formation (Chinle Group). *1.1*

7.5 On left, the basal limestone of the Todilto Formation is well exposed, overlying the yellowish to orangish (becoming redder down-section) Entrada Sandstone. Beneath the Entrada Sandstone lies reddish-brown, litharenite sandstones and intra-formational conglomerates of the Correo Sandstone Bed of the Petrified Forest Formation. The Entrada and Todilto formations were deposited in the Middle Jurassic (ca. 165–160 Ma) in an arid environment. Between the yellowish Entrada sandstone cliff and the Correo Bed are orangish sandstone and siltstone, locally cyclically bedded, of the lower part of the Entrada Sandstone. Thus, the Entrada here can be divided into two members: the Dewey Bridge Member for the lower, reddish beds and the Slick Rock Member for the upper, yellowish sandstones (Lucas and Heckert, 2003; Lucas, 2021). The Dewey Bridge Member can be traced northwestward across the Four Corners to the Carmel Formation (its equivalent) and represents coastal plain deposits landward of the Carmel sea, which occupied parts of northern Utah-Idaho early in the Middle Jurassic. The Slick Rock Member displays the classic eolianites of the Entrada and represents an erg that extended eastward from eastern Utah and northeastern Arizona to western Oklahoma, crossing Colorado and northern New Mexico. Cross-bed azimuth directions in the Slick Rock Member indicate wind directions headed southwest, so the nexus during this part of Middle Jurassic time was in the zone of prevailing easterlies and probably no more than 10–15°north of the paleoequator. Eventually, Middle Jurassic subsidence or sea level rise allowed a shallow body of salty water to flood the area. Evaporation of the brackish water precipitated limestone followed by ~60–100 ft (~20–30 m) of deposition of gypsum (probably initially anhydrite) of the Todilto Formation (Anderson and Lucas, 1996). *0.5*

8.0 Strongly cemented terrace deposit caps the low ridge to right (northeast). *0.1*

8.1 Highway crosses Cuchillo Arroyo (a south-flowing tributary of the Rio Salado) and turns north. As seen near Arroyo Peñasco, the Cuchillo valley is walled by the Todilto-Entrada-Petrified Forest Formation sequence (Fig. 2.6). *0.5*

FIGURE 2.6. Exposure of the Jurassic-Triassic strata that forms the western wall of the valley of Cuchillo Arroyo (taken at mile 9.4). White, gypsum-dominated strata of the Todilto Formation (Jt) cap the ridge. The basal limestone bed of the Todilto Formation (3–5 ft, 1–1.5 m thick) is annotated. Beneath the Todilto lies 70–80 ft (20–24 m) of orange to reddish-brown Entrada Sandstone (Je; to south-southeast of here, the upper part is yellow). The two members of the Entrada Sandstone are shown: the Slick Rock Member (top, Jesr) and the Dewey Bridge member (bottom, Jedb). A substantial disconformity separates the Middle Jurassic Entrada Formation from the Upper Triassic Petrified Forest Formation, a hiatus of about 25 my. Lowest slopes are underlain by the reddish-brown Petrified Forest Formation (Trpf). Most of the Petrified Forest Formation consists of smectitic mudstones, but the top of the formation in this area is capped by 1–2-m-thick, resistant, litharenite sandstones (and minor intraformational conglomerates) of the Correo Sandstone Bed (Lucas et al., 1987; Lucas, 1991; Lucas and Heckert, 1996). Holocene valley fill in the area is typically underlain by the erodible Petrified Forest Formation.

8.6 Excellent exposures of the white Todilto Formation overlying yellow-orange Entrada Sandstone. Reddish-brown Petrified Forest Formation lies in the lower slopes, capped by the 1–2-m-thick Correo Sandstone bed (Fig. 2.6). *0.1*

8.7 At 2:00, in the distance are a series of pediments and terraces, many of which are capped by travertines and related travertine mounds. *0.2*

8.9 In the far distance at 1:00 is a view of crystalline rocks of the Nacimiento Mountains (Fig. 2.7). At 2:00 is a dip slope of Agua Zarca sandstone dipping 12–45° west. The Nacimiento fault separates the Agua Zarca Sandstone from Proterozoic gneiss, granite, diorite, and monzonite, which underlie the steep slope on the right (Woodward et al., 1977; Woodward and Ruetschilling, 1976). *0.5*

9.4 To left (west), more exposures of the gypsum and sandstone (Todilto and Entrada Formations, respectively) that rims the Cuchillo Arroyo valley, which are disconformably underlain by the Petrified Forest Formation (Fig. 2.6). *0.7*

10.1 At 12:00, note the gentle eastward dip of Triassic strata. *0.6*

10.7 Slight right bend in highway. Reddish-brown mudstones of Petrified Forest Formation in roadcuts on both sides of highway here and 0.3 mi to north. *0.5*

11.2 Left bend in highway. Outcrop of reddish-brown Petrified Forest Formation on right. Straight ahead (1.5 mi) is an east-southeast-trending ridge capped by white gypsum of the Todilto Formation. This ridge is called Cuchilla Blanca ("white knife") and is part of the northeastern limb of a northwest-plunging anticline (Fig. 2.8). *0.5*

11.7 Proceed northward along the wide valley incised into relatively soft Triassic strata of the Petrified Forest Formation of the Chinle Group. Slopes to immediate right (west) are capped by a terrace deposit with a tread of ~90 ft (~27 m) above the general level of the Holocene valley floor. *0.4*

12.1 To right (east) lies the former site of the Warm Springs Resort. An oil well drilled here in the 1920s along the axis of the aforementioned northwest-plunging anticline reached a total depth of 2008 ft. The well failed to produce oil or gas, but it did yield warm, artesian water (Van Hart, 2013). *0.4*

12.5 On left (west), good exposures of reddish-brown mudstones of the Triassic Petrified Forest Formation (Chinle Group). At 10:00, note how the overlying Todilto-Entrada couplet bends in a westward direction from northwest-striking to north-northeast-striking. This bend marks the approximate axial plane of a northwest-plunging anticline (Fig. 2.8), one of many along the Nacimiento fault. These folds are interpreted by Baltz (1967) to have formed as a result of right-lateral wrench faulting during the Laramide. To right lies the Zia Hot Well. *0.4*

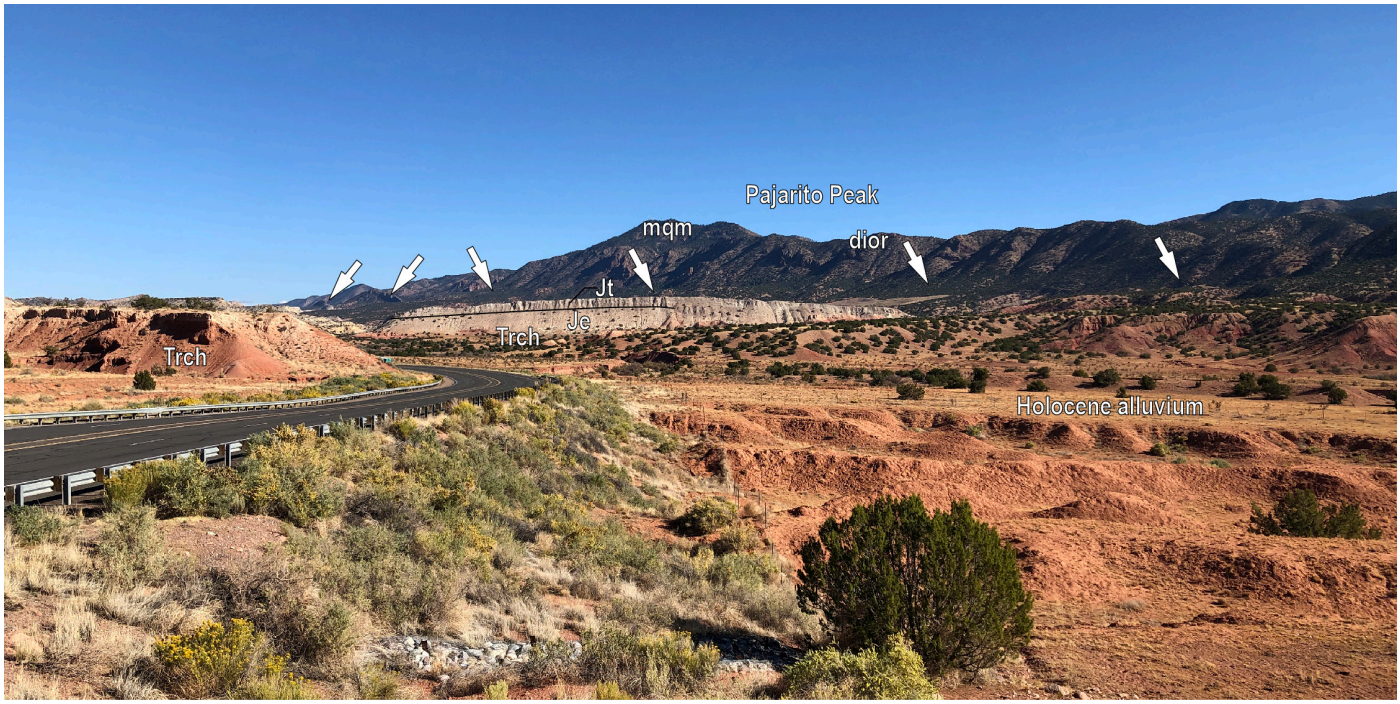

FIGURE 2.7. View to north of Pajarito Peak and the crystalline-cored Nacimiento Mountains (skyline). The Proterozoic rocks seen in the photo are mainly granite and gneiss, with local diorite (dior) and muscovite-bearing quartz monzonite (mqm). These basement rocks are fault-juxtaposed (by the Nacimiento fault) alongside white gypsum of the Todilto Formation (Jt), hard-to-see Entrada Sandstone (Je), and reddish-brown Chinle Group (Trch) in the middle part of photo. Approximate fault trace shown by white arrows. The north-trending valley of Cuchillo Arroyo is floored by Holocene alluvium that overlies the Petrified Forest Formation.

12.9 Cross the Todilto-Entrada couplet on the east limb of the northwest-plunging syncline. As we drive north, we proceed up-section across nicely exposed Jurassic strata. *0.1*

13.0 On left is a strike valley developed in the relatively non-resistant sandstones, siltstones, and mudstones of the Summerville Formation (Jurassic) (Fig. 2.9). To right (east) is Cachana Spring. Woodward and his students mapped the Summerville as part of the Morrison Formation throughout the region around the Nacimiento uplift (see Woodward, 1987). However, the Summerville (up to 260 ft [80 m] thick in the nexus) can be separated as a distinctive rock unit underlying the Morrison Formation; in this area it should instead be included in the upper part of the San Rafael Group. The lower part of the Summerville Formation is maroon or grayish-red siltstone and silty mudstone. Similar, overlying strata of the upper Summerville also include beds of cross-stratified, fine-grained sandstone. Anderson and Lucas (1996) suggested these sandstone beds are of eolian origin and may be equivalent to the Bluff Sandstone to the west/northwest. Regionally,

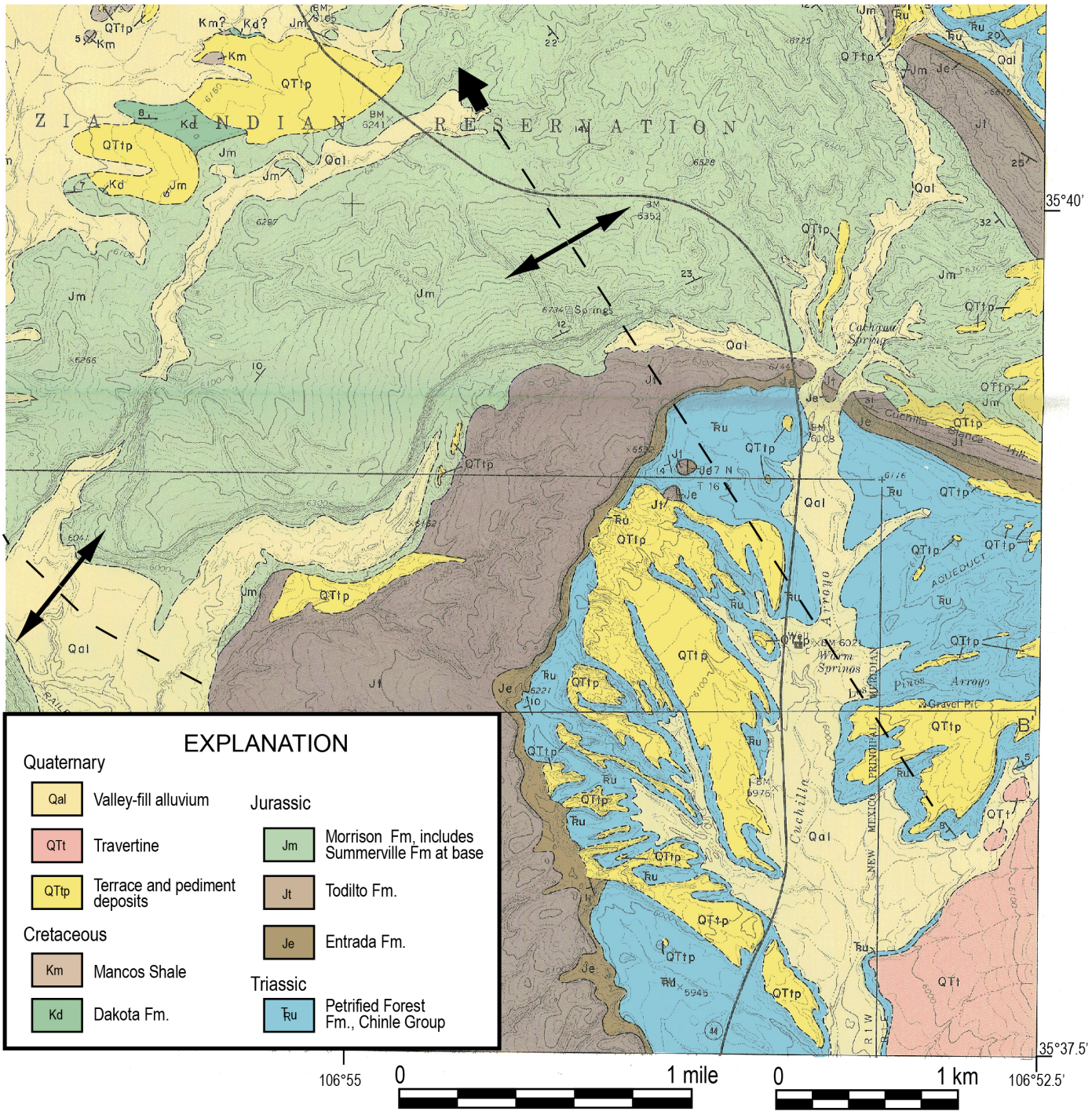

FIGURE 2.8. Southeast portion of the geologic map of the Holy Ghost Spring quadrangle (Woodward and Martinez, 1974). Approximate axes of anticlines are noted by dashed black lines with opposing arrows. Plunge direction noted by the arrow on the end of the dashed black line.

FIGURE 2.9. View to west up a strike valley developed in the erodible Summerville Formation (Js), flanked to the left and right, respectively, by the Todilto (Jt) and the Morrison formations. Two members of the Morrison can be differentiated: the sandstone-dominated lower Salt Wash Member (Jmsw) overlain by interbedded mudstones and sandstones of the Brushy Basin Member (Jbb). The Summerville Formation is composed of reddish-brown sandstones and mudstones that are in thick, tabular beds. The Salt Wash Member consists of yellowish-tan, medium-grained, feldspathic to subfeldspathic arenite sandstones that are commonly cross-stratified. The Brushy Basin Member was deposited by northeast-flowing rivers across a vast flood basin and is famous for hosting sauropod fossils, including Seismosaurus, which is now considered to be a species of the more widely known Diplodocus (Lucas et al., 2006).

Summerville strata extend across the Middle–Late Jurassic boundary (Anderson and Lucas, 1996). *0.3*

13.3 Road bends to left. Cross tannish-yellow sandstone of the Salt Wash Member of the Morrison Formation (Fig. 2.9). *0.3*

13.6 Pastel-colored Brushy Basin Member of the Morrison Formation (Fig. 2.10). Mudstones are greenish (minor reddish), and sandstones are yellow. In contrast to the eastern provenance of Triassic strata, sandstones in the Morrison Formation have a western provenance from the volcanic arc that was building up at the time near what is now California. The pastel colors in the mudstones may be due to varying ash content controlling redox reactions during shallow diagenesis and to varied zeolite clay minerals. *0.3*

FIGURE 2.10. View to northeast of Brushy Basin Member of the Morrison Formation.

13.9 Cross ridge underlain by Brushy Basin Member. *0.3*

14.2 Nice view to right of interbedded tannish-yellow sandstones and pastel-colored and reddish mudstones characteristic of the Brushy Basin Member. *0.6*

14.8 Tannish, resistant sandstones of the Jackpile Member of the Morrison Formation, capped to west by a veneer of Pleistocene sand and gravel. The Jackpile has generally been considered a member of the Morrison Formation and is only found across part of central New Mexico. Up to ~100 ft (~30 m) thick, the Jackpile consists mostly of white, kaolinitic, fine- to coarse-grained, cross-bedded sandstone with some beds of silica-pebble conglomerate and minor interbeds of pale green mudstone and siltstone. The age of the Jackpile is uncertain; it is commonly assigned a Late Jurassic age, but it may be an Early Cretaceous equivalent of the Burro Canyon Formation to the north and northwest. The base of the Upper Cretaceous Dakota Sandstone on the Jackpile Member is a substantial unconformity that represents a hiatus of as much as 50 my, separating strata of Late Jurassic age(?) and strata of early Late Cretaceous (Cenomanian) age. This contact was observed close-up on Day 1. *0.3*

15.1 Road bends to right. View ahead of smooth, relatively low topography underlain by yellowish to light-greenish yellow, weakly resistant Mancos Shale. *0.2*

15.3 At 1:00–2:00 is yellowish-tan sandstone that was correlated to the upper Morrison Formation by Woodward and Martinez (1974). *0.2*

15.5 Cabezon Peak at 9:00. *0.4*

15.9 Pleistocene sand and gravel deposit on right. *0.4*

16.3 Ridge capped by gravelly terrace deposit, which overlies light yellowish to light greenish-yellow Mancos Shale. *0.7*

17.0 CCC camp ruins to the right. *0.1*

17.1 Cross Arroyo Semilla and head due north. At 2:00, low ridge just left (northwest) of the main arroyo was correlated to the Dakota Formation by Woodward and Martinez (1974). *0.4*

17.5 At 9:00, Mancos Shale is capped by a sandstone interval ~10 ft (3 m) thick; its correlative to the southwest is uncertain (possibly the Tocito Sandstone). *0.4*

17.9 Turn left (west) on State Road 279. To the north lies Jemez Pueblo and to the south lies northeastern Zia Pueblo. Sandstone exposed in right (north) roadcut is possibly correlative to the Tocito Sandstone.

0.0 RE-ZERO ODOMETER at intersection of State Road 279 and U.S. Route 550. *0.1*

Waypoint 3 [35.711576°, -106.938385°]

0.1 Expansive view of the middle Rio Puerco Valley ahead (the upper Rio Puerco Valley is considered to be centered in the area around Cuba). The valley and surrounding mesas are underlain by Upper Cretaceous strata interspersed with Quaternary valley fills and high-level terrace and pediment deposits. Late Cretaceous strata consist of Mancos Shale with subordinate tongues of sandstone, the latter typically being several tens of feet (a few tens of meters) thick. We are in the southeast corner of the San Juan Basin, which subsided in the Late Cretaceous through Paleogene. Subsidence occurred mainly due to west-down movement on the Nacimiento fault system at the western foot of the Nacimiento Mountains (1.2 km of maximum stratigraphic separation, per Woodward, 1987). There has also been a substantial component of right-lateral slip along this fault. Estimates of the magnitude of this slip have varied: 5 km (Baltz, 1967); 5–20 km (Woodward et al., 1997); 20–33 km (Cather, 1999), 6–18 km (Pollock et al., 2004), but all agree there was more Laramide strike slip than dip slip across this fault (Cather et al., 2006). At 9:00, note Upper Cretaceous strata dipping gently westward into the San Juan Basin. On the southern skyline, we can see Cabezon Peak and many of the Rio Puerco necks, in addition to Mesa Prieta and Mesa Chivato (Fig. 2.11). *0.8*

0.9 Cross broad valley underlain by Holocene alluvium. *0.3*

1.2 Mancos Shale outcrops in road cuts. *0.2*

1.4 Mile 7 road post. Driving across a small valley underlain by Holocene alluvium. *0.2*

1.6 Mancos Shale exposure on the left. *0.2*

1.8 Sparse vegetation on the surrounding landscape consists of juniper trees, cholla, and grasses that include grama and sacatone. *0.5*

2.3 Ascend a low ridge underlain by Mancos Shale. View of southern skyline includes Mesa Prieta (9:00), volcanic necks of the Rio Puerco Valley (9:30), Cabezon Peak (10:00), Mount Taylor (10:00–10:30), and Mesa Chivato (10:00–11:00) (Fig. 2.11). Mount Taylor is a 3.72–1.26 Ma composite stratovolcano consisting of coalesced domes, flows, plugs, dikes, ash, and debris flows composed of trachyandesite

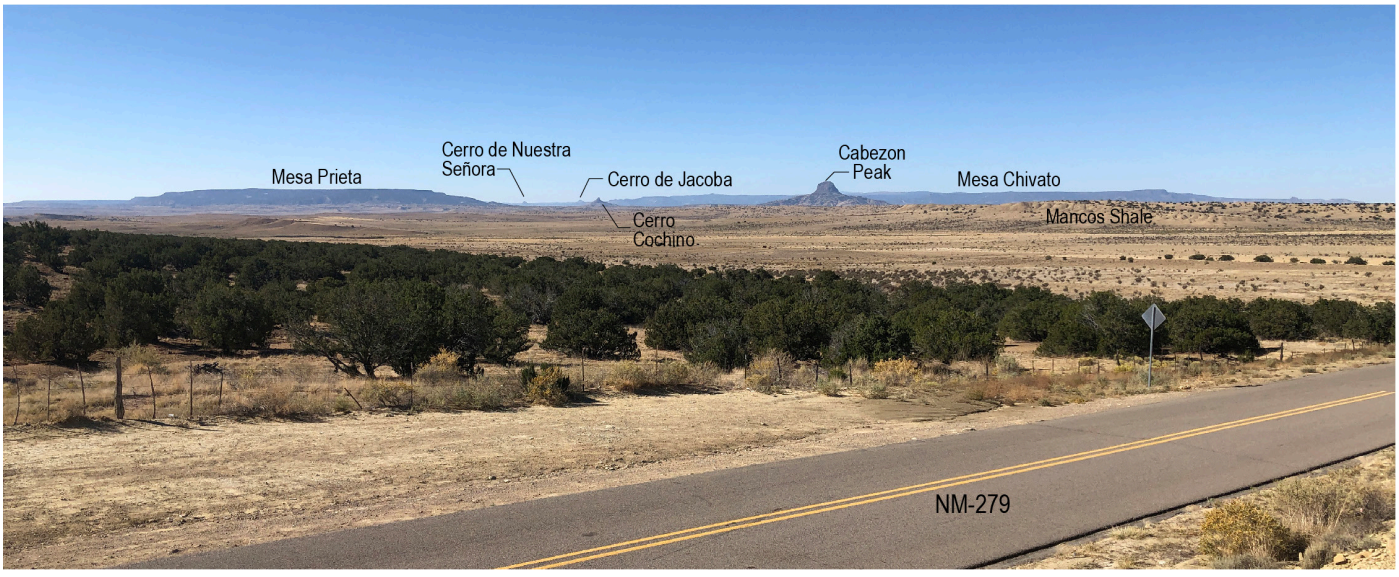

FIGURE 2.11. View southwest from near the intersection of State Road 279 and U.S. Route 550. On the skyline, from left to right, are Mesa Prieta, various Rio Puerco necks (Cerro de Nuestra Señora, Cerro de Jacoba, Cerro Cochino, and Cabezon Peak), and Mesa Chivato.

to rhyolite and minor trachybasalt (Goff et al., 2019). *0.1*

2.4 Rolling landscape underlain by erodible Mancos. *0.1*

2.5 View straight ahead of Point Lookout Sandstone overlying the upper Mancos Shale. *0.5*

3.0 Road makes a left jog. *0.5*

3.5 Road bends left and goes southward. Cabezon Peak and other Rio Puerco necks visible between 12:00 and 1:30. *0.6*

4.1 Road bends right (west). Views ahead (west) and to right (north) of the middle Rio Puerco Valley, the Rito Leche terrace, and the edge of a mesa capped by the Point Lookout Sandstone (Fig. 2.12). *0.3*

4.4 Crossing the entrenched arroyo of the Rio Puerco. The name of this river can be "River of Pigs" in Spanish (though *cochino* is a more typical Spanish word for pig), but its usage in the Southwest is better translated as "muddy river" (Julyan, 1998). Prior to American annexation, two explorers, Josiah Gregg (1844) and Fray Francisco Dominguez (1776), remarked on the muddiness of the river's water (Julyan, 1998). Its length is ~230 mi (370 km), and its drainage basin area is 7350 mi^2 (19,000 km^2), although 1130 mi^2 is probably noncontributing (https://wdr.water.usgs.gov/wy2009/pdfs/08353000.2009.pdf). The river heads in the San Pedro Peaks area of the northern Nacimiento Mountains and flows southward near the margin of the Colorado Plateau and Rio Grande Rift, joining the Rio Grande near Bernardo, located 30 mi (50 km) south of Albuquerque. North of Interstate 40, the Rio Puerco has carved a wide canyon mainly in Cretaceous strata, whereas south of Interstate 40 the valley is eroded in Upper Cenozoic sediment of the Santa Fe Group. This ephemeral river has a notably high amount of suspended load (Nordin, 1963). As will be discussed at Stop 3, an astonishing amount of incision has occurred since 1885 on this river, resulting in an inner, steep-walled arroyo that is commonly 20–30 ft (6–9 m) deep and meandering. *0.2*

4.6 Straight ahead are Rio Puerco terrace deposits, where 6–10 ft (2–3 m) of sandy gravel overlie Mancos Shale. The tread of this terrace is about 100 ft (30 m) above the valley floor near the modern arroyo and correlates with the Rito Leche terrace of Bryan and McCann (1936). *0.2*

4.8 Road crosses an abandoned acequia (filled in and hard to see) and bends to left (south). An acequia is a community-owned and operated irrigation system which uses ditches to divert water from rivers or streams to water crops. In New Mexico, acequia systems were developed by Hispanic farmers over the past couple of hundred years. *0.1*

4.9 Mancos Shale exposed in right roadcut. To left (east) are former agricultural fields irrigated using water delivered by the aforementioned acequia. *0.3*

5.2 Mancos Shale exposed in right roadcut. Further to right (0.2 mi) is a gravel-capped terrace deposit, which is locally well-cemented. The tread of this terrace is ~100 ft (~30 m) above the unincised Holocene valley floor near the recently entrenched arroyo, and it correlates to the Rito Leche surface of Bryan and McCann (1936). *0.2*

5.4 Intersection of State Road 279 and Lobato Trail. Enter north part of the town of San Luis. On Google Earth, remnants of agricultural fields are apparent between the acequia (just east of the highway) and the incised Rio Puerco. *0.4*

5.8 Small knob of Mancos Shale on left. *0.3*

6.1 Victors Road. Cross low ridge underlain by Mancos Shale. *0.1*

6.2 On right are bluffs offering good exposures of the

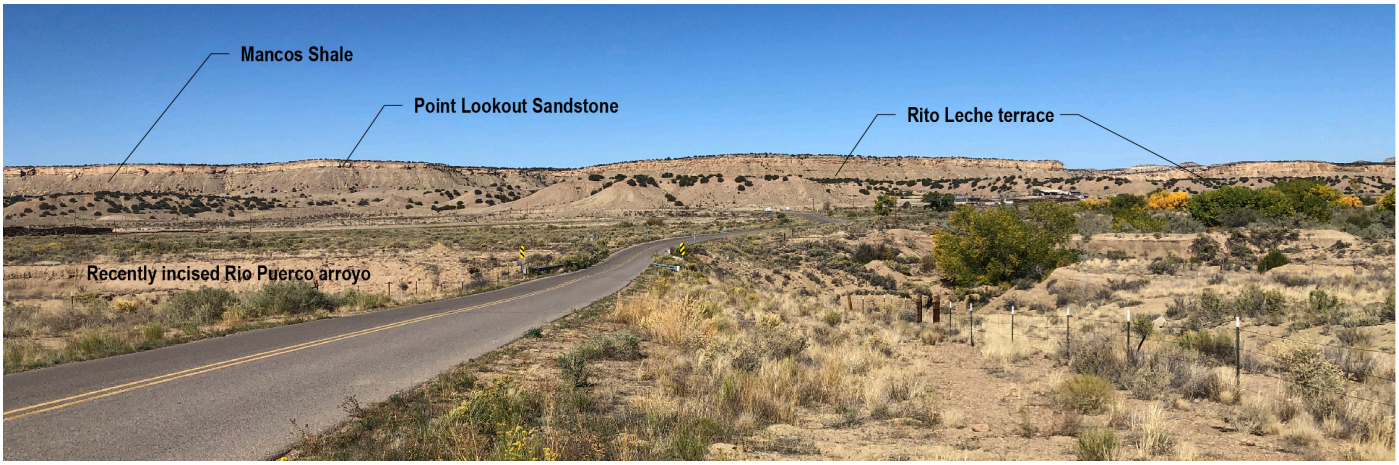

FIGURE 2.12. View to west of State Road 290 crossing over the recently incised arroyo of the Rio Puerco. Rapid incision of a deep, continuous arroyo occurred after 1885 CE (Bryan, 1928; Aby, 2017). The lower set of bluffs on the west edge of the Rio Puerco Valley is the Rito Leche terrace of Bryan and McCann (1936), composed of ~6–10 ft (2–3 m) of sandy gravel, which overlies the upper Mancos Shale. The higher bluff on the skyline is the east edge of the San Luis Mesa, capped by resistant Point Lookout Sandstone.

Satan Tongue of the Mancos Shale overlain by Point Lookout Sandstone. Seen here of the Point Lookout Formation is interpreted to have been deposited in the lower shoreface and the lower shoreface–offshore transition zone facies (Wright and Hayden, 1988; Wright-Dunbar, 1992b). Note that the Point Lookout shoreface sandstones have been removed by a large channel, having a width of ~1300 ft (~400 m) and a maximum scour depth of 50 ft (15 m). The Cretaceous channel trends northwest-southeast, roughly parallel to the inferred geometry of the paleoshoreline in the area (Lucas et al., 1992). *0.2*

6.4 Mile marker 2. The flat valley floor to left (east) hosted agricultural fields in the first half of the 20th century (Fig. 2.13). Excellent view to right of the steep bluff flanking the east side of Mesa San Luis, where the Point Lookout Sandstone transitions down-section into the upper Mancos Shale. In local folklore, the San Luis area, including the mesa to the west, was a site of supernatural phenomena that commonly involved lights and sparks or mysterious dark objects (García, 1987, 1992; Harris, 2003). *0.9*

7.3 To the right (west) are a morada (gathering place for Penitentes) and a Catholic cemetery, and to the left (east) is the San Luis Catholic Church. Similar to today, San Luis in the early 20th century stretched for 3 mi north of here, with houses built on the west (uphill) side of fields irrigated via an acequia that carried water diverted from the Rio Puerco (Widdison, 1959); the remnants of the acequia were crossed at mile 4.8. There were four principal communities in the middle Rio Puerco Valley: San Luis, Cabezon, Guadalupe, and Casa Salazar. Spaced approximately 4–6 mi (6–10 km) apart, these towns offered store-supplied provisions, dance halls, and a Catholic church for the predominantly Hispanic farmers that settled this part of the Rio Puerco Valley. Irrigation infrastructure, built and maintained by the local community, provided water for growing corn, beans, chile, and wheat (Widdison, 1959). Secondary crops included alfalfa, oats, and vegetables, and there were some apple, pear, plum, and cherry trees (Widdison, 1959). The head of an acequia coincided with a dam on the river, which would wash out in big floods. Irrigated fields were located on middle-upper Holocene alluvium that sloped gently toward the Rio Puerco channel. Large numbers of livestock (cattle, goats, sheep, and horses) were grazed in the valley and surrounding uplands (Widdison, 1959; García, 1992, 1994).

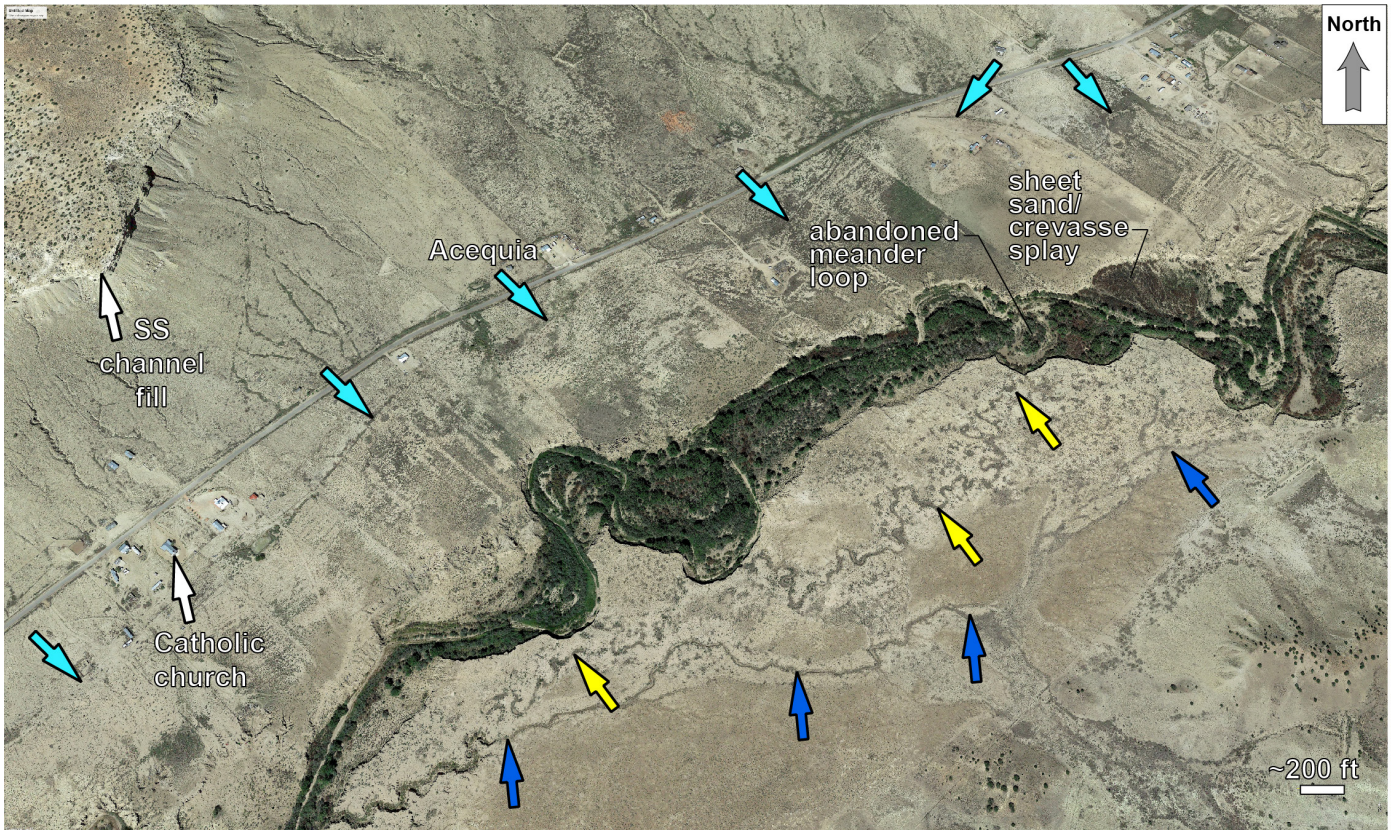

FIGURE 2.13. Google Earth image showing the Rio Puerco Valley floor northeast of the San Luis Catholic Church. The church and the large sandstone channel fill in the lower Point Lookout Sandstone (mile 6.2) are noted by the white arrows. Note the trace of the acequia (light blue arrows) on the north side of abandoned irrigated fields, which often have striped ground patterns. These fields were presumably abandoned in the 1930s to 1950s, when people gradually left the area (García, 2015). Note the well-vegetated nature of the Rio Puerco inner arroyo, suggesting a lack of major flood scouring over the past few decades. Also of interest are two channel patterns south of the Rio Puerco inner arroyo. The channel demarcated by the yellow arrows is highly meandering, whereas the channel noted by the dark blue arrows is much straighter. The sharpness of the latter suggests it is younger, and it seems to be capturing side-stream runoff. The northwestern channel (yellow arrows) may be the former channel of the Rio Puerco. The main channel was narrow and small prior to 1885, and the felling of one cottonwood tree was able to divert water in the main channel to an irrigation ditch (Bryan, 1928).

The four towns were permanently settled starting in 1870–1872 after cessation of Navajo raiding, and irrigation infrastructure was built in 1872. Farming and grazing were largely for subsistence and were relatively successful through the 1920s, but the area's population decreased between World War I and the early 1950s (García, 2015). Several factors made the traditional farming lifestyle difficult: (1) dramatic deepening and widening of the Rio Puerco arroyo made it costly and difficult to maintain irrigation dams (Widdison, 1959), (2) a severe drought during the mid-1930s killed more than half the cattle (García, 1994), (3) passage of the Taylor Grazing Act by the U.S. Congress in 1934 regulated grazing on public lands and ended in rangers shooting cattle (García, 1994), and (4) external events and opportunities lured the population away. These events included men enlisting oversees in WWI and WWII as well as relatively abundant job opportunities in communities along the Rio Grande, especially Albuquerque, in the mid-1940s through the 1950s. Only two families were living in San Luis by the end of the 1950s, but since then, the population has rebounded to 185 people (2021 U.S. Census: https://datausa.io/profile/geo/san-luis-nm/). Although there are several ranches in the area, it appears that most people commute for jobs, probably to Cuba or Torreon (based on the average commute time of 26.8 minutes reported in https://datausa.io/profile/geo/san-luis-nm/). *0.1*

7.4 1 mile sign post. *0.5*

Waypoint 4 [35.678325°, -107.056376°]

7.9 **Just beyond the cattle guard, turn right onto a dirt road.** Follow the dirt road to the west-northwest

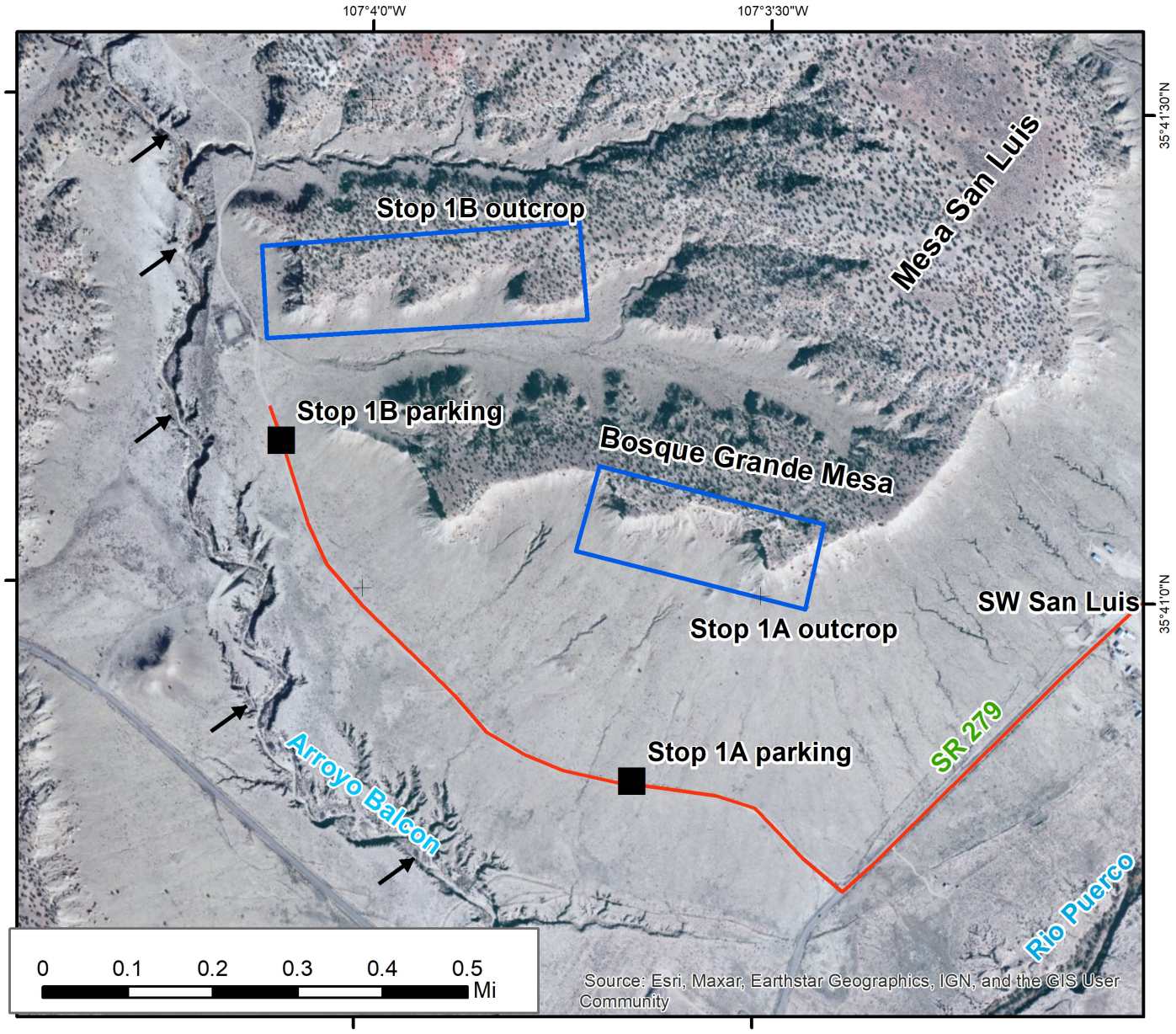

FIGURE 2.14. Map of the area around Stop 1. Note the incised nature of Arroyo Balcon (black arrows). Outcrop areas are shown in blue rectangles.

across valley-floor alluvium. To the right lie sandstone-capped bluffs that we observe at Stop 1. These bluffs form the southeast edge of Bosque Grande Mesa, a thin extension of Mesa San Luis (Fig. 2.14). *0.3*

8.2 STOP 1A. Stratigraphy and sedimentology related to an 84–81 Ma regression of the Cretaceous Western Interior Seaway (upper Mancos Shale overlain by Point Lookout Sandstone) and Quaternary geology of the middle Rio Puerco Valley.

Waypoint 5 [35.680039°, -107.060795°]

Pull off alongside the dirt road. Stop 1 consists of two parts (1A and 1B), and the map in Figure 2.14 shows the stop relative to surrounding physiographic features and roads. We briefly stop here (Stop 1A) to view the Upper Cretaceous stratigraphy exposed in the cliffs 0.3 mi to the north. More time will be spent at Stop 1B, where easier slopes allow participants to walk up to the stratigraphic interval seen in Stop 1A and look at outstanding sedimentologic features characteristic of wave- and storm-influenced shoreline environments. These environments are encapsulated in two transgressive-regressive parasequences (1–3 m thick) developed during a long-term shoreline progradation. At Stop 1B, we also discuss the geomorphology of this part of the Rio Puerco Valley, which is characteristic of much of the larger San Juan Basin and southeastern Colorado Plateau. On the valley floor 0.1–0.23 mi to the south and southwest of the road, one can see steep-walled, narrow gullies related to post-1885 incision of the Rio Puerco. Also, along the foot of the sandstone-capped bluffs are scattered sandstone boulders (up to several meters long) that fell from the mesa-capping Point Lookout Sandstone, reflective of the mass wasting processes integral to valley widening. What exactly are the geomorphic processes driving arroyo incision and slope retreat? What is the timing of incision and mass wasting, and how might they relate to one another?

Point Lookout Sandstone

Late Cretaceous setting

The Western Interior Seaway (WIS) flooded the middle of the North American continent during the Late Cretaceous and between 95 and 80 Ma, connecting the Gulf of Mexico with the Arctic Ocean (Fig. 2.15; https://deeptimemaps.com/map-lists-thumbnails/western-interior-seaway/). The WIS formed due to: (1) dynamic regional subsidence caused by shallowing of the subducting Farallon flat slap (Chang and Liu, 2021); (2) crustal loading during the Sevier orogeny, which generated a wide foreland basin east of the Sevier highlands (Pang and Nummedal, 1995; Liu and Nummedal, 2004; Miall et al., 2008); (3) globally high sea levels related to a greenhouse climate (resulting in minimal, if any, glacial ice and thermal expansion of seawater); and 4) extensive mid-ocean ridge volcanism displacing seawater onto continents (Hay, 2008).

Long-term sea levels peaked during the late Cenomanian through the earliest Turonian (94–92 Ma), then progressively fell in the remainder of the Late Cretaceous, resulting in long-term northeastward shoreline progradation and eventually terrestrial conditions across New Mexico by ~70 Ma. However, the long-term fall was interrupted by relatively stable sea levels during the Coniacian through Campanian (86–75 Ma; Haq, 2014). Superimposed upon long-term (10^7-yr) sea-level changes were shorter term (10^5–10^6-yr) sea-level oscillations, many of which were eustatic (e.g., Nummedal, 2004; Gale et al., 2008; Lin et al., 2019). During the Late Cretaceous, the WIS western shoreline trended approximately northwest-southeast, with rivers and associated deltas flowing northeast into the WIS (Fig. 2.16; Wright-Dunbar et al., 1992; Wright-Dunbar, 1992a, Lin et al., 2019). Shorelines between local deltas were characterized by strandplains (broad shorelines with well-defined parallel sand ridges separated by shallow swales), beach ridges, barrier islands, and back-barrier environments, the latter including lagoons and estuaries (Shetiwy, 1978; Zech, 1982; Wright, 1986; Devine, 1991; Katzman and Wright-Dunbar, 1992; Wright-Dunbar, 1992a; Nummedal, 2004).

FIGURE 2.15. Schematic paleogeography of the Late Cretaceous Western Interior Seaway on the North American continent during the Late Cretaceous. Tan and green = land mass; blue = seaway (from https://www.cretaceousatlas.org/geology/).

The repeated, short-term transgressions and regressions, superimposed on a long-term shoreline progradation during WIS retreat, resulted in a stratigraphic succession characterized by interfingering of marine mudstones with nearshore sandstone tongues, such as that generalized in Figure 2.17 for the Coniacian through early Campanian. The shaly mudstones are assigned to the Mancos Shale. The intervening nearshore sandstone tongues are each formally named but terminate to

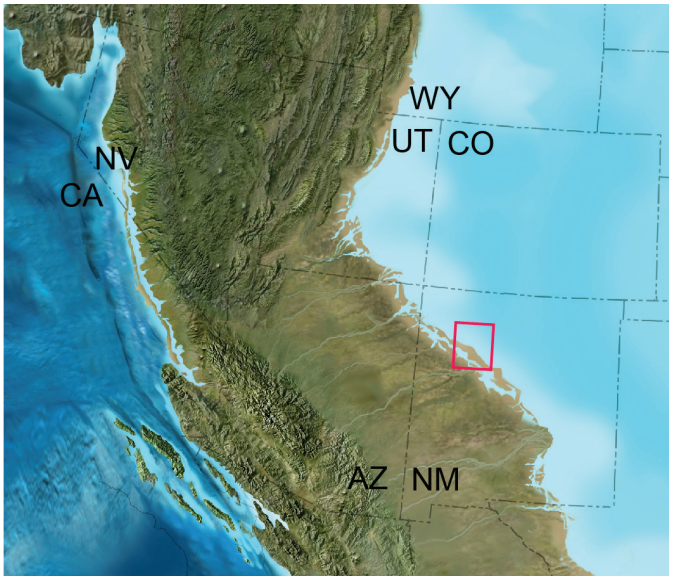

FIGURE 2.16. Paleogeography of the southwestern United States at 82.9 Ma (early Campanian). Red rectangle denotes the approximate area of the NMGS field trip (specifically, between what is now Grants [lower left corner] and Gallina [upper right corner] in New Mexico). From the web page https://deeptimemaps.com/map-lists-thumbnails/western-interior-seaway/.

the northeast (seaward) and grade landward (southwest) into terrestrial deposits. Where present, the sandstone tongues also allow the Mancos Shale to be locally divisible into formally named tongues (Fig. 2.17). In this field trip, the stratigraphic sequence we will see includes the following lithologic units, listed in ascending order with approximate thicknesses in parentheses: Gallup Sandstone (50 ft, 15 m), Mulatto Tongue of Mancos Shale (500 ft, 155 m), Dalton-Sandstone tongue (30–50 ft, 12–15 m), Satan Tongue of the Mancos Shale (310 ft, 95 m), and Point Lookout Sandstone (70–85 ft, 22–26 m). The Point Lookout Sandstone grades upward into coal-bearing, terrestrial deposits of the Menefee Formation.

The sandstone tongue underlying the Satan Tongue is called the Hosta Tongue by Hunt (1936) and New Mexico Bureau of Geology and Mineral Resources (2003). However, as shown in Optional Stop 2, this sandstone records a regression and, in that sense, is more akin to the Dalton Sandstone (Fig. 2.17). No terrestrial deposits are observed. To honor precedent and the regressive nature of the sandstone, for the purposes of the field trip we use the hyphenated Dalton-Hosta sandstone to describe this laterally extensive sandstone body (Fig. 2.17), which we cross frequently in the remainder of the Second-Day Road Log.

Parasequences

In Stop 1A, we look northward at cliffs flanking the south edge of Bosque Grande Mesa (Fig. 2.14). These excellent exposures depict the upward transition from the Mancos Shale to the Point Lookout Sandstone, illustrating a major progradation or shoreline regression (relatively interchangeable terms as used here, with progradation referring to the lateral movement of environments/sediment and regression referring specifically to offshore-directed shoreline migration) that occurred in the latest Santonian to early Campanian (84–81 Ma). Ammonite data support a primarily early Campanian age for the Point Lookout Sandstone in this area (Sealey and Lucas, 2019). More details of the Point Lookout progradation and how it and other sandstone tongues relate to sequence stratigraphic concepts are in Koning (2024). It suffices to say here that the Point Lookout Sandstone is an important component of a major early Campanian regression, and it is manifested in the stratigraphic record by the upward transition of mudstones of the Mancos Shale to nearshore sandstones (Point Lookout Formation) to fluvial-deltaic mudstones and sandstones (Menefee Formation). There must have been significant basin subsidence and sediment influx to preserve this 70–85-ft-thick (22–26 m) progradational succession, and, since longer-term sea level was relatively static at this time (Haq, 2014), these two processes were probably important drivers of the progradation.

The Point Lookout Sandstone was studied in detail by Robyn Wright in the 1980s and early 1990s (Wright, 1986, 1988; Wright and Hayden, 1988; Wright-Dunbar, 1992a, 1992b; Wright-Dunbar et al., 1992). Although the Point Lookout represents a long-term progradation or regression, their work recognized many meter-scale transgressive-regressive units termed parasequences (a conformable succession of genetically related beds that are bound by marine flooding surfaces or their correlative surfaces; Van Wagoner et al., 1988). We look at two such parasequences, represented by the lithologic couplets T1-R1 and T2-R2 (T = transgressive, R = regressive; Fig. 2.18). Units T1 and T2 in the lower part of these couplets are primarily mudstones deposited in relatively deep marine settings, whereas the overlying R1 and R2 units are sandier and deposited in shallower marine settings. The T2 subunit is tabular in geometry and was termed the marker shale by Wright and Hayden (1988) and Wright-Dunbar (1992b).

In the traditional sequence stratigraphic literature, which is dominated by studies in siliciclastic deposits, parasequences are described as repeated, upward-coarsening units bound by discrete flooding surfaces. Flooding surfaces are characterized by an abrupt change in grain size indicating rapid deepening (Van Wagoner et al., 1988). The parasequences observed in the Point Lookout do not follow all of these traditional characteristics; we explore how they differ at Stop 1B and discuss possibilities of why they differ.

Parasequences are the fundamental or smallest scale component of sequence stratigraphy, which seeks to understand a sedimentary system by subdividing and relating unconformity-bounded units within a lithostratigraphic unit(s). For an overview of sequence stratigraphy concepts and terms, see the Society of Sedimentary Geology (2023) webpage. Original publications related to the subject include Posamentier et al. (1988) and Van Wagoner et al. (1987, 1988).

Parasequences are commonly ascribed to ~20–400-ky eustatic sea-level changes (as is inferred for late Cenomanian through Santonian strata; Nummedal, 2004; Lin et al., 2019). A possible alternative explanation for the parasequence formation seen here could involve changes in sedimentation rates due to varying discharge and channel-mouth locations of rivers on the nearby coastal plain (termed autocyclic or autogenic processes; Muto and Steel, 1992; Hajek and Straub, 2017).

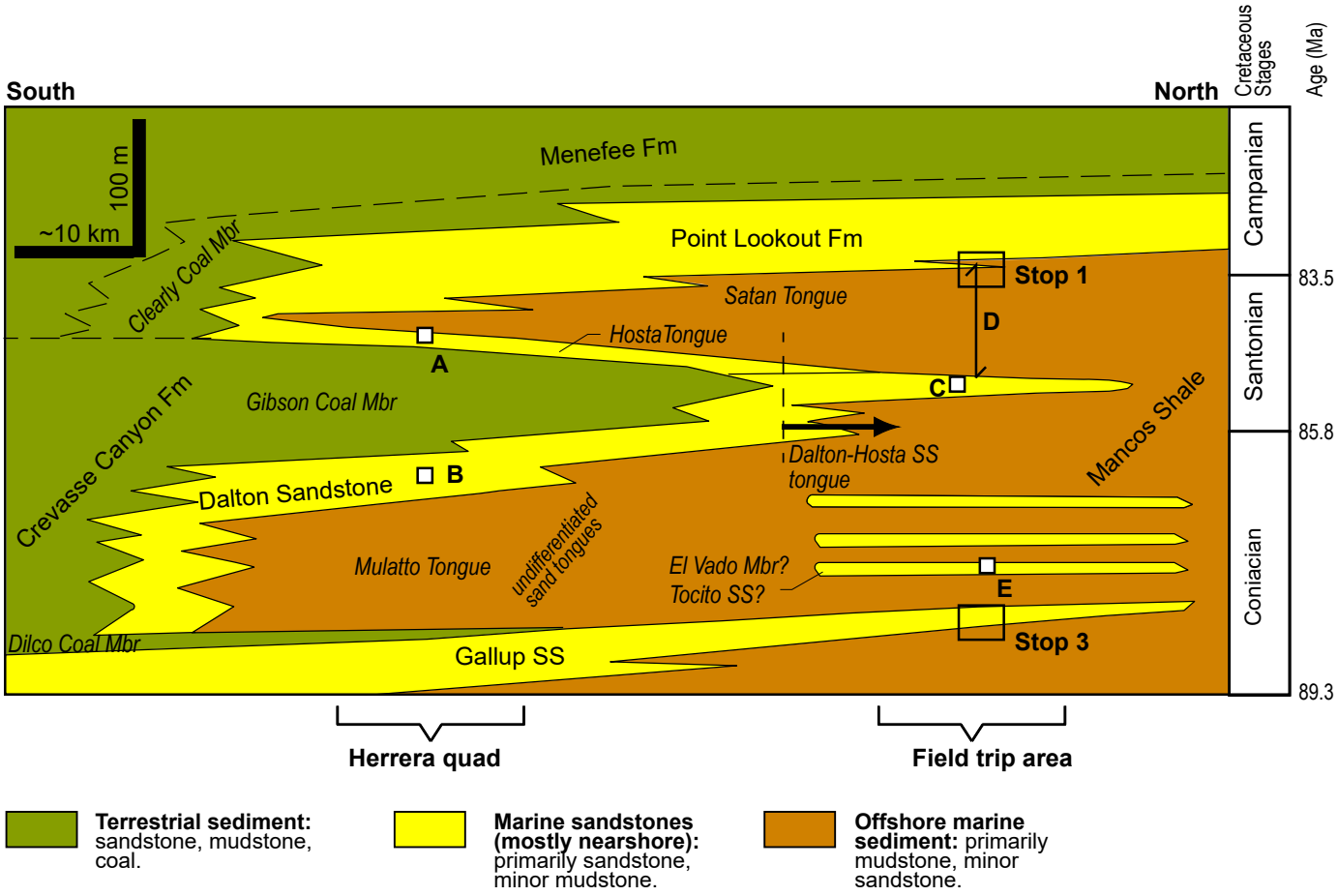

FIGURE 2.17. Schematic, north-south cross section illustrating the Late Cretaceous stratigraphy of the Rio Puerco Valley between Interstate 40 and San Luis. Note that the trend of section is oblique to the northwest-southeast trending paleoshoreline. Thicknesses and stratigraphic relations from the Herrera quadrangle (~10 mi, 16 km, north of Interstate 40) are from geologic mapping of Rawling and Koning (2019), Koning and Rawling (2017), and Koning and Jochems (2014). General thicknesses and stratigraphic relations for the field trip area are from New Mexico Bureau of Geology and Mineral Resources (2003), Koning (unpubl.), Hunt (1936), and measurements in Google Earth; thicknesses have up to 10 m error, except for the Satan Tongue (5 m error). Ages for Late Cretaceous stages are from https://timescalefoundation.org/resources/geowhen/timelinestages.html (accessed January 6, 2024). Age and thicknesses at specific localities (A through E) are from: (A) Bourdon et al. (2011), (B) Johnson and Lucas (2003), (C) and (D) Koning (unpubl.), and (E) Williamson and Lucas (1992). Figure slightly modified from Koning (2024).

Given long-term tectonic subsidence in the foreland basin, periodically reduced sediment fluxes could be expected to result in increased relative water depths and a local transgression. However, the repeated occurrence and meter-scale nature of the parasequences recording rapid transgression followed by gradual regression is reported in Upper Cretaceous strata throughout the WIS (Elder et al., 1994; Gale et al., 2008) and globally (Haq, 2014; Ray et al., 2019), arguing for eustatic origins rather than due to local variations in autogenic sediment supply and subsidence processes.

The Late Cretaceous is well known for being one of the warmest time intervals of the last ~200 My (Hay, 2008; https://doi.org/10.1016/j.cretres.2008.05.025), casting doubt on glacio-eustatic drivers for the widespread parasequences. However, thermo-eustasy (climatically controlled thermal expansion/contraction of seawater) and aquifer-eustasy (climatically controlled filling and emptying of groundwater reservoirs) are plausible mechanisms to explain the observed eustatic changes with the climate changes driven by variations in Earth's orbit-

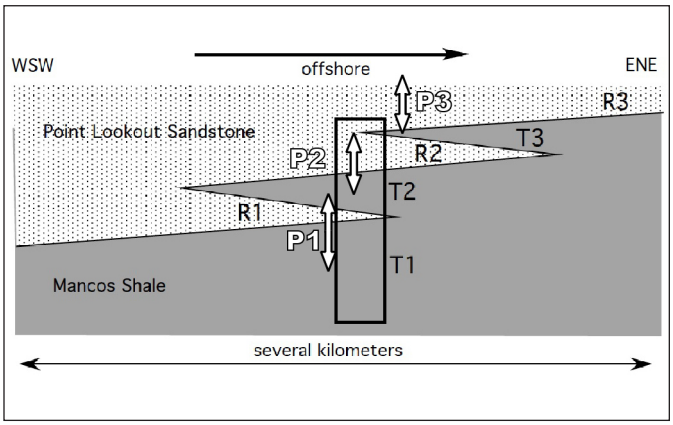

FIGURE 2.18. Schematic illustration of the parasequences (and their component T1-R1, T2-R2, and T3-R3 lithologic units) that developed during long-term Point Lookout progradation. Note that the shallower water sandstones pinch out seaward (northeast of us), while mudstone tongues of the Mancos Shale pinch out landward (southwest of us). The vertical box outlines the portion of the Point Lookout progradation observed at Stop 1.

al parameters (or Milankovitch climate changes) occurring on ~20 ky, ~40 ky, ~100 ky, and ~400 ky periods (Berger, 1988; https://doi.org/10.1029/RG026i004p00624).

The cliff face to the north nicely illustrates three parasequences that we informally refer to as parasequences 1 through 3 (P1, P2, P3). In outcrop, these three parasequences are associated with the T1-R1, T2-R2, and T3-R3 lithologic units of Wright (1986) and Wright and Hayden (1988) that reflect transgressions and regressions (Figs. 2.19, 2.20). These workers have found that the transgressive units (e.g., T2, T3) thick-

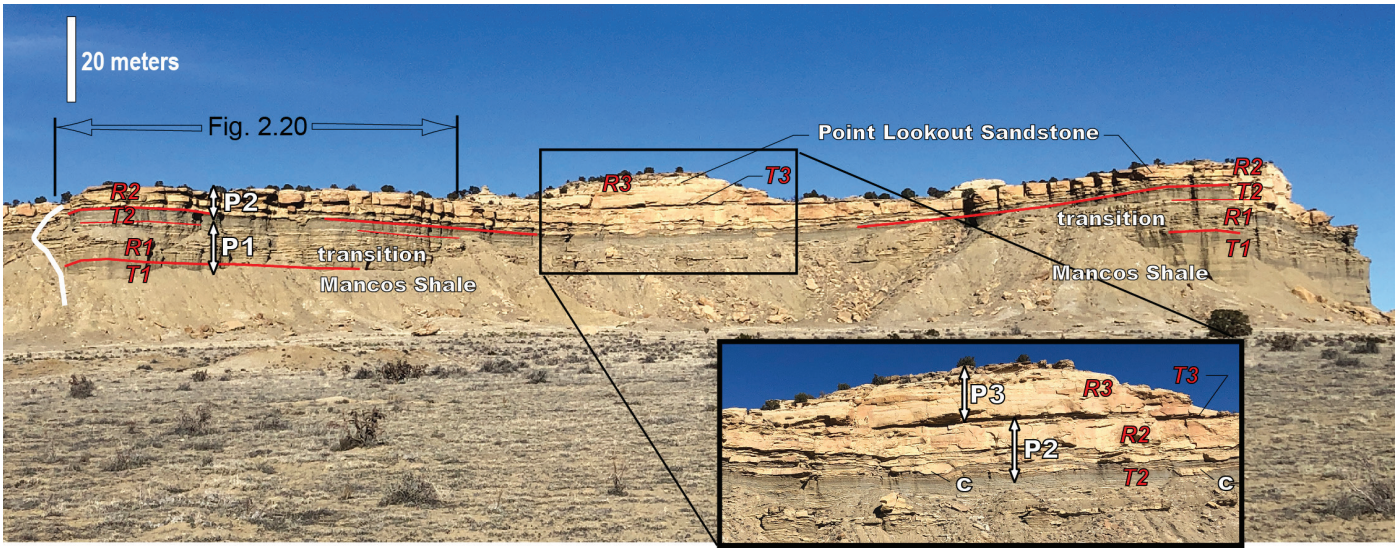

FIGURE 2.19. Annotated outcrop face of the southern end of Bosque Grande Mesa (outcrop 1A shown in Fig. 2.14). View to the north. There are three meter-scale parasequences (denoted by opposing white arrows and labeled P1, P2, P3) composed of transgressive-regressive, lithologic couplets labeled T1-R1, T2-R2, and T3-R3, oldest to youngest (Wright, 1986; Wright and Hayden, 1988; Wright-Dunbar, 1992b). Both T2 and T3 thicken basinward to the northeast (Wright, 1986). Sandstone-dominated strata are correlated to the Point Lookout Sandstone (R2, T3, R3). A 12-m-thick transition zone (R1 through T2) separates these sandstones from the underlying, mudstone-dominated Mancos Shale (T1 and lower strata). A close-up of the western cliff face is shown in Figure 2.20. The white line on left is the location of the stratigraphic section depicted in Koning (2024). Note the ribbon-like channel forms in the inset, enlarged photo of the central part of the outcrop (these features are also seen in Fig. 2.20). These forms are particularly common at the base of R2 and upper R1.

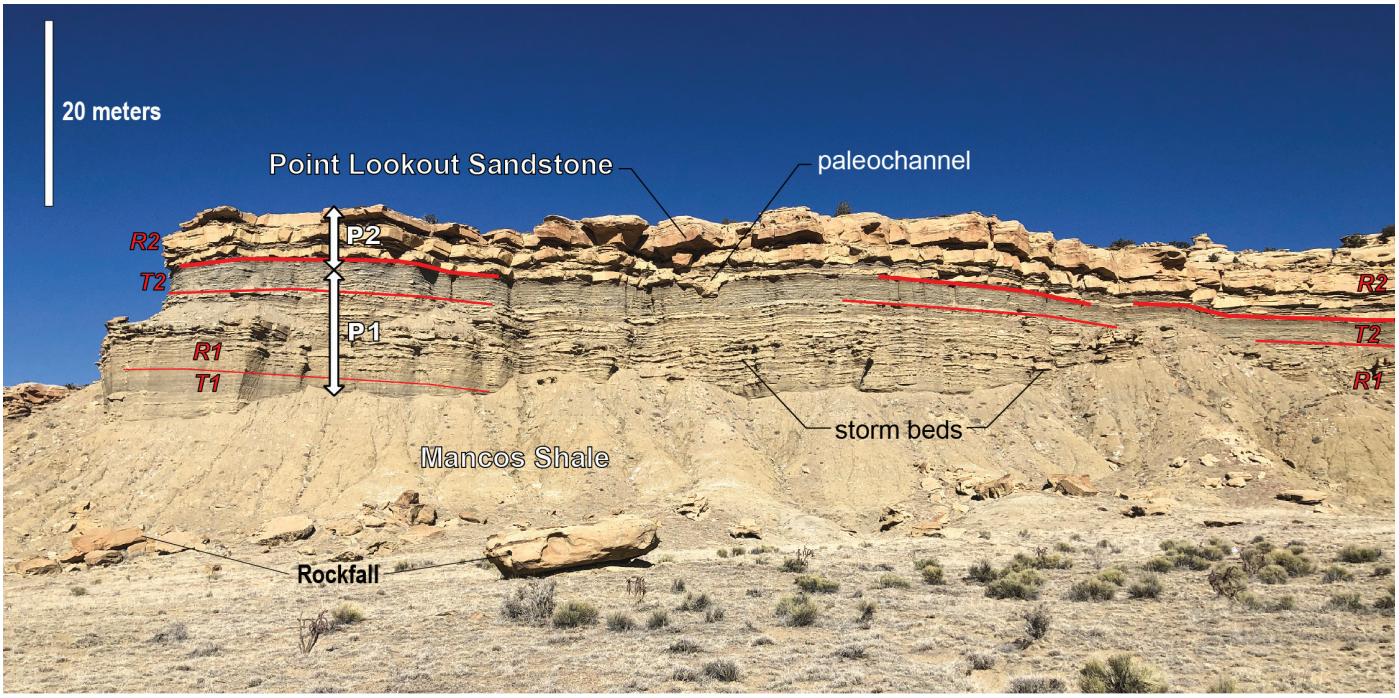

FIGURE 2.20. Close-up of the western side of the cliff depicted in Figure 2.19. A 12-m-thick transition zone (units R1 and T2) separates the Point Lookout Sandstone from the underlying, mudstone-dominated Mancos Shale. The two parasequences studied at Stop 1 (P1 and P2) are shown by the double-sided white arrows. The transgressive and regressive lithologic units of Wright (1986, 1988; also Wright-Dunbar, 1992b) are annotated and labeled in red.

en basinward (to the northeast), whereas the regressive units (R2, R3) thin basinward. Stop 1B allows participants to closely inspect these parasequences (i.e., transgressive-regressive couplets), and using sedimentologic features, one can interpret relative water depth and oxygen curves (as a function of stratigraphic height). At Stop 1B, we also discuss where to interpret parasequence boundaries.

The cliff exposure to the north exhibits many lenticular to channel-shaped sandstone beds with scoured bases and sharp tops (Figs. 2.19, 2.20), in addition to the tabular beds often characteristic of nearshore environments and turbidites (cf. the lower Gallup Sandstone at Stop 3). The lenticular and channel-shaped beds are probably related to storm-generated currents (Wright, 1986; Wright Dunbar et al., 1992; Lucas et al., 1992). Trip participants will measure the orientation of the channels at Stop 1B and decide if their trends are consistent with a storm interpretation. **Return to vehicles.** *0.4*

8.6 Pass gate. Make sure gate remains closed if you found it closed. *0.3*

8.9 STOP 1B. Park alongside road on southeast side of a cattle tank (shallow excavation on ground to collect surface runoff that is rimmed by tamarisks). Three topics are discussed at this stop: (1) Nearshore paleoenvironments and regressive-transgressive parasequences in the lower-middle Point Lookout Formation, (2) slope geomorphology, and (3) gully incision and headward propagation.

Waypoint 6 [35.686722°, -107.068845°]

1) Lower-middle Point Lookout Sandstone sedimentologic and paleontologic features; interpretation of depositional environments and parasequences and how these relate to transgressions-regressions

Stop 1B allows us to access to the regressive (R1, R2) and transgressive (T2) units that approximate parasequences 1 and 2 (Wright, 1986; Wright and Hayden, 1988; Wright-Dunbar, 1992b). These outcrops are found on the north side of the canyon extending east from here (Figs. 2.14, 2.21). There, we divide into smaller groups, each led by those familiar with the outcrop, to facilitate access and discussion. On the outcrop, look for sedimentologic features that allow one to infer relative water depth, dissolved oxygen content, depositional environments, paleoflow directions, and transitions between environments (Figs. 2.22–2.24). Three depositional environments are present, which are summarized below and in Figure 2.22.

Offshore facies (below storm wave base)

The offshore region lies below the effects of storm and fair-weather waves so is dominated by the suspension settling of fine-grained deposits (mudstone, siltstone, very fine sandstone). Sparse interbeds of very thin to thin sandstone lenses or tabular beds accumulate (but are not reworked) from offshore storm (lenticular) or turbidity current (tabular) transport. The mudstones have abundant organic matter, imparting a dark color, and vertical burrows may be seen. On the knoll to the south of the canyon, bivalve molds (likely not in-life position) are present in a sandstone bed interbedded in mudstone (Fig. 2.25).

Lower shoreface facies (between storm wave base and fair-weather wave base)

Interbedded sandstones (primarily during storms) and mudstones (during fair weather). Sandstone layers and lenses commonly have sharp bases (planar to irregular due to erosion) and hummocky cross-stratification characterized by convex to concave tops and variably dipping, low-angle stratification (Fig. 2.26). Hummocky cross-stratification develops during storms when sands eroded from the upper shoreface are transported and reworked into three-dimensional hummocks and adjacent swales; they can form in the lower and upper shoreface but are commonly reworked by longshore currents or homogenized by bioturbation in the upper shoreface and erased. There are symmetric ripplemarks (caused by waves) on sandstone surfaces (Fig. 2.27) and spectacular sandstone-filled paleochannels up to 0.7 m thick and with vertical walls (Fig. 2.28). Look for tool marks on bed bottoms to assess paleoflow directions (Fig. 2.29). Interbedded sandstone-mudstone intervals beds exhibit vertical burrows, probably correlative to *Skolithos* (Fig. 2.30). The depth of storm wave base likely varies through time, so absolute or strict boundaries between offshore and lower shoreface environments can be difficult to assess.

FIGURE 2.21. North wall of east-west canyon at Stop 1B. R1, T2, and R2 lithologic units of Wright (1986), Wright and Hayden (1988), and Wright-Dunbar (1992b) are annotated in red. The corresponding parasequences are shown in white, double-sided arrows and labels.

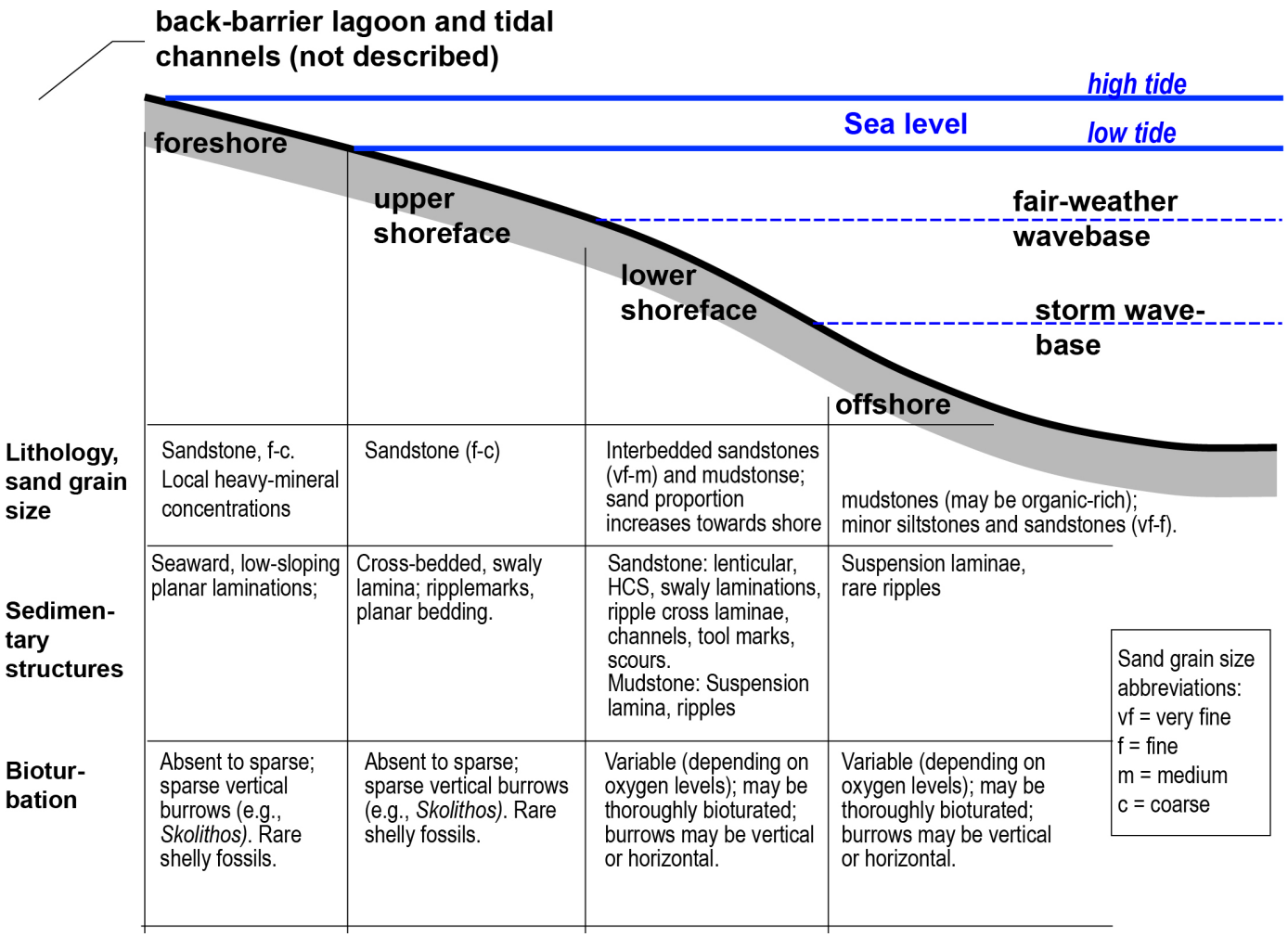

FIGURE 2.22. Depth-related depositional environments in a nearshore, marine setting applicable for Stop 1. Below are specifics of the sedimentologic and paleontologic features that can be used to recognize these environments.

Upper shoreface facies (generally above fair-weather wave base and below low tide)

Relatively continuous fair-weather wave activity characteristic of the upper shoreface results in the deposition of dominantly coarser grain sediments (sandstones, locally with pebbles) which can be reworked by longshore and rip currents generating shore-parallel to offshore-directed cross-bedding and ripples. Point Lookout upper shoreface facies are typically medium- to thick-bedded sandstone with abundant bioturbation homogenizing many original sedimentary structures (i.e., massive sandstone beds; Figs. 2.23, 2.24, 2.31). Locally preserved are swaly (concave-up) and horizontal laminations, rare cross-bedding, and iron-rich dolomite concretions and layers/nodules.

Foreshore (between low and high tide)

Relatively continuous swash and back wash currents characterize foreshore environments, generating horizontal to sub-horizontal laminae (may be gently dipping in seaward direction) that may be homogenized by bioturbation. Some laminae may be defined by alternating dark (mafic-rich) and light (quartz-rich) grains.

At this outcrop, we suggest participants focus their observations to address these key questions:

1) Draw a relative water-depth curve next to the outcrop photograph shown in the handout replicating Figure 2.23 (sans the water depth curve), and interpret and label the depositional environments of each genetically related unit using the criteria outlined in Figure 2.22. Using this water-depth curve, draw the boundaries of the parasequences. Is there evidence for abrupt deepening (flooding "surface") or abrupt shallowing? How do your observations differ from the traditional parasequence, as defined by Van Wagoner et al. (1988)?

2) Using the presence/absence of bioturbation (including individual burrows and the absence of sedimentary layering due to homogenization by bioturbaters) and organic matter abundance (dark color in sediments), draw a relative oxygen level curve next to your water-depth curve.

3) How do the water-depth and O_2 curves compare (e.g., do they covary, or are they offset from each other? What physical factors explain the relationship between water depth and O2 curves?)

4) Measure the orientation of tool marks and channel geometries to estimate the paleoflow direction of sandstone transport.

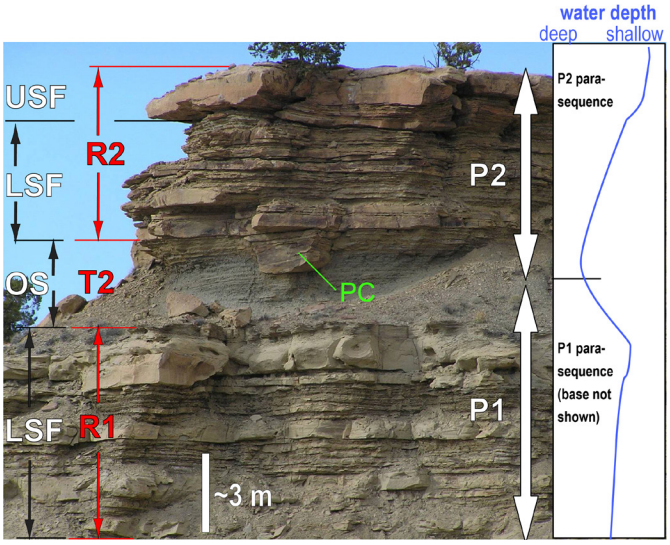

FIGURE 2.23. Annotated outcrop along south-facing bluff visited in Stop 1B. Depositional environment interpretations shown in white text on left side of figure: OS = offshore; LSF = lower shoreface; USF = upper shoreface. Original transgressive-regressive units of Wright (1986) are illustrated with red arrows and text. Parasequences are illustrated on right by white, double-sided arrows and labeling. On extreme right is inferred water depth curve. Wright and Hayden (1988) recognized that the lower part of T2 contained notable thicknesses (several tens of centimeters) of transgressive deposits with maximum water depths represented by the finest-grained interval near the middle of the T2 unit (rather than at the base of T2, as would be expected for a "flooding surface" in a typical coarsening-upward parasequence). Related revision of the parasequence boundary is shown by the white, double-headed arrows. PC = paleochannel.

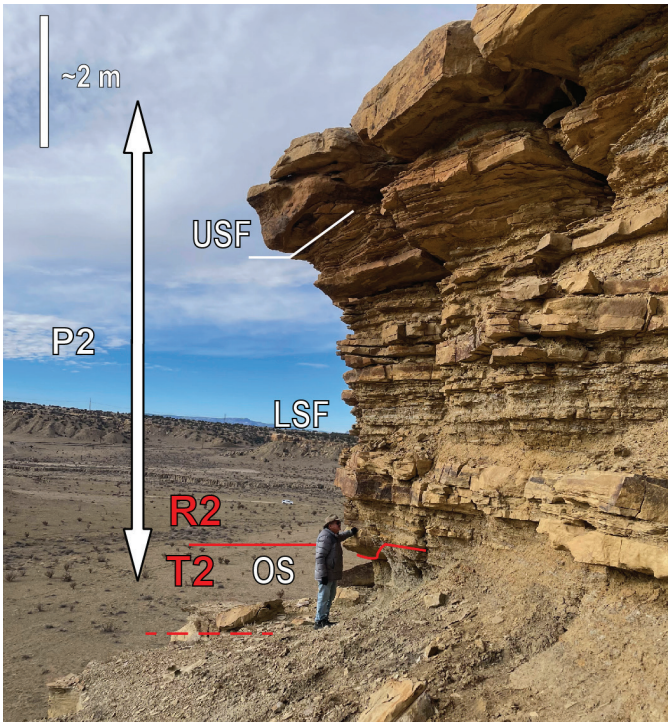

FIGURE 2.24. Illustration of the stratigraphic interval encompassing parasequence 2 (P2, including the upper part of T2 and all of R2) above the interval of maximum water depth in T2. Note upward increasing sandstone proportions in the parasequence. Paleoenvironmental abbreviations as in Figure 2.23.

What types of currents (e.g., storm currents, longshore currents, rip currents) might have transported these sands? What is the relationship between the interpreted paleoflow and the regional paleoshoreline trend?

2) Slope geomorphology in southeastern Colorado Plateau

Two important features of slope geomorphology that demonstrate slope erosion processes are visible at Stop 1B. The first is abundant rockfall at the base of the slopes, occurring in a zone extending ~30 m away from the toeslope (e.g., Fig. 2.20). Based on the thick dimensions of these slabby rockfalls, most of the boulders are sourced from the more thickly bedded R2 unit in the upper part of the cliff. Most of the boulders appear not to be buried, but rather lie on the surface of the Holocene valley fill and thus post-date it. The approximate elevation of the top of the fill, less possibly ~1 m, has existed for the past ca. 1000 years (Stop 3C of Day 2; Pippin, 1979; Niels, 2003; Baker and Durand, 2003).

Geomorphic processes in the exposed ledges of Point Lookout Sandstone that are responsible for the rockfall include fracture sets and under-cutting (erosion) of the weak mudstones underlying the sandstone ledges. Extensive fractures likely relate to past regional stresses, with a 000–030° set being relatively common (Gorham et al., 1979; Estrada et al., 2009; Nelson, 2019). Fractures expand due to water-related freeze-thaw or clay hydration. Fracture growth and expansion eventually result in the fall of a sizeable sandstone boulder (0.5 m to several meters in length). The rockfalls may occur via sliding or by fast

FIGURE 2.25. Bivalve molds in a thin, fine-grained, calcareous sandstone interbed in the uppermost Mancos Shale. Found on the knoll on the south side of the east-west canyon.

FIGURE 2.26. Hummocky cross-stratification seen low in the slope at Stop 1A with rock hammer for scale. Note that on the left individual laminae can be followed from the swale (trough) over the hummock top and down into the adjacent swale, which is diagnostic of storm-generated hummocky cross-stratification. The structures are typical of fine sandstone deposits in lower shoreface environments (between storm wave and fair-weather wave bases). The overlying and underlying strata are mudstone-dominated and part of the uppermost Mancos Shale.

FIGURE 2.27. Symmetrical ripplemarks from middle of unit R2, formed from oscillatory wave motion (black arrows)

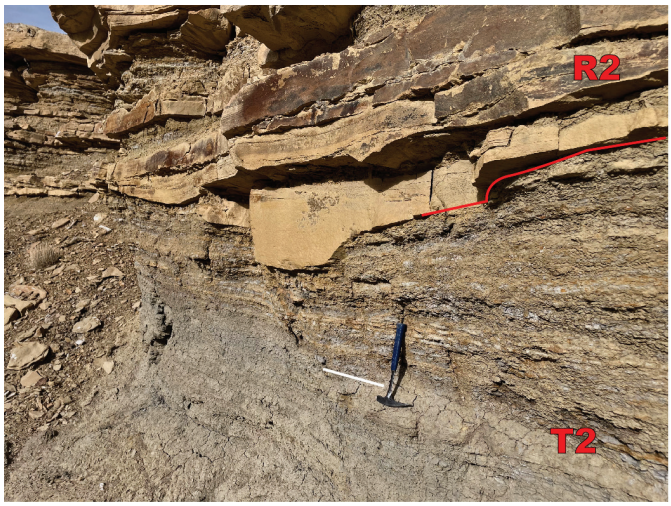

FIGURE 2.28. Unit T2 overlain by unit R2 sandstones. The finest-grained, middle part of T2 is found just below the white line and coincides with interpreted maximum water depths. Above the hammer head and white line, note the increasing proportion of light-colored siltstone lamina and very thin beds, which reflect progressively shallowing water depth of the early R2 regression. Also, note the sandstone paleochannel (base of unit R2) eroding into the top of T2.

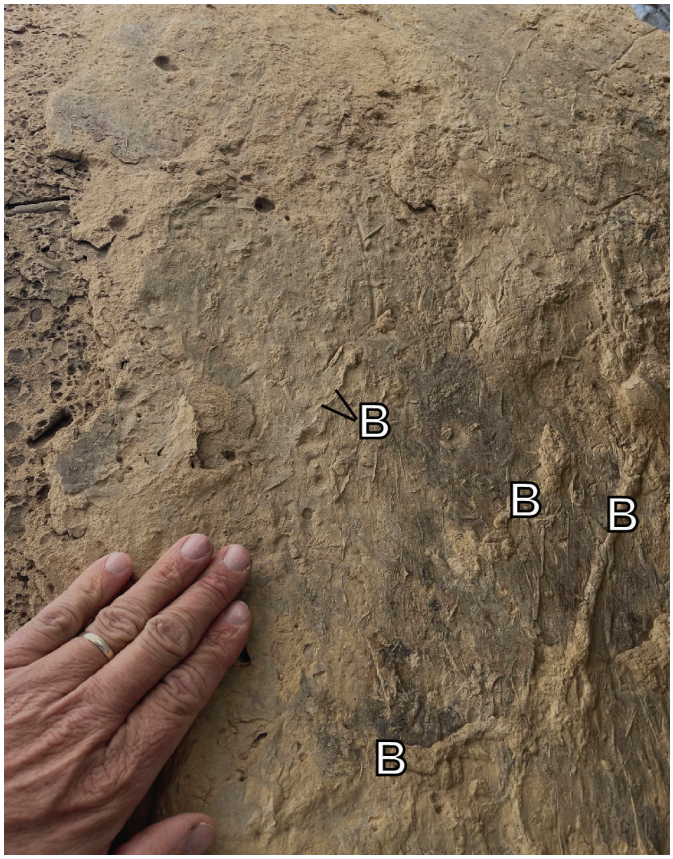

FIGURE 2.29. Photograph looking up to the bottom of a sandstone bed at the base of R2. Note the centimeter-wide burrows (labeled B) and the thinner, parallel-aligned toolmark grooves. The toolmarks trend north-south and were likely generated by offshore-directed storm currents dragging pebbles/fossils along the seafloor orthogonal to oblique to the paleoshoreline (northwest-trending).

rotational (rolling) rockfall. It may be that colder climates of the Little Ice Age (16th to 19th centuries) may have enhanced the freeze-thaw process and increased the rates of rockfall.

Other geomorphic processes commonly responsible for slope erosion include landslides and grain-size "plucking" of sand, the latter promoted by hydration of clayey cements in the

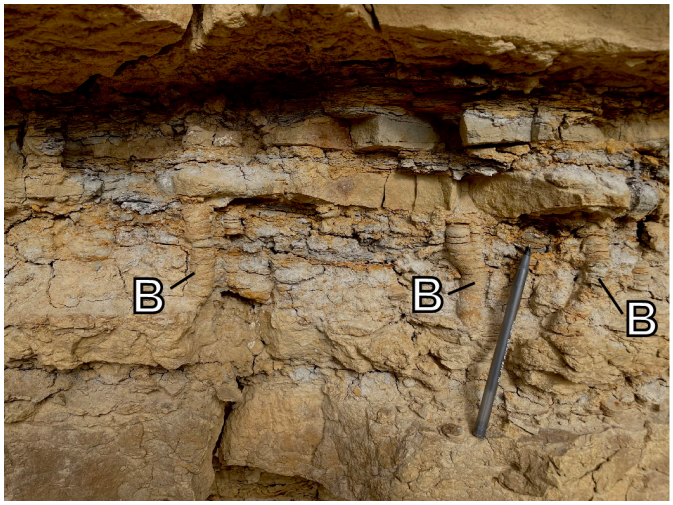

FIGURE 2.30. Vertical burrows (labeled B and probably *Skolithos*) found in the lower part of the R2 unit, indicating sufficient dissolved oxygen was available to support limited animal life. Pen for scale, just to the lower right of one such burrow.

FIGURE 2.31. Horizontal paleoburrows (*Thalassinoides*?*)* near the base of the capping, 2–3-m-thick sandstone. This capping sandstone is massive due to homogenizing from bioturbation.

sandstones. Landslides are very sparse to absent, but the lead author can attest to sand-size particles raining down from the cliff face during times of high winds. Rockfall is probably the dominant process by which sandstone-capped slopes retreat with time, all the while maintaining their characteristic steep profile (i.e., parallel slope retreat).

The second slope-related feature seen here is related to slope aspect, which is the direction of the slope faces. Looking eastward up the valley where Cretaceous outcrops are located, note how the north-facing slope is mantled by thick colluvium and generally not a cliff, whereas the south-facing slope has low to no colluvium and exhibits cliffs (Fig. 2.32). Rockfall is concentrated at the foot of the south-facing slope but is rare on the north-facing slope. The Cretaceous bedrock stratigraphy is the same on both slopes; the main difference is aspect, with less evaporation and moister surfacial sediment on the north-facing slope allowing a higher density of grassy and shruby vegetation. Higher vegetative density promotes colluvial development by (1) capturing more eolian fines (by slowing down wind velocity) and (2) retarding the erosive effects of slopewash. Moister conditions in fine soils in turn drive clay hydration in the sandstone cements and consequently promote sandstone weathering under the colluvial mantle, further increasing the thickness of the colluvium. Colluvium buildup on the slope buries potential ledges and prevents the slope-undercutting that can promote rockfall. Previous works noting the importance of slope-aspect on slope profiles and hillslope erosion on the Colorado Plateau and/or semiarid, badland landscapes provide the conceptual basis of the foregoing discussion on geomorphic processes and include Melton (1960), Churchill (1981, 1982), Kirkby et al. (1990), Burnett et al. (2008), McAuliffe et al. (2014), and McFadden et al. (2005).

FIGURE 2.32. Photograph looking east up the canyon at Stop 1B. Note that the north-facing (right) slope has a colluvial cover, whereas the south-facing (left) slope exposes Mancos Shale and the Mancos-Point Lookout transition zone. Also note the abundant rockfall on the south-facing slope and lack of rockfall on the north-facing slope.

3) Recent-historic gully incision

From the Cretaceous outcrops at Stop 1B, one is afforded views of steep-sided, deep (~5–10 m) gullies in the Holocene alluvium underlying the valley floor along Arroyo Balcon. One can walk ~400 ft (~120 m) south of the vehicles to appreciate the steep headwalls and knick-point migration occurring at the heads of gullies feeding into the mainstem gully (Fig. 2.33). How do these gullies form? The following is based on personal observations by the lead author. During intense summer monsoons, one would expect sheets of water (sheetflooding) to flow southward from the mouth of the canyon at Stop 1B toward the lowest part of the valley floor (south of the vehicles). There, meter-scale free fall of the cascading water at the heads (and to some extent the sides) of the gullies creates the energy

for direct erosion of the gully headwalls (Fig. 2.34). The flow of deep (concentrated) water in the gullies facilitates further incision and gully widening, the latter via toe-cutting and mass wasting.

What will be the fate of this gullying? Will the gullies extend to the footslope of the bluffs? Will all the alluvium of the valley floor be removed, and will the increased vertical relief facilitate slope erosion on the bluffs? Or will the hundreds of meters of distance between the incised gullies and the mesa flanks allow dampening of the headward-migrating gully erosion, so that slope processes are relatively independent of such gully incision? More about historic gully erosion will follow on the field trip, particularly at Optional Stop 1 and Stop 3. **RE-ZERO ODOMETER at intersection of dirt road and State Road 279.** *0.4*

Waypoint 4 [35.678325°, -107.056376°]

0.4 Low ridge underlain by Mancos Shale. *0.2*

FIGURE 2.33. View of incised valley floor of Arroyo Bacon. White truck for scale.

FIGURE 2.34. Headwall of a northward-propagating gully in Holocene valley fill. View to the northeast. Sheetflooding on the right-sloping (southward-sloping) valley floor, generated during intense rainfall events, cascades over the headwall, and the associated kinetic energy wears down the vertical face.

0.6 Cross Arroyo Balcon. Paved road turns sharply right (Power Line Road). Continue straight on dirt road (State Road 279). *0.6*

Waypoint 7 [35.669520°, -107.061078°]

1.2 Cross buried natural gas pipeline. *0.6*

1.8 To right is an extensive terrace developed on a 6-ft-thick (2-m-thick) Rio Puerco sandy gravel, which overlies Mancos Shale. This correlates to the Rito Leche terrace of Bryan and McCann (1936). Its tread is about 80–100 ft (24–30 m) above the valley floor adjoining the entrenched Rio Puerco arroyo. *0.1*

1.9 Intersection with dirt road leading to right. *0.1*

2.0 Intersection with dirt road leading to left. This follows a utility line and can be used to access the north end of Mesa Prieta and the Ojito Wilderness Area. *0.1*

2.1 Straight ahead is a view of the northern part of Chivato Mesa, with Cerro Cuates in the foreground. At 1:00–2:00 are bluffs capped by Point Lookout Sandstone, correlating to the same strata visible at Stop 1. *0.2*

2.3 Gravel-capped knolls to right correlate to the Rito Leche terrace. *0.5*

2.8 Cross a low ridge underlain by Mancos Shale, beyond which road bends slightly left. Skyline ahead (Fig. 2.35) includes these volcanic necks (left to right): Cabezon Peak (9:00–10:00), Cerro Chato (behind which lies the taller Cerro de Guadalupe), Cerro de Santa Clara, and Cerro Cuate (1:30–2:00). *0.5*

3.3 Cross under an electrical transmission line and a cattle guard. *0.3*

3.6 To left is the head of a recently incised gully. *0.2*

3.8 Road bends right on top of a ~30 ft (10 m) topographic rise. Cabezon Peak (10:00) towers above the valley. The sandstone ledge below the dark-colored basalt is probably the Point Lookout Sandstone, underlain by 200–300 ft (60–90 m) of Mancos Shale. *0.2*

4.0 Good view of Point Lookout Sandstone on right. *0.4*

4.4 Y-intersection with well-graded, dirt road (BLM Road 1114) leading to the southeast. **Turn left. RE-ZERO ODOMETER.**

Waypoint 8 [35.632253°, -107.107980°]

Route from State Road 279 to Cerro de Guadalupe and Cerro de Santa Clara (Stop 2 and Optional Stop 1)

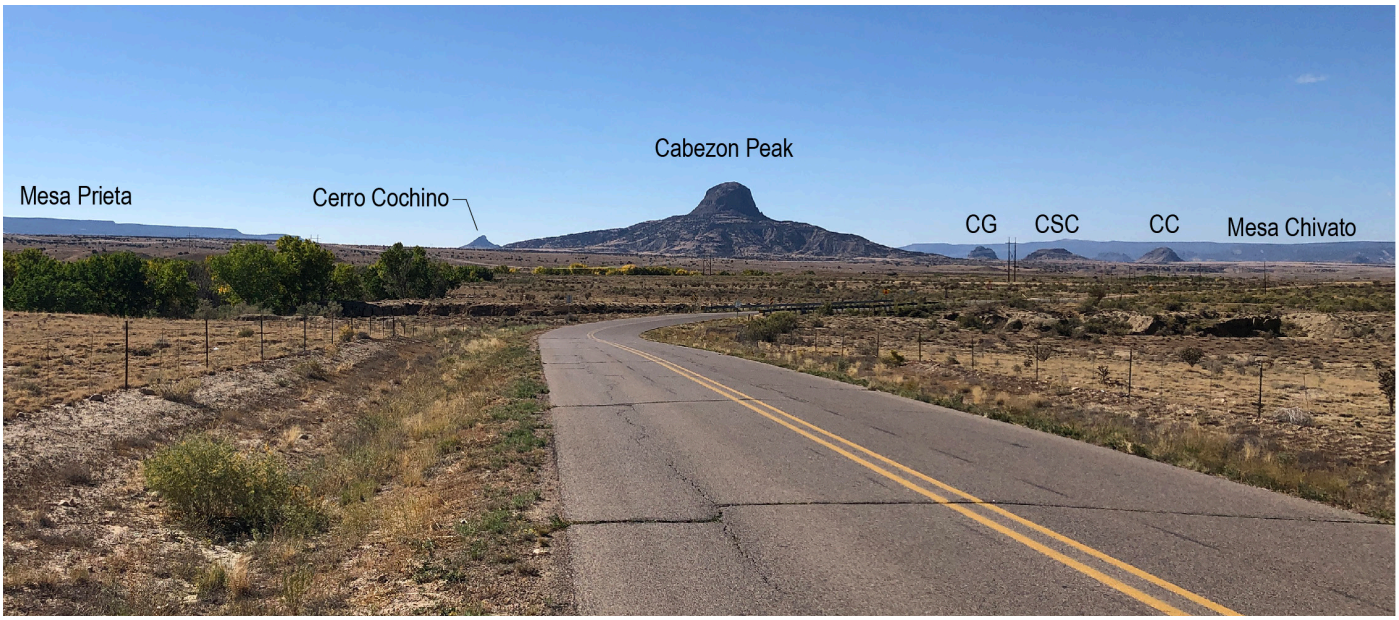

FIGURE 2.35. View looking south-southwest down the Rio Puerco Valley. Mesa Prieta and Mesa Chivato flank the valley on the left and right, respectively. Between lie the Rio Puerco volcanic necks, including two which we will visit on this field trip (left to right): Cerro Cochino, Cabezon Peak, Cerro de Guadalupe (CG), Cerro de Santa Clara (CSC), and Cerro Cuate (CC).

This part of the road log allows observation of a variety of sedimentary strata and 3.5–2.5 Ma volcanic necks that are the prominent landscape feature of the middle Rio Puerco Valley (Fig. 2.35). Sedimentary sections are well-exposed in both Cretaceous and middle-late Holocene alluvial valley fill, respectively exposed on the sides of buttes and on the sidewalls of recently incised arroyos.

From the road junction, we can see several volcanic necks framed by Mesa Prieta to the left (east) and Mesa Chivato to the right (west), bounded on the south by Mount Taylor. From left to right (east to west), the volcanic necks include Cerro Cochino, Cabezon Peak, Cerro de Guadalupe, Cerro Chafo, Cerro de Santa Clara, and Cerro Cuate (Fig. 2.35).

The Rio Puerco volcanic necks lie within the northeastern extension of the Mount Taylor volcanic field, so it is useful here to discuss the larger volcanic context of this field. Mount Taylor is the principal volcanic edifice within the field, located at the south end near Grants. It is a composite stratovolcano composed of coalesced domes, flows, plugs, dikes, ash, and debris flows reflective of trachyandesite to rhyolite compositions; there are also a few trachybasalt cones and flows (Crumpler, 1982, 2010a; Goff et al., 2021). The Mount Taylor volcano and surrounding volcanic field, including the Rio Puerco volcanic necks, developed 3.7–1.26 Ma (Hallett et al., 1997; Goff et al., 2008; Goff et al., 2010). Much of the upper volcano, composed of thick trachydacite lavas, was erupted between 2.5 and 1.26 Ma (Goff et al., 2021).

Extending 27 mi (44 km) northeast from Mount Taylor, Mesa Chivato is a classic distributed volcanic field. Eruptions on Mesa Chivato include a sequence of alkali mafic, 3.5–2.5 Ma flows that are compositionally diverse. These flows include (1) an early sequence of basanites/alkali basalts to hawaiites (basanites to sodic-trachybasalts using classification of Le Bas et al. [1986]) with sodic benmoritic (sodic-basaltic trachyandesite) to trachytic (trachyandesite) domes and viscous lava flows (~3.5–2.5 Ma; Crumpler, 1980; Schrader et al., 2012) and (2) a late series of basaltic lava flows, many of which contain prominent megacrysts consisting of angular pyroxene-plagicloase gabbroic clots. Schmidt et al. (2016) argued these megacrysts could be from a deep crustal sill cumulate confined below Mesa Chivato, "sampled" by basaltic magmas ascending upward from the mantle. On the other hand, while the Rio Puerco volcanic necks are a northeastern extension of the Mount Taylor field, there are no evolved (e.g., high silica) compositions in the necks. In the model of Schmidt et al. (2016), similar xenocrysts are absent in the Rio Puerco basalts because the deep crustal reservoir (sill) that resulted in gabbroic cumulates of plagioclase and pyroxene beneath Mesa Chivato never developed in the northeastern part of the field.

Compositionally, the Rio Puerco necks include basanitic/trachybasaltic compositions similar to the basaltic lavas of Mesa Chivato. While gabbroic megacrysts like that seen in the late lava flows on Mesa Chivato are generally absent, there is a notable abundance of mantle peridotite xenoliths and rare gneissic crustal xenoliths. Pyroxenite and lherzolite xenoliths are the most common types in basalts of the volcanic necks.

Eruptions responsible for the necks range in age from 3.36±0.06 Ma to 2.56±0.02 Ma (Hallett et al., 1997; Perkins et al., 2006; Porreca et al., 2006; Crumpler, 2010b), essentially contemporaneous with the volcanism in Mesa Chivato and highlighting the fact that it is part of the Mount Taylor volcanic field. The Rio Puerco volcanic necks have been the site of numerous geochemical studies, and the petrology and geochemistry of the necks and the mantle xenoliths associated with them is relatively well studied (Brunton, 1952; Brown, 1969; Kudo et al., 1971; Wilshire et al., 1988; Hallet, 1994; Hallett et al., 1997; Porreca et al., 2006; Schmidt et al., 2016).

Ironically, despite the fact that the Rio Puerco volcanic

necks are among the best exposed and most concentrated examples of shallow volcanic structure in the world, the structure and details of their origin revealed by these unusual exposures have been relatively unexplored, except for studies by Hallett (1992) and Hallett et al. (1997). The imposing and monolithic appearance of many of the necks is deceptive, as a significant number consist of various tuff-breccias, scoria, dikes, and lava ponds. In short, the Rio Puerco volcanic necks are not simple intrusions; they are instead a result of in-filling of the middle-lower part of volcanic craters. This in-filling consists of recycled pyroclastic materials, lava ponds, and shallow intrusions of magma, the latter occurring either lower in the necks or as through-going, vertical dikes (Hallett, 1992; Hallett et al., 1997). Relatively symmetrical volcanic plugs that result from infilling of most of the conduit by magma, which then slowly solidifies, is less common, but ironically it includes the most prominent volcanic neck—Cabezon Peak.

Based on an inventory of the structures and lithologies observed within the Rio Puerco necks, a basic summary of the origin of the volcanic necks is shown in Figure 2.36. A large fraction of the necks are a combination of several variations that include (1) massive lava ponds, (2) scoria cone crater fill lavas and breccias, and (3) tuff-breccia crater fills.

Understanding the structure is useful because it means one can potentially determine if the observed structures developed within or immediately beneath the paleogeomorphic vents, and the necks may therefore be used to approximate the height of the paleoground surface (Hallett, 1994). The principal difficulty with this assumption is determining the paleodepth that each neck represents, which is dependent on the morphometric context of the crater. Are they crater fills largely formed within a volcanic cone rising above the level of the paleosurface? Or are they shallow (100–200 m deep) conduit and explosive craters, like maars, and therefore represent masses emplaced below the original ground surface? Estimates of the paleosurface therefore are subject to 100–200 m errors within our current understanding of what depth within small volcanic vents the necks are actually preserving.

Many of the necks are elongated along the strike of regional faulting (northeast) throughout the Rio Puerco area, as are several exposed dikes, two of which are crossed in this road log (Fig. 2.37). As a result, some of the necks may represent the interior of former fissure line eruptions or may be a collection of several overlapping, nearly-aligned eruption centers, which further complicates their interpretation. *0.2*

0.2 Intersection with dirt road. The right road goes back to State Road 279. The gated left road leads to the ghost town of Cabezon, which is on private property and now the site of a ranch headquarters. Cabezon has long been rated as one of the best ghost towns of New Mexico, having 15–20 abandoned buildings (as of the 1970s) and the dramatic backdrop of Cabezon Peak to the east (Sherman and Sherman, 1975; Varney, 1981). But vandalism has been a problem since it was abandoned in the early 1950s (e.g., García, 1987), and for many decades the private property of the town has been officially off-limits and posted against trespassing (Varney, 1981). During its heyday (1870–1920s), this town was the largest of the four communities mentioned earlier (with San Luis, Guadalupe, and Casa Salazar). The community was originally called La Posta and in its early days was an important station on the stagecoach route between Santa Fe and Fort Wingate (Varney, 1981). The town's name changed to Cabezon when the post office began operations in 1891, and by 1915, the town boasted as many as four saloons, a few general stores, dance halls, a blacksmith shop, and a population of 375 (Widdison, 1959; Sherman and Sherman, 1975; Varney, 1981). A leading citizen of Cabezon was Richard Heller, who lived in a large (11-room) house in town and at one time owned as many as 10,000 sheep and 2,000 cattle (Sherman and Sherman, 1975). "Ricardo" Heller and his wife were well liked by the local, pre-

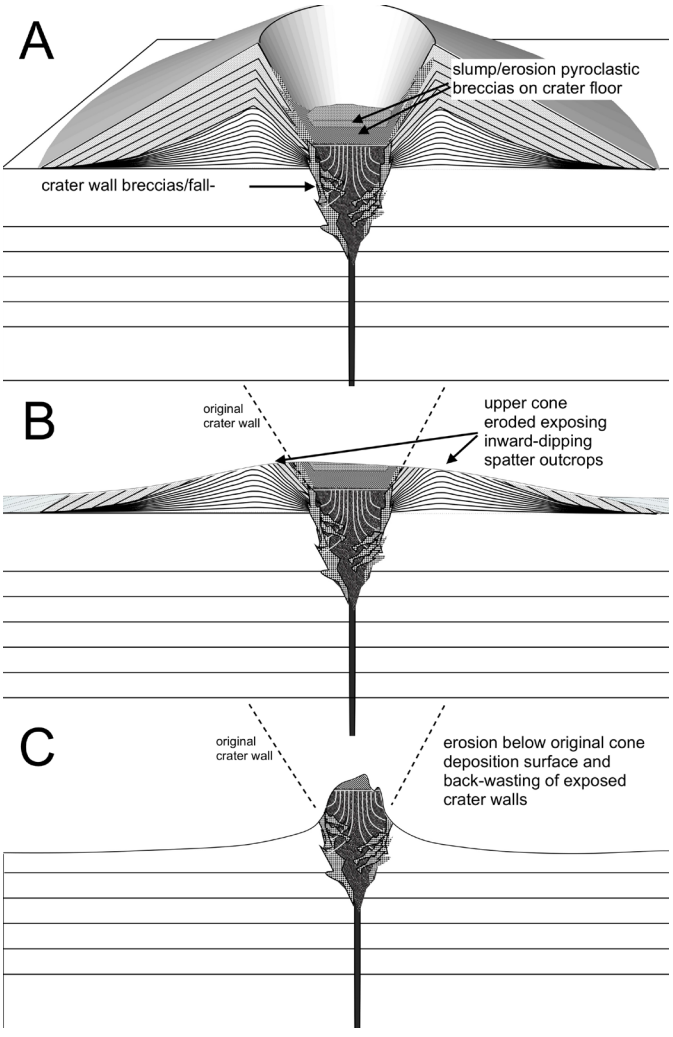

FIGURE 2.36. Relationship between the original cone and the current exposures in the volcanic necks of the Rio Puerco, based on observed necks around Mesa Chivato that are in proximity to their associated surface edifices. (A) Model of typical scoria cone with interior lava ponding at the vent. The height of the lava pond surface varies by tens of meters. The funnel narrows to the feeding dike at variable depths (~50–100 m), as observed around Mesa Chivato. (B) State of erosion in scoria cones of ages equivalent to the Rio Puerco necks on the surrounding mesa tops. (C) Volcanic necks are the remains of the massive "cores" of small volcanic vents. Where observed on Mesa Chivato and Mesa Prieta, the main mass of the neck is near the level of the surface that existed at the time of eruption.

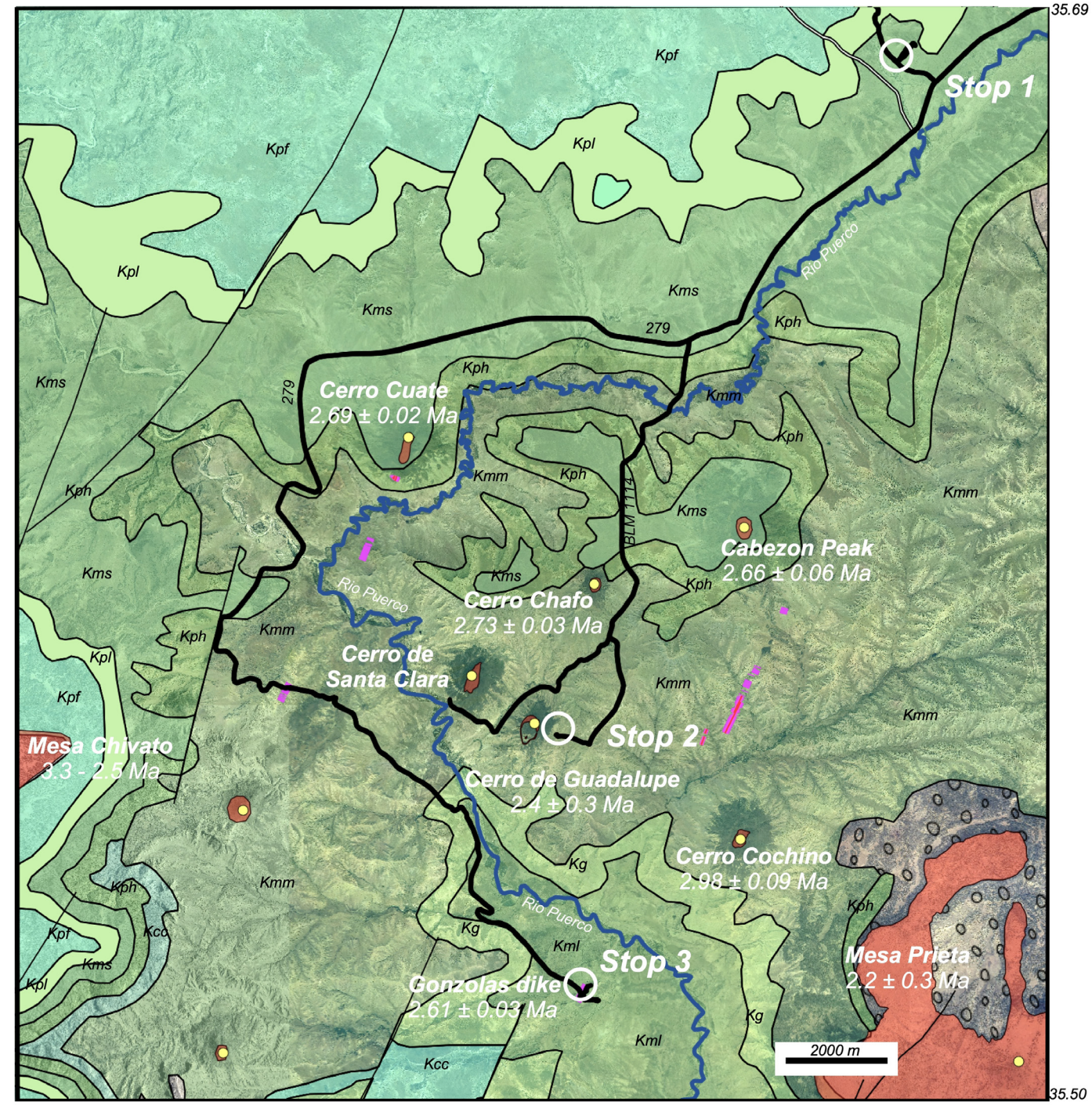

FIGURE 2.37. Map showing the Second-Day route and stops in the Rio Puerco Valley and their relation to Mesozoic stratigraphy. The geologic setting and ages of the six volcanic necks in the vicinity of Cabezon Peak along the route to Stops 2 and 3 are also shown. Geologic map base is from New Mexico Bureau of Geology and Mineral Resources (2003). Kpf = Menefee Fm; Kpl = Point Lookout Fm; Kms = Satan Tongue of the Mancos Shale; Kph = Dalton-Hosta sandstone tongue (see text); Kmm = Mulatto Tongue of the Mancos Shale; Kg = Gallup Sandstone; Kml = lower Mancos Shale. Quaternary sedimentary deposits not shown. Yellow dots are inferred vent center locations. Pink lines are basaltic dikes.

dominately Hispanic populace because of their generosity and helpfulness (Sherman and Sherman, 1975). For example, Heller provided much-appreciated economic opportunities to Nasario García's grandfather (García, 1994). The town's population steadily dwindled between WWI and the 1950s due to (1) transportation and related commerce becoming increasingly concentrated along what is now U.S. Route 550 and Interstate 40 (Widdison, 1959; Sherman and Sherman, 1975), (2) the difficulty of maintaining dam and related irrigation infrastructure as the Rio Puerco progressively deepened and widened (Widdison, 1959), (3) a drought in the mid-1930s (García, 1994), and (4) the economic opportunities present in Albuquerque and other towns along the Rio Grande (Widdison, 1959; García, 1994). *0.2*

FIGURE 2.38. View of the upper Holocene deposits comprising the northern bank of the Rio Puerco at the Rio Puerco crossing of BLM Road 1114. Sandy sediment is yellowish, and clayey fine sand is dark brown. Beds are generally tabular. Note the paleochannel developed on top of the clayey interval to the left, which was completely filled by the lower part of the upper sandy unit. The black arrow denotes the level of the main valley floor, which is ~30 ft (~10 m) above the bottom of the arroyo. The upper surface (tread) of a lower gravelly terrace deposit (light gray arrow) is 25 ft (8 m) above the main valley floor, and the tread of an upper gravelly terrace (dark gray arrow) is ~90–100 ft (27–30 m) above. Note the cementation seen in the upper terrace, which likely correlates to the Rito Leche terrace of Bryan and McCann (1936).

0.4 Road descends southward toward the Rio Puerco arroyo. On either side of the road are scattered exposures of a laterally extensive, nearshore sandstone located ~500 ft (~155 m) above the Gallup Sandstone and ~310 ft (~95 m) below the base of the Point Lookout Sandstone (Fig. 2.17). Here and in the next 2 mi, we see exposures illustrating an upward-increasing proportion of sandstones (relative to mudstones) in the unit we informally call the Dalton-Hosta tongue (see Stop 1 text; Fig. 2.17). About 25 mi (40 km) to the south (landward in the Late Cretaceous), the uppermost beds of the Hosta Tongue, which clearly overlie terrestrial sediment of the Gibson Coal Member (Crevasse Canyon Formation), yield Santonian selachian fauna (Bourdon et al., 2011). However, terrestrial sediment does not overlie nor underlie this sandstone tongue near Cabezon. *0.2*

0.6 At 9:00, the towering Cabezon Peak commands the horizon on the left and lies above a sandstone ledge likely correlative to the Point Lookout Sandstone. Below the Point Lookout are exposures of the Satan Tongue of the Mancos Shale, which overlie the Dalton-Hosta sandstone tongue. *0.1*

0.7 Ridge to right is capped by a cemented terrace deposit (Fig. 2.38) that is 90–100 ft (27–30 m) above the unincised parts of the valley floor alluvium and correlated to the Rito Leche terrace of Bryan and McCann (1936). Road is on the lowest Rio Puerco gravel terrace level; its tread is ~25 ft (~8 m) above the main unincised valley floor. *0.2*

0.9 Road bends left and crosses the well-vegetated, inner arroyo of the Rio Puerco (Figs. 2.38, 2.39). *0.2*

1.1 On left (9:00) is a 40-ft-tall (12 m) bluff capped by the Dalton-Hosta sandstone tongue; note the upward increase in the proportion of sandstone beds in the Dalton-Hosta sandstone, which can be interpreted as Cretaceous water depth decreasing up-section. *0.1*

FIGURE 2.39. Soil piping erosion occurring on the southwest bank of the Rio Puerco near the BLM Road 1114 bridge crossing. This is an important geomorphic process for widening of steep-walled arroyos in Holocene sediment; it is discussed further at Optional Stop 1. The arroyo floor of the Rio Puerco is well vegetated here and elsewhere in the middle Rio Puerco Valley, reflecting the lack of scouring floods over the past few decades.

1.2 Road bends left and crosses cattleguard. *0.5*

1.7 Drive southward up a small canyon flanked on either side by bluffs where Dalton-Hosta sandstone is underlain by yellowish Mancos Shale. *0.2*

1.9 Ascend onto mesa underlain by a 3–6-ft-thick (1–2 m) cemented sandstone (part of the Dalton-Hosta tongue). Turn left and follow the wide, graded dirt road. Volcanic necks to the south and southwest include Cerro Chapo with Cerro de Guadalupe behind it (1:00), Cerro de Santa Clara (2:00), and Cerro Cuate (4:00). *0.5*

2.4 Cross cattle guard. *0.1*

2.5 The behemoth of Cabezon Peak rises dramatically at 9:00 (Fig. 2.40). Cabezon Peak (2.66±0.06 Ma; Hallet et al., 1997) is the largest and most visually impressive volcanic neck in the Rio Puerco Valley. Despite its size, the neck is relatively simple in structure and lithology compared to many others in the valley, most of which are geometrically complex pyroclastic and breccia masses intruded by thin dikes and sheets of basalt. Petrographically, the main mass of Cabezon Peak, like most of the dense basalts in the other necks of the Rio Puerco Valley, consists of trachybasalt largely devoid of vesicles and contains almost no phenocrysts of note.

The view of this peak from the west (Fig. 2.40) is dominated by the 500-m-diameter, 240-m-high, largely cylindrical mass of mostly vertically oriented columnar basalt that makes up the bulk of the volcanic neck. Near the base, columns rotate outward 30–45° (Hallet, 1994). Since the fractures defining columns propagate perpendicularly to isotherm in the cooling mass and away from the nearest cooling interface (e.g., Spry, 1962; Ryan and Sammis, 1978), heat loss in the observed mass of the neck must have been mostly vertically orientated (i.e., toward the surface). Outward orientation of columns near the base of the peak, on the other hand, implies that the cooling gradient in the now mostly eroded periphery of the plug was controlled more by the enclosing margins of the pond. Additional complications in history, convection, and irregularities in input to the pond would locally alter these controls. But the roughly cylindrical geometry of the basaltic mass and loss of heat to the sides and bottom of the original crater and feeding conduit is responsible for the commonly observed patterns of columns in well-known intrusive plugs.

At the top of the massive basalt, the gently rounded summit consist of reddish-oxidized basaltic scoria and breccias capping the upper part of the basaltic neck. The presence of basaltic scoria is interpreted to represent the remains of a basaltic scoria cone associated with the original emplacement of the neck as a whole. Similar upward-trending basalt to pyroclastic scoria sequences occur in other volcanic necks throughout the valley and support the concept that the volcanic necks represent the near surface interiors of small volcanoes.

The original geometry of the basalt mass, however, is somewhat less constrained. Based on some of the characteristics outlined above, the so-called "plugs" of volcanic necks like that of Cabezon are generally interpreted as being the interior of a monogenetic scoria cone, representing a former crater-filling lava pond and associated feeder dikes rather than a large intrusive mass. This means that volcanic necks are the very-near surface interior of small scoria cones and related phreatomagmatic (tuff cone/maar) eruptions and represent the interior volcanic structure within ~600 ft (~200 m) of the surface. The necks are resistant to erosion because lava ponds, near-vent spatter, and welded agglomerate filling small summit craters in each case has left a resistant, very welded mass at the core of the former cone. This mass of basalt and breccias remains after erosion of the surrounding, more loosely lithified scoria-dominated cone and underlying Cretaceous sedimentary rocks.

The large diameter of Cabezon poses some problems to this simple model. If the cylindrical mass of basalt at Cabezon represents a former lava pond, it is somewhat large for the interior of typical scoria cones. Lava ponds of this size are more common in the large, platform-style vent complexes of large flow fields rather than scoria cones. Examples of vents of this type in New Mexico include the Jornada del Muerto and McCartys lava flow fields. In both of these examples, small, late-stage scoria cones rest on the surfaces of inflated, presumably thick platforms composed of basalt. So the summit pyroclastic breccias could represent the remains of a late scoria cone resting on the mass of the pond. In this interpretation, Cabezon might represent the former vent for a large-volume flow field instead of a small pyroclastic cone; the capping scoria in this interpretation would be from a late scoria cone formed during waning stages of the eruption. Alternatively, Hallet (1994) suggested that rates of magma input may play a role in defining the difference between the massive basaltic plugs and those dominated by pyroclastic breccias. Slower arrival of magma at the vent would enable more interaction with groundwater and corresponding explosive phreatomagmatic activity. Higher volume rates would restrict the interaction with water-saturated country rock and yield more massive basaltic intrusions. Given the elevated position of the original vent for Cabezon relative to many of the necks farther west, it may also have been above the saturated water table at the time of the eruption. *0.3*

FIGURE 2.40. Cabezon Peak, view from the west. From this perspective, columnar jointing is mostly vertical and locally can be seen to have rotated outward closer to the base, where scree covers the contact with the underlying sandstone. The slightly rounded and smoother cap on the summit consists of reddish scoria.

Waypoint 9 [35.595649°, -107.121848°]

2.8 Intersection with road heading east to the Cabezon Peak parking lot. Continue straight on BLM Road 1114. Nice view of Cerro Chafo at 2:00. Cerro Chafo (2.73 Ma) is an instructive contrast with Cabezon and is a somewhat unusual volcanic neck, consisting mostly of inward-dipping tuff breccias instead of the massive basaltic cap at Cabezon and some of the other local volcanic necks (Fig. 2.41A). Differential erosion along the inward-dipping structure at Cerro Chafo has etched out a concave-up summit that opens southward. Cerro Chafo has the structure and lithology typical of a deeply eroded phreatomagmatic explosion center and is either the near-surface (<100–200 m depth) interior of a maar (Aubele et al., 1976; Fig. 2.41B) or a partly eroded tuff cone (Hallet, 1994; Fig. 2.41C). The interpretation as a deeply eroded former maar (i.e., a diatreme) is based on the fact that a large fraction of the outcrops consist of non-juvenile, fragmented material in which outcrops are a complex mixture of accidental blocks of underlying sandstone and shale, scoriaceous agglomerate with welded sandy matrix, and greenish-gray ash and cemented tuffs. Many of these characteristics are similar to the deep interiors of maars exposed elsewhere in New Mexico (Aubele et al., 1976). The alternative interpretation that Cerro Chafo is a partly eroded tuff cone (Fig. 2.41C) is based on the assumption that there has been very little erosion and that the topographic bench of the Dalton-Hosta Tongue that Cerro Chafo currently rests on was present at the time of eruption. The structure shown in Figure 2.41 is speculative, and the disparity in the two interpretations means that the original depth below the surface of the currently observed exposures at the time of eruption cannot be confirmed. But Cerro Chafo should be considered as the inward-funneling of breccias that accumulated in the lower section of a crater, extending from 300 to 1000 ft (100 to 300 m) depth, that formed primarily by maar-like to tuff-cone explosive activity.

Regardless of original style of eruption, the outcrops are an interesting study in the complexity of phreatomagmatic eruptions. At least one block of Mancos Shale, resting within comminuted basaltic lapilli and sandy fines, was heated in the vent to such an extent that when subsequently chilled around the margin, it developed radial columnar mini-joints. Many of the volcanic necks preserve outcrops in their lower sections of similar phreatic pyroclastic sequences, implying that phreatomagmatic explosive eruptions were common in the opening phases of eruptions at most of the volcanic necks. This is evidence that the local rocks were fairly saturated in groundwater at the time of the eruptions.

Estimates of the depth of the necks below the original ground surface at the time of the eruptions are important because they permit estimates of the timing of erosional surfaces, paleorelief, and drainages that are useful for establishing landscape evolution during the late Cenozoic. Based on the interpretation of the elevations of paleotopographic surface on which these volcanic centers originally erupted, considerable relief existed across the current valley at the time of eruptions, ca. 3.5–2.5 Ma (Hallet, 1994). If so, substantial groundwater would have been present in the paleovalley floor at that time, resulting in water-magma interactions and explosive eruptions of the type that formed Cerro Chafo.

Just beyond the intersection with the side road to Cabezon, the road descends into a south-draining canyon. Just below the mesa top is a 15-ft-thick (4–5 m) sequence of yellowish sandstone comprising thin to medium (minor thick), tabular beds correlated to the Dalton-Hosta sandstone tongue. Note the upward increase in the proportion of sandstone beds. *0.4*

3.2 To left are recently incised gullies on the floor of the unnamed, south-draining canyon. *0.1*

3.3 Road bends right. View to southwest of Cerro de Guadalupe. *0.3*

3.6 Note the lack of a gully on the valley floor here. Instead, this area of the valley is occupied by a low-relief, elongated, relatively recent alluvial fan at the lower end of the aforementioned canyon-floor gully. Ongoing erosion of the gully supplies the sediment for recent aggradation of this alluvial fan. *0.3*

3.9 Mancos Shale outcrop to right, containing notable sandstone beds. These strata are locally folded and deformed. *0.1*

4.0 Road makes a left jog. Mancos Shale exposed in right (west) roadcut. *0.1*

Waypoint 10 [35.579520°, -107.124135°]

4.1 Road intersection. Take the left fork, following BLM Road 1114. *0.1*

4.2 Excavated cattle tank to right on the floor of the valley. *0.4*

4.6 Cross low ridge underlain by Mancos Shale. *0.1*

4.7 Ascend onto broad ridge; road bends right. *0.5*

5.2 Good view to left (southeast) of Cerro Cochino. *0.4*

5.6 Road turns sharply left (southeast) at a road intersection. Turn right on the less-defined dirt road that travels west on the broad ridge. *0.4*

Waypoint 11 [35.560737°, -107.127888°]

6.0 Road turns slightly right and ends near the eastern foot of Cerro de Guadalupe. *0.7*

STOP 2. Cerro de Guadalupe and lunch stop.

Waypoint 12 [35.562264°, -107.34991°]

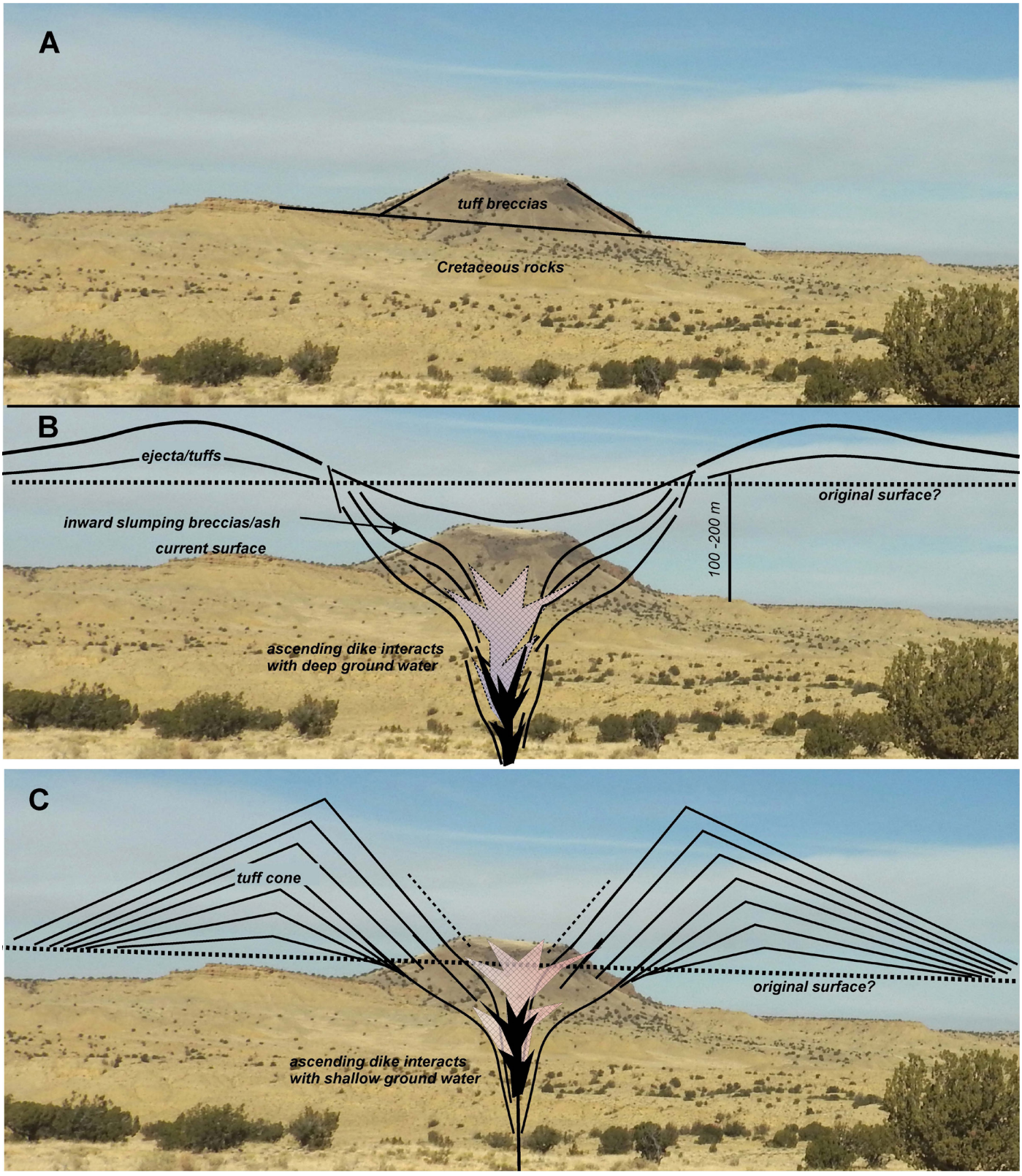

FIGURE 2.41. (A) Cerro Chafo, as viewed from the south (looking north) from Stop 2. The exterior slopes are defined by inward-dipping, coarse tuff breccias. (B, C) Speculative section showing former structure and crater-like form of tuff breccias; two models for the location of the original ground surface at the time of eruption. (B) This interpretation assumes that Cerro Chafo is the internal breccia mass associated with a maar-type eruption. The surface at the time of eruption could have been as much as 200 m above the current general land surface, although this estimate is poorly constrained and the depth could be greater. (C) This interpretation assumes that Cerro Chafo is the remains of a former phreatomagmatic tuff cone, a morphology in which the cone rests directly on the surface existing at the time of the eruption. If it were a tuff cone, then the surface at the time of eruption would be closer to the current surface.

Park at the end of the road near the eastern foot of the towering Cerro de Guadalupe. At this location, we will have an opportunity to examine one of the more challenging volcanic necks to interpret due to the complexity of its dikes, breccias, and phreatomagmatic tuffs.

Cerro de Guadalupe is one of the more complex volcanic necks and illustrates the fact that not all volcanic necks are simple "plugs" of basalt. Multiple generations of basaltic intrusions, including basalt conduit wall sheets, and scoriaceous breccias form shell-like marginal walls around the exterior of the main upright mass (Fig. 2.42). Basalt conduit wall sheets (Fig. 2.42A) refer to basalt that has either intruded along the periphery of the conduit or to basalt that originally filled the conduit and remains following the emplacement of later materials (like the tuff breccias).

Additional parts of the story are in the slopes on the south side, where a few exposures consist of phreatomagmatic tuff breccias (Fig. 2.42B) locally overlain or intruded by basalt. The most unusual characteristic on the south side is an arcuate dike intruding Cretaceous sediments and enclosing phreatomagmatic tuff breccias, arcing 360 m out to the south and back (Fig. 2.43).

The basalt of Cerro Guadalupe is a dense, dark, aphyric trachybasalt frequently characterized by an unusual spotted appearance on weathered surfaces (Fig. 2.44), a characteristic seen in many of the lavas around the Mount Taylor field and in nearby volcanic fields and volcanic necks. Float in the colluvium on the east side of the lower colluvial slopes offers an opportunity to search for small (1–2 cm) peridotite mantle xenoliths. These include Cr-diopside peridotites, lherzolite, websterites, pyroxenites, and wehrlite. Pyroxenites are mostly composed of clinopyroxene, lessor orthopyroxene, and olivine, although the latter is mostly absent in individual samples. Where lherzolite and pyroxenite are in contact, the cross-cutting relations almost always imply that the pyroxenite postdates the lherzolite. At least one study (Porreca et al., 2006) suggested that the pyroxenite originated by metasomatic alteration of lherzolite to pyroxene under the influence of carbonatite melt metasomatism.

From this stop, Mesa Prieta dominates the eastern skyline. There are two volcanic necks in that direction: Cerro Cochino (2.98±0.09 Ma; Hallet et al., 1997) on the left and Cerrito Cochino in the distance on the right. Mesa Prieta stands approximately 400 m above the surrounding surfaces and extends 12 mi (20 km) from north to south. The surface on top of the basalts drops 200 m in elevation southward and may represent a paleovalley at the time of eruption of the lavas now capping it (e.g., Bryan and McCann, 1936). If so, the paleovalley appears to have been relatively high in the landscape and perhaps not fully graded to the main valley, an inference based on the young ages of the capping lavas and their height above the majority of older necks (Hallett, 1994), in addition to apparent lack of river gravel on the western slopes of the mesa.

There are two volcanic flows capping the mesa. The source vent for the upper flow (west side of mesa) is a low scoria and lava cone near the north end, whereas the source for the lower flow (east side of mesa) is less clear. A 0.6-mi-diameter (1 km) crater with a low rim and local elevated accumulations of basalt, which may represent former vents, is present in the middle of the mesa along its western margin (Fig. 2.45).The crater is possibly a maar, based on accidental clasts of sedimentary rocks on its west margin. It could also be a simple late explosive crater associated with a short fissure, which was further widened by backwasting of what would have been originally steep crater walls. Several prominent northeast-trending faultline scarps, up to 85 ft (25 m) tall, offset the mesa-capping lava flows.

The upper lava flow was dated at 2.05±013 Ma and 2.36±0.30 Ma by Hallet et al. (1997). The lower lava flow was dated at possibly 2.2±0.03 Ma by Armstrong et al. (1976). These dates mean that Mesa Prieta eruptions were somewhat younger than most of the eruptions responsible for the Rio Puerco volcanic necks, an important observation that needs to be taken into account when attempting to reconstruct the paleolandscape. The upper of the two flows capping Mesa Prieta is also distinctly different from the basalts of the volcanic necks and the Mount Taylor field in general, being subalkaline and consisting of plagioclase-phyric texture (Hallet et al., 1997). These characteristics are much more akin to lavas within and marginal to the Rio Grande rift (located to the east) than the high-sodic alkali, dense, generally olivine-phyric lava flows typical throughout most of the Mount Taylor field. The source of the melts responsible for the volcanism of Mesa Prieta therefore appears to be unrelated genetically to the Mount Taylor volcanic field volcanism. Thus, one might infer that lavas on Mesa Prieta may potentially mark a transition in characteristics of eruptions associated with different mantle sources and/or tectonic environments.

Return back to BLM Road 1114. RE-ZERO ODOMETER at road intersection. Turn left and head north, retracing our route.

0.7 Crest low drainage divide. *0.6*

1.3 Descend onto valley floor. Excavated cattle tank on left. *0.1*

1.4 **T-shaped intersection, turn left for Optional Stop 1. (Optional Stop 1 mileages proceed from this intersection.) To continue with the Second-Day Road Log, take a right, and after 4.6 mi return to State Road 279.** *0.3*

Waypoint 10 [35.579520°, -107.124135°]

1.7 Road winds around low hills of Mancos Shale to right (west), which belong to the Mulatto Tongue. *0.2*

1.9 Canyon widens and road makes a rightward jog. Recently incised gully head abuts road on left (southwest). Runoff from the road probably facilitated erosion of this particular gully. *0.1*

2.0 On the right (west), ~15–20-ft-thick (4–6 m) sandstone-rich interval in the Mancos Shale. The

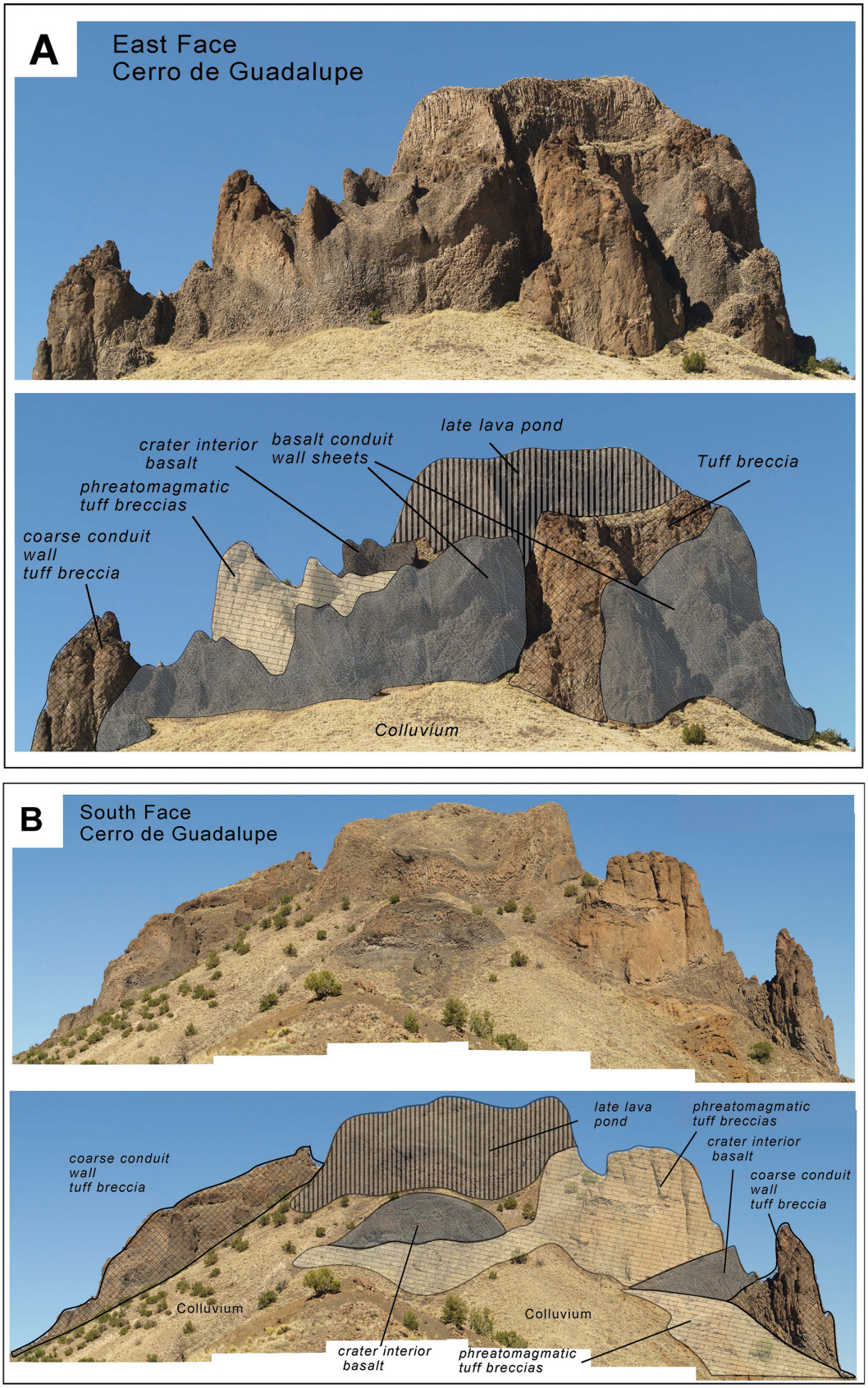

FIGURE 2.42. Views of the eastern and southern faces of Cerro de Guadalupe and corresponding geologic sketch maps. (A) The east face consists of complexly-sheeted, vertical masses of coarse tuff breccias bearing large basaltic pyroclasts, blocks, and bombs and vertically foliated masses of denser basalt. Distinctly horizontal and vertically columnar basalt rests at the summit. (B) The south face exposes an underlying, thick section of phreatomagmatic tuff breccias in the mostly colluvium-covered slopes.

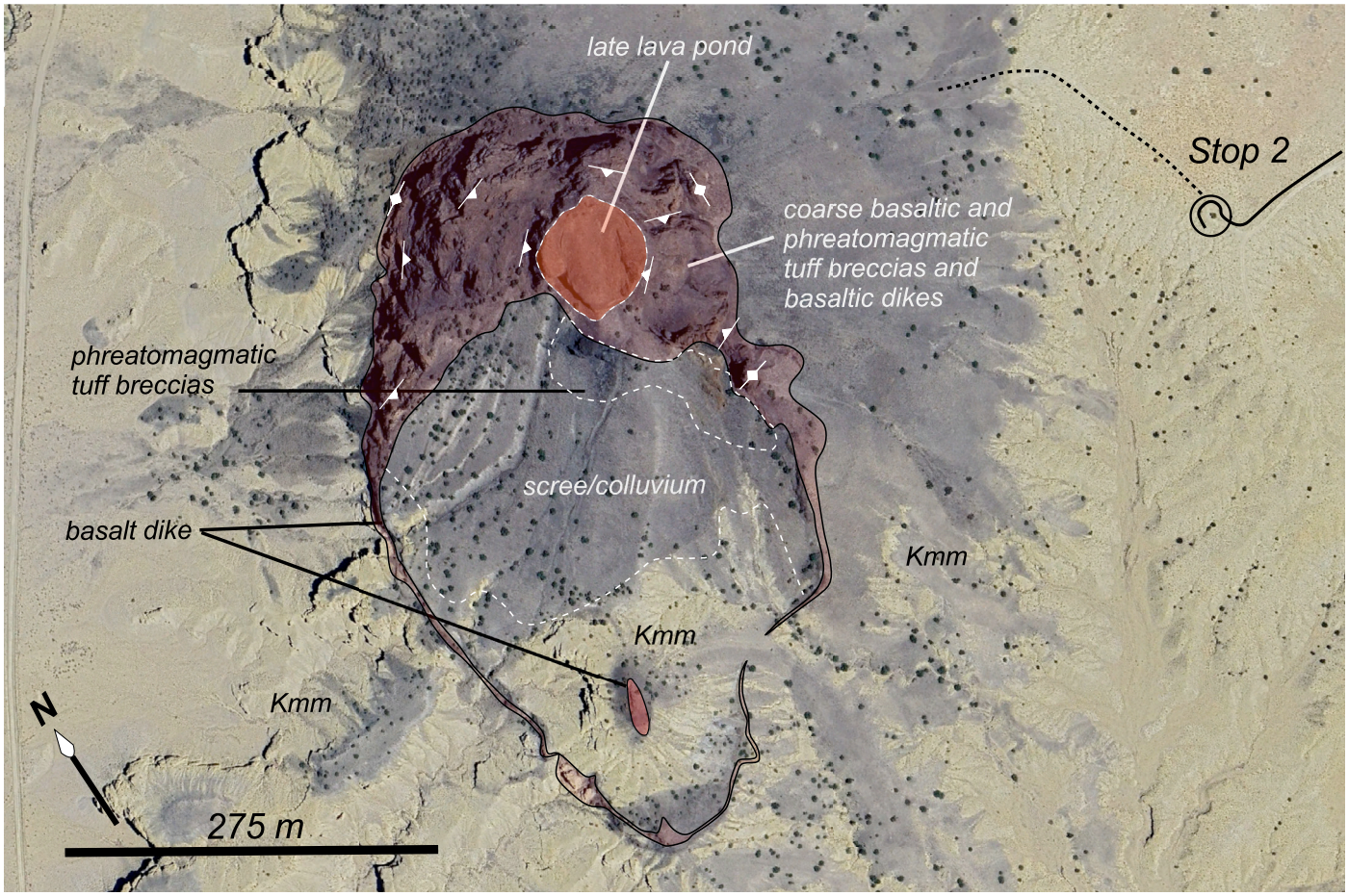

FIGURE 2.43. Geologic sketch map of the principal features of the Cerros de Guadalupe volcanic neck. The summit occupies the northern end of an arcuate dike that locally includes basaltic breccias. Vertical foliations in basalt dikes and basaltic breccia masses form a carapace on the neck's circumference. Inward, there appears to be layering within the basaltic tuff breccias that dips approximately inward toward the center of the summit area. The summit consists of a lava pond with undulating basalt columns. Lower in the south slopes, and presumably lower in the section, extensive fine phreatomagmatic tuffs are more common, suggesting that the earliest eruptive phase was more explosive and that eruptions evolved to more juvenile pyroclastic materials.

FIGURE 2.44. Typical mantle xenoliths in dense, basaltic rock of the Rio Puerco volcanic necks. The dark xenolith is pyroxenite and the lighter colored xenolith is lherzolite. Many xenoliths are rounded, reflecting their rapid transport from the mantle in dikes feeding the volcanic neck. The white spots in this basalt are a surficial weathering phenomena common to many of the sodic-trachybasalts of the Mount Taylor volcanic field.

FIGURE 2.45. Aerial view looking northeast across the southern half of Mesa Prieta at one of two identified vent areas on the mesa, a large 0.6-mi-diameter (1 km) crater near the western margin that has the characteristics of a maar. Note linear, northeast-trending, west-down fault scarps to the right of the crater.

proportion of sandstone beds appears to increase up-section, and the beds are mostly very thin and tabular. This ledge-forming sequence can be followed throughout the upper part of his canyon, about 100 stratigraphic feet (30 m) above a lower sandstone-rich interval observed near Optional Stop 1. (This lower sandstone interval is depicted in Figure 2.46.) *0.2*

2.2 Road jogs left. Good exposure of Mancos Shale on the right. *0.1*

2.3 Road turns left (southeast) and crosses the arroyo incised in the valley floor. *0.1*

2.4 Road makes a 90° bend to west on a wide expanse of middle to late Holocene alluvium. Cerro de Guadalupe rises impressively 0.4 mi to south-southwest. *0.1*

2.5 Exposure of sand-poor Mancos Shale in left road cut. *0.3*

2.8 Road on top of middle-late Holocene alluvium, following the canyon west and southwest as it winds around the north end of Cerro de Guadalupe. Deep arroyo to the right. *0.4*

3.2 Good exposures of Mancos Shale on either side of wide canyon. *0.2*

Waypoint 13 [35.562475°, -107.148000°]

3.4 **Dirt road intersection. Turn right and cross modern gully-bottom arroyo.** To left (east) of road intersection, the Mancos Shale is capped by a ~20-ft-thick (~6 m) interval with abundant sandstone beds (Fig. 2.46). This interval lies about 50 ft (15 m) above the top of the Gallup Sandstone. *0.2*

FIGURE 2.46. A ~20-ft-thick (~6 m) sandstone-rich interval in the yellowish Mulatto Tongue of the Mancos Shale. The basaltic mass of Cerro de Guadalupe rises behind these bluffs. Another sandstone-rich interval (~15–20 ft [4–6 m] thick) occurs 100 ft (30 m) above here (e.g., at mile 2.0 after Stop 2 in this road log). White arrow points to a cemented bed that probably correlates to the cemented sandstone bed noted at mile 3.8. The Mulatto Tongue in the Rio Puerco Valley is overall more sandy than the Satan Tongue.

3.6 Rounded ridges underlain by Mancos Shale at right, capped by a resistant sandstone-rich interval (the same pictured in Fig 2.46). *0.2*

3.8 Ascend topographic saddle, with a flat-topped butte to the southwest. This butte is capped by sandy gravel and sand of a terrace deposit with tread about 60 ft (18 m) above the adjoining valley floor. Beneath the gravel lies 27–30 ft (8–9 m) of interbedded sandstone and mudstone, capped by a 1.5-ft-thick (0.5 m) bed composed of well-cemented, cross-stratified sandstone. Inoceramid shell fragments are found in the lower part of this bed. *0.2*

4.0 Dirt road to right leads to the spring of Ojo de los Jaramillos, which we visit at Optional Stop 1. *0.1*

4.1 Pull over on right side of road for Optional Stop 1. This is the site of a former homestead. Adjacent farmed land and some structural remains are still present but are diminishing year by year. Four decades ago, segments of the whitewashed, interior walls of the residence were present; today little remains of even the foundation. The rectilinear pattern of former tilled rows on the valley floor between the road and the recently incised arroyo of the Rio Puerco (Fig. 2.47) can be identified on Google Earth and other aerial imagery.

OPTIONAL STOP 1. Ojo de Jaramillo Spring, post-1885 Rio Puerco arroyo incision, and exposure of deep vent facies and volcanic neck stratigraphy of Cerro de Santa Clara.

Waypoint 14 [35.566463°, -107.157015°]

This stop has three components. The first observes slow discharge coming from a sandy interval of the Mulatto Tongue (Mancos Shale), a spring known as Ojo de los Jaramillos. The second component is a southwestward view of the Rio Puerco Valley from Ojo de los Jaramillos, which allows discussion of relatively recent geomorphic features and arroyo incision related to this river. The last component focuses on a spectacular exposure on the southern foot of Cerro de Santa Clara, where a buttress contact separates basaltic lava of the neck from yellowish, sandy mudstone of the Mulatto Tongue of the Mancos Shale. Obey all signs posted against trespassing, which mostly apply to private land south-southwest of the road.

Ojo de Jaramillo Spring and the Mulatto Shale aquifer

Walk northeast toward Cerro de Santa Clara, aiming for the end of the dirt road at the foot of the peak. Near the end of the dirt road, stop at a spring catchment box (Fig. 2.49). Note how the water is discharging from the base of a 6-ft-thick (2 m) sandstone-rich interval in the yellowish Mulatto Tongue of the Mancos Shale. The sandstone-rich interval lies roughly 40 ft (12 m) below the cemented sandstone bed described at mile 3.8. Sandstone comprises ~75% of the strata in this interval (the rest being interbedded mudstones) and occurs in tabular-lenticular, laminated to very thin beds. The source of this

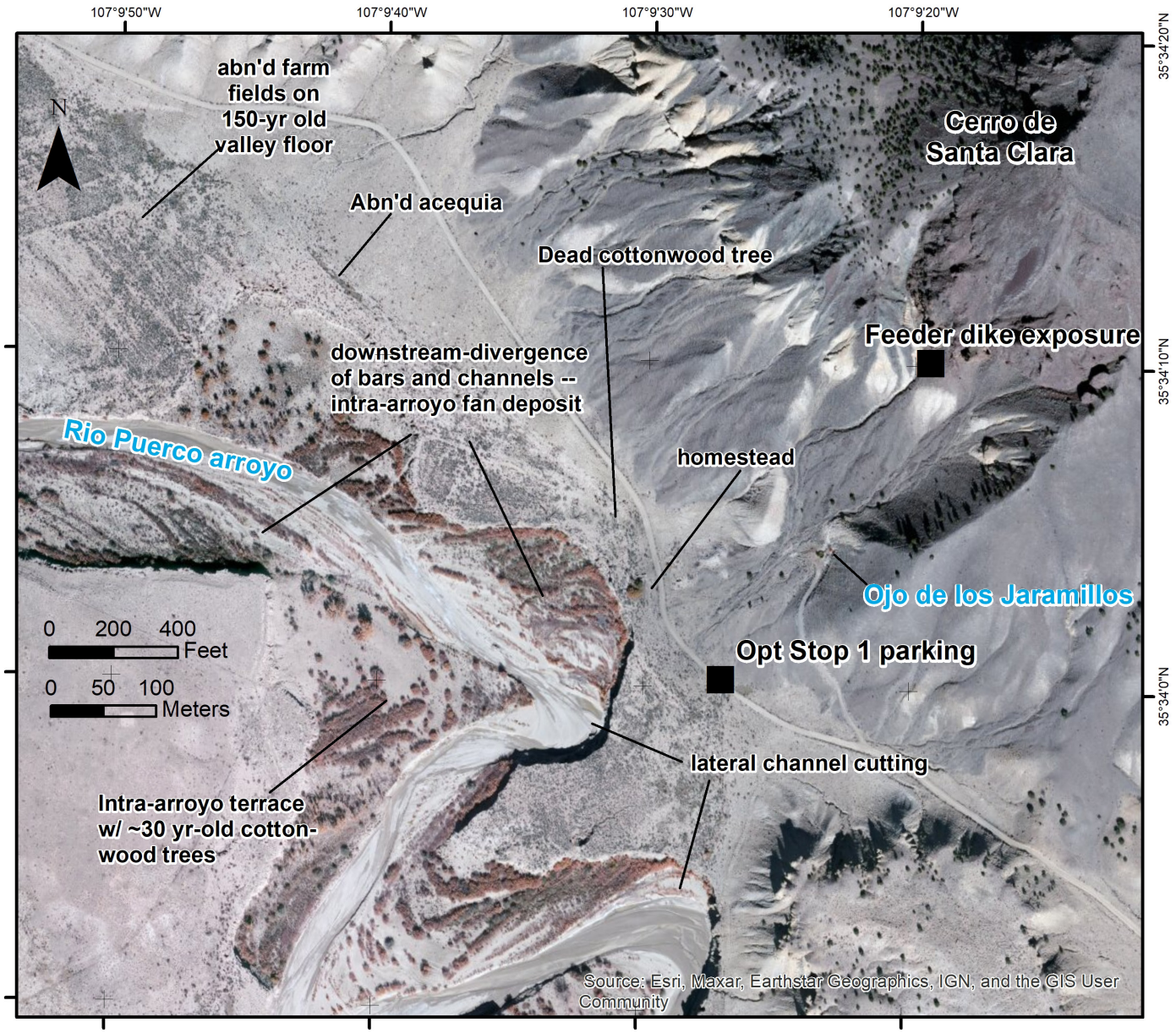

FIGURE 2.47. Geomorphic, geologic, and cultural features near Optional Stop 1. Abn'd = abandoned.

water is not known, but given its relatively high topographic position relative to the surrounding Mancos landscape, one wonders if groundwater could be upwelling along fractures in the feeder dike of Cerro de Santa Clara or possibly from recharge in the volcanic neck itself.

Post-1885 incision of the Rio Puerco arroyo

From the spring, we have a good view of the incised, meandering Rio Puerco arroyo to the south (Fig. 2.49), which is ~30 ft (~10 m) deep here. Locally on the outer part of meander bends, note how modern stream flow promotes undercutting and bank collapse of the arroyo sidewalls (labeled "lateral channel cutting" on Fig. 2.47). Another way the bank is eroding here is through soil piping (Fig. 2.50). This geomorphic process occurs in many types of surficial sediments, but in central New Mexico, piping is common in silty-clayey sand interbedded with sandy, sodium-rich clays. The clays give the sidewalls cohesion and allow vertical arroyo faces to be maintained. Expansive (commonly smectitic) clays commonly form cracks in the near-surface sediment that initiate the piping process, and the presence of nearby, deep arroyos creates the hydraulic head necessary for piping. Surface water enters the cracks during storm events, through infiltration or directly from sheetflooding, and once in these cracks, it erodes sediment and forms subsurface channels (pipes) before draining out of the pipes into an adjoining, incised arroyo. These pipes further erode and enlarge with subsequent storm-related runoff events. Pipes can be seen elsewhere on this trip where the road log crosses the Rio Puerco, but here they are on private property. References regarding soil piping include Parker (1964), Heede (1971), Masannat (1980), and Parker et al. (1990). Wells et al. (1983) summarized conditions favorable for piping, compared this

FIGURE 2.48. Adobe wall remains of a former homestead at Optional Stop 1 (as it looked ca. 2012). Although there may have been local (discontinuous) arroyos along the Rio Puerco Valley in the mid 19th century, a continuous, deeply incised (20–30 ft, 6–10 m) and wide arroyo (several hundred feet, a few hundred meters) like that seen in this photograph was formed between 1885 and ~1940. This arroyo incision resulted in eventual destruction of diversion dams and subsequent abandonment of the acequia systems critical for farming; presumably it also lowered the groundwater table. These adverse consequences of incision spelled the end of irrigation farming in the Guadalupe area by the mid-1930s. Today, the walls of the homestead are almost entirely gone. Four decades ago, a small dwelling was still present. The north end of Mesa Chivato comprises the left skyline, with the small peak to the right known as Bear Mouth.

process to lateral cutting of the Rio Puerco near State Highway 6, and concluded that piping is just as important as lateral channel cutting for widening of incised arroyos.

One cannot help but be impressed by the size and depth of the modern Rio Puerco arroyo, which is continuous from Cuba to the river's intersection with the Rio Grande at Bernardo. It is even more impressive in light of the fact that this incision largely occurred between 1885 and the mid-20th century (Bryan, 1928; Aby et al., 2024). In the decades prior to 1885, arroyo incision by the main river was not continuous nor generally as deep as today. Deep gullying of the valley floor by the main river occurred locally (e.g., a 20–30-ft-deep [6–10 m], 100-ft-wide [30 m] gully was noted in the Simpson expedition 5 mi [8 km] north of Cabezon). But it is certain that a continuously entrenched arroyo comparable in dimensions to the modern did not exist. In many places, the main channel was relatively shallow and the valley floor was subjected to widespread flooding. Such a "spillover" near Casa Salazar, located 5–6 mi (8–10 km) southeast, was a favored place for past residents to gather driftwood (firewood) after large floods (García, 1987, pp. 81–82). Accounts from settlers in Cabezon and Guadalupe

FIGURE 2.49. Catchment box for the Ojo de los Jaramillos spring, with the Rio Puerco arroyo behind. View to southwest.

FIGURE 2.50. Soil pipe extending >2 m^3. Foot for scale.

state that between 1870 and 1885, the river was easily crossed by small bridges (<8 ft [<2.4 m] long) and river water could be diverted into a ditch by felling of a single cottonwood tree (Bryan, 1928; Aby et al., 2024).

Bryan (1928) constrained the initiation of rapid Rio Puerco arroyo incision to between 1885 and 1890 and compiled depth and width measurements of the arroyo at various localities. This timing of this incision compares well with the initiation of

major arroyo incision across the American Southwest from the 1880s through 1910 (Aby, 2017). Presently, the arroyo is about 30 ft (10 m) deep, and its width is highly variable. At a location 1.5 mi (2.3 km) upstream of here (to the northwest), currently the arroyo width is 600–1000 ft (180–300 m). This location approximately corresponds with the northern boundary of the former Ignacio Chavez land grant, where Bryan (1928) documented changes in the depth/width of the Rio Puerco arroyo versus time (time given in calendar years in parentheses): 8 ft/175 ft (1879), 30 ft/735 ft (1910), and 30 ft/240 ft (1927). Note that the apparent narrowing of the arroyo between 1910 and 1927 is probably due to slightly different measurement locations and the spatially variable width of the arroyo. Consistent with other data in Bryan (1928), rapid incision of the Rio Puerco in the field trip area occurred between the years 1885 and 1915 to depths similar to what we see today.

How arroyos such as the Rio Puerco evolved with time is summarized by Aby et al. (2024) and in a generic model presented in Gellis et al. (2012). The Gellis model (Fig. 2.51) predicts initial rapid and narrow incision, followed by steady widening of the arroyo during a stable base level that then slowly rises. The data compiled by Bryan (1928) supports rapid initial incision. We can see that the Rio Puerco channel is presently widening, at least locally, and a study of its lower reach indicates upstream progression of arroyo widening and filling (Friedman et al., 2015). That the base level is relatively stable in the field trip area is indicated by a relatively vegetated valley floor and aggradational fluvial geomorphic features such as intra-arroyo, fan-like deposits (Fig. 2.47). In the arroyo, we can also see a 3–6-ft-high (1–2 m) terrace that supports a growth of ~30-year-old cottonwood trees. If the Gellis model (Fig. 2.51) proves correct, widening will extend only partly across the valley floor before the incised arroyo is completely backfilled.

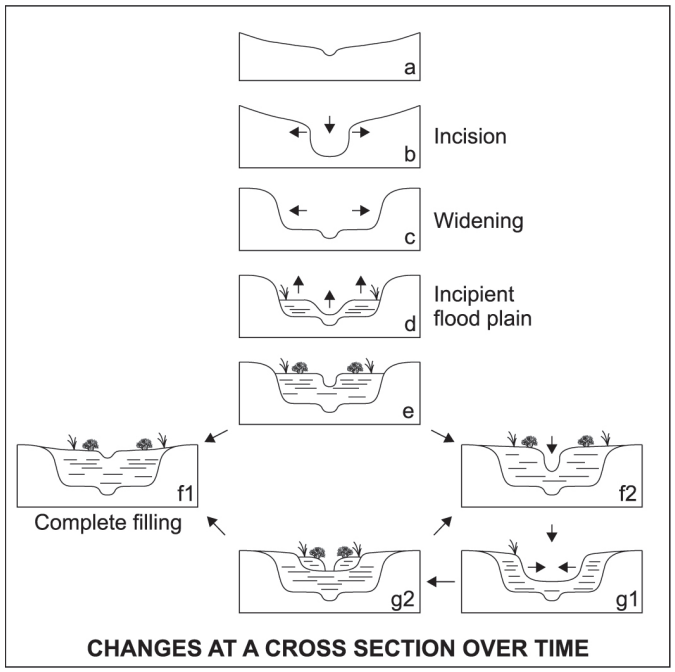

FIGURE 2.51. Stages of arroyo evolution at one place over time: (a) pre-incision; (b) vertical incision; (c) widening through lateral erosion; (d) inner floodplain development; (e) decrease in channel width, inner floodplain stabilization, and aggradation; (f) complete filling of the arroyo channel; and (g) re-incision of the channel. The Rio Puerco arroyo now has a stabilized floodplain and is experiencing aggradation (d and e). Figure, caption, and interpretations are from Gellis et al. (2017).

What initiated major, late-19th- to early-20th-century arroyo incision on the Rio Puerco and other Southwestern arroyos has been a matter of long debate (summarized in Aby, 2017, and references therein). It definitely is a natural process that operated throughout the Holocene, and remnants of former paleoarroyos can be seen in the sidewalls of the modern arroyos (e.g., Stop 3C; Gellis et al., 2012, fig. 1). However, the magnitude and timing of erosion since 1885 may have been influenced by overgrazing (Bryan, 1928; Widdison, 1959) and other anthropogenic activities (such as road and acequia building; see Aby, 2017).

The flat valley floor between the road and the arroyo once hosted farm fields irrigated with water from an extensive acequia system between ca. 1872 and 1936. Water was fed into this acequia from a diversion dam located 2.5 mi (4.0 km) northwest (upstream) of here, 1.5 mi (2.4 km) upstream of the intersection of Arroyo Chico with the Rio Puerco (Widdison, 1959, fig. 17). Remnants of the acequia can still be traced using aerial imagery along the valley-floor terrace on the east and northeast sides of the modern arroyo. In many areas between the acequia and the modern arroyo, striped patterns on the ground surface indicate former agricultural fields (Fig. 2.47). For many decades after the post-1885 incision of the Rio Puerco, Hispanic farmers were able to maintain a dam constructed using pine trees weighed down with large rocks; no cement was used (García, 1992, pp. 25–27). The dam washed out several times and accidently burned another in one instance (García, 1992; Widdison, 1959), but the width and depth of the arroyo was such that it was practical to rebuild the dam. However, a severe flood in 1936 washed away the last dam (Widdison, 1959) and presumably further widened the arroyo. Given that Hispanic farmers were already leaving the area (starting ca. World War I; García, 1994, 2015) due to reasons enumerated above for San Luis and Cabezon (e.g., easier ways to make a living in the Rio Grande valley), there was not the wherewithal to put in the labor to rebuild another, probably larger dam structure. Although the federal government paid $3697 for the materials for a log-and-stone dam near San Luis, they decided not to do the same for the dam serving the Guadalupe area (García, 2015; Widdison, 1959). The farmer's livelihoods were doomed without the irrigation system, as dry farming proved unviable due to the progressive drying of the climate from the mid 1930s through the 1950s (García, 2015).

Volcanic neck stratigraphy of the south face of Cerro de Santa Clara

The south face of the Cerro de Santa Clara neck is wonderfully exposed at this optional stop (Fig. 2.52) and illustrates a fundamental characteristic of the shallow and near-surface emplacement and structure of volcanic necks that is frequently misunderstood—namely that volcanic necks are actually near-surface features rather than deep intrusive "plugs." The

main basaltic mass of Cerro de Santa Clara is 720 ft (220 m) wide and elongated 2100 ft (640 m) along the general northeast-southwest strike of both faulting and dikes elsewhere within the Rio Puerco Valley. Looking north from this stop, a vertical exposure illustrates a dike 60–100 ft (20–30 m) wide cutting through thick, finely comminuted tuff breccias. The dike continues upward to feed a massive cap of basalt responsible for the upper and most visible parts of the volcanic neck.

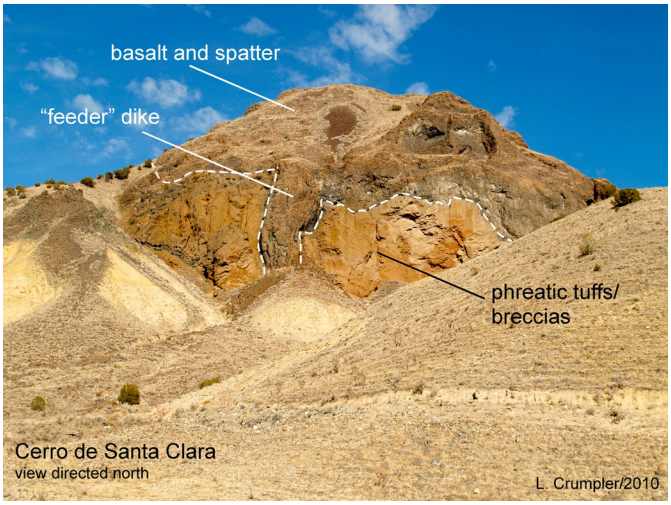

FIGURE 2.52. Natural cross section on the south face of Cerro de Santa Clara. The exposure shows a sequence of early tuff breccias cut by a vertical feeder dike that supplied thick masses of basaltic lava to the surface, most likely along a fissure vent, and associated local lava pond. The view is along the strike of the neck-elongation (N28E) and general trend of faulting and dikes within the Rio Puerco Valley. Fragments of the lava scattered in the alluvium often include small (centimeter-size) ultramafic xenoliths (mostly lherzolites and a few pyroxenites).

FIGURE 2.53. View of Cerro de Guadalupe from the southwest that shows part of the ring dike that forms a semicircle south of the neck (identified by arrows). The dike locally abuts tuff breccias in the slopes proximal to the "plug." These tuff breccias probably filled a former conduit/crater prior to further development of the main center of eruption forming the peak. The geometry between the Cretaceous sediments and the tuff breccias is not well exposed because of the extensive slope debris and colluvium on the south slopes. Based on the apparent sequence of emplacement of these diverse lithologies, it seems likely that Cerro Guadalupe began as a phreatomagmatic event, much like many of the other necks, and subsequently evolved to a pyroclastic cone built at the northern end of the former crater.

The contact between the dike and the tuff breccias is distinct enough to lay a finger on. Visible thermal effects are moderate. Immediately adjacent to the mass of the dike are small 2–4-mm-wide veins of gypsum(?) extending at right angles into the adjacent tuff breccia.

The contact between tuff breccias and the underlying Cretaceous rocks that formed the surface at the time of the eruption forms a low angle funnel that is locally below the mostly horizontal contact between the basalt cap and the underlying Cretaceous sediments (that the contact is horizontal is best appreciated by geologic mapping and not obvious in Fig. 2.52). Assuming the horizontal contact represents the unconformity defined by the original surface at the time of the eruption, the thick section of tuffs here appears to be deposited in the funnel of a crater excavated during the opening phreatomagmatic phase of the eruption. Examination of exposures and drill logs throughout the Rio Puerco Valley confirms much the same conclusion, namely that volcanic necks are not large intrusions, but rather local masses of basalt and tuff breccias accumulated at or above the ground surface at the time of their emplacement.

Return to State Road 279 via the way we came (7.3 mi from Optional Stop 1). The return trip offers a good view of the southwest side of Cerro de Guadalupe (Fig. 2.53). *7.3*

RE-ZERO ODOMETER at the intersection with the main dirt road (corresponds to the northeastern apex of the triangular road intersection in this area). Travel west (left).

Waypoint 8 [35.632253°, -107.107980°]

0.2 Northwest-southeast trending dirt road that leads to the ghost town of Cabezon. In 0.1–0.2 mi, it intersects BLM Road 1114 and continues on to the former town of Cabezon. *0.5*

0.7 Cross cattle guard. Water distribution facility on the left. *0.1*

0.8 At 11:00 is Cerro Cuate, a basaltic neck with a 020–025° feeder dike. *0.2*

1.0 Road bends right slightly. Cabezon Community Reservoir lies 0.1–0.2 mi (0.15–0.3 km) to the right (north). *0.3*

1.3 Road bends left. Straight ahead (12:00–2:00) is a butte held up by Point Lookout Sandstone. *0.1*

Waypoint 15 [35.635498°, -107.132218°]

1.4 **Cross a recently incised arroyo followed by a road intersection. Proceed straight.** Dirt road to right leads to the La Lena Wilderness Study Area and accesses the Continental Divide trail. From this road intersection, one could walk 0.2 mi (0.3 km) southwest (~200°) to see an example of active headwall retreat of a small arroyo incised into middle–late Holocene alluvium. *0.2*

1.6 View southward toward Cerro Cuate (Fig. 2.54). *0.4*

2.0 Short road to left leads to cattle watering trough. From here, one can walk 0.5–0.7 mi northward across BLM land to the nicely exposed butte capped by Point Lookout Sandstone (Fig. 2.55). These strata correspond to what we visited at Stop 1. Note the rockfall boulders on the southeast-facing slopes. *0.5*

2.5 Low, rolling landscape developed on upper Mancos Shale (Satan Tongue). Topographic low areas (broad swales) are generally underlain by Holocene alluvium and sheetflood deposits. *0.3*

2.8 Cattle guard. Straight ahead, in the distance, lies the volcanic neck called Cerro Parido. *0.1*

2.9 To left (south) there is a 025° dike leading toward the Cerro Cuate volcanic neck. *0.5*

3.4 Ascend a low topographic rise underlain by upper Mancos Shale. To left (south) lies Cerro Cuate (Fig. 2.54). *0.1*

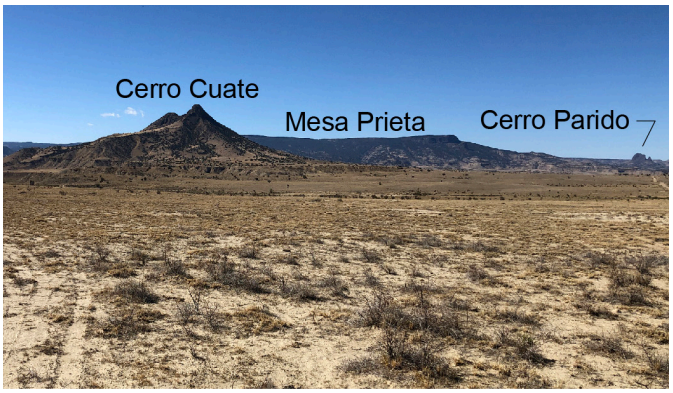

FIGURE 2.54. View to south of Cerro Cuate. This Rio Puerco neck is elongated along the strike of feeder dikes. Lower slopes to right consist of Mancos Shale with the 15–20-ft-thick (4–6 m) Dalton-Hosta sandstone tongue.

FIGURE 2.55. View to northwest of a butte offering good exposure of the transitional contact between the Point Lookout Sandstone and underlying Mancos Shale. In the foreground lies middle–late Holocene alluvium on easily erodible Mancos Shale. The landscape and paucity of vegetation seen here is typical of the Rio Puerco Valley near the volcanic necks.

3.5 Cattle guard and topographic rise underlain by upper Mancos Shale. *0.3*

3.8 On right of road is 1–2 ft (0.3–0.6 m) of cemented, Pleistocene gravel overlying Mancos Shale. *0.2*

4.0 Road descends into a valley. Straight ahead is a nice view of the north end of Chivato Mesa. Note the volcanic neck (Bear Mouth) at the extreme north end of mesa. *0.2*

4.2 Good exposure on right of yet another butte showing Point Lookout Sandstone underlain by the Satan Tongue of the Mancos Shale. This exposure is on private land. *0.3*

4.5 Cross cattle guard. *0.2*

4.7 Road turns left and ascends low ridge underlain by Mancos Shale. *0.1*

Waypoint 16 [35.626347°, -107.190631°]

4.8 **Road intersection. Follow main road to the left.** The right road parallels the Chico Arroyo on its northern bank. Good view to left (east) of Cerro Cuate. To the southwest lies Chivato Mesa and the tooth-like Bear Mouth peak just north of it. *0.1*

4.9 Subdued topographic relief of the larger area is reflective of erosion of weakly resistant mudstones of the upper Mancos Shale. *0.5*

5.4 Cross cattle guard. *0.6*

6.0 Nice view to left of Cerro Cuate (Fig. 2.56). At foot of this neck are exposures of the ledge-forming Dalton-Hosta sandstone tongue, which overlies the easily eroded middle tongue (Mulatto Tongue) of the Mancos Shale. *0.3*

FIGURE 2.56. Cerro Cuate (left) and Cabezon Peak (right). View to the northeast. Photograph taken at mile 6.3.

6.3 Road bends sharply right. Just before the tight curve, pull off on the dirt road heading east.

Waypoint 17 [35.604937°, -107.187138°]

OPTIONAL STOP 2. View of Rio Puerco Valley and Puerco necks, Dalton-Hosta sandstone tongue, high-level terrace gravel.

Walk to the south edge of the mesa for a great view of the middle Rio Puerco Valley and the north end of Mesa Chivato (Figs. 2.57, 2.58). This secluded and picturesque segment of the middle Rio Puerco Valley, flanked on either side by Mesa Chivato and Mesa Prieta, is one of the most scenic places in New Mexico, due in large part to the geologic features and processes that have been spotlighted on this field trip. Here, the Rio Puerco has incised into Late Cretaceous strata that consists of Mancos Shale with two prominent sandstone tongues lying stratigraphically below the Point Lookout Sandstone we visited in Stop 1 (listed in ascending stratigraphic order): Gallup Sandstone and the combined Dalton-Hosta sandstone. The Dalton and Hosta sandstones are combined because terrestrial Crevasse Canyon strata that typically divide the Dalton and Hosta sandstones do not extend this far to the northeast; hence the two nearshore sandstones appear as one unit (as discussed in Stop 1). The Dalton-Hosta sandstone tongue is nicely exposed in the roadcuts to the west (Fig. 2.59). The Mancos Shale tongue between the Gallup and Hosta sandstones is ~750 ft (~230 m) thick and is informally referred to as the "middle Mancos tongue," or formally as the Mulatto Tongue of the Mancos Shale.

Walk down the road, turning right and crossing a small

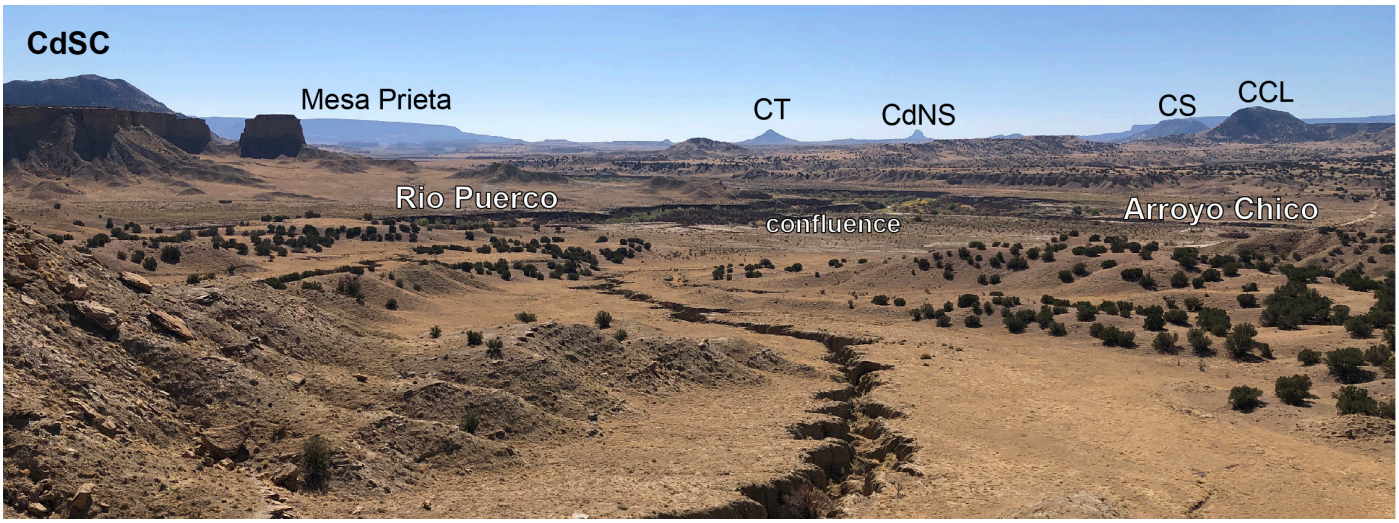

FIGURE 2.57. View to the southeast of the confluence of the Rio Puerco and one of its larger tributaries, the Rio Chico. The former diversion dam for the abandoned Guadalupe acequia system was located about 0.6 mi (1 km) on the Rio Puerco to the left of the left margin of the photograph. Volcanic neck abbreviations are: CdSC = Cerro de Santa Clara, CT = Cerro Tinaja, CdNS = Cerro Nuestra Senora, CS = Cerro Salado, and CCL = Cerro Chamisa Losa.

FIGURE 2.58. Looking southwest at the north end of Mesa Chivato. The embayed buttes in the middle ground are held up by the Dalton-Hosta sandstone tongue. The light-colored cliff just above the white arrow correlates to the Point Lookout Sandstone.

east-down fault, to view the sandstone tongue (Fig. 2.59). The sandstone has a noteworthy, 2-m-thick main body that overlies a heavily scoured erosional contact. The main body is mostly massive, with 1-5% swaly laminations, and consists of very fine– to fine-grained sand. Below the erosional contact lies subequal mudstone and siltstone, with minor very fine–grained sandstone in very thin to laminated, horizontal-planar beds. In this fine-grained interval are ~10% lenticular to channel-shaped, very fine–grained sandstone, bodies. The upper ~1 m of the exposure consists of well-defined, darker-brown sandstone beds that are slightly wavy, becoming more distinctly hummocky cross-stratified in its upper part.

The presence of marine fossils (mainly bivalve molds that are best seen at the top of the bluff) and the stratigraphic position of the sandstone tongue between Mancos Shale tongues indicates a nearshore depositional environment. Here, and along the field trip route near Cabezon, the Dalton-Hosta sandstone tongue clearly coarsens upward, in the sense that the proportion of sandstones to mudstones increases up-sections, so it mainly reflects deposition during a shallowing of sea level (i.e., regression). What is noteworthy here is the heavily scoured contact at the base of the main sandstone body, perhaps reflective of a forced regression. The interbedded sandstone and mudstone best correlates with the distal lower shoreface. The channelized to lenticular sandstone bodies are likely storm deposits, such as those inferred for the Point Lookout Sandstone at Stop 1, and have a similar orientation: 170-180°. The main, 2-m-thick sandstone body can be interpreted as a proximal lower shoreface that is massive due to bioturbation. The presence of subtle hummocky cross-stratification in the upper 1 m

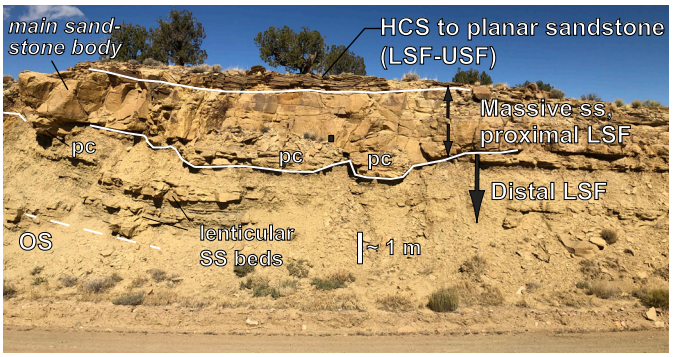

FIGURE 2.59. The Dalton-Hosta sandstone tongue, which we see frequently in our drive between Stops 1 and 3. Stratigraphically above this outcrop lie 300–330 ft (90–100 m) of Mancos Shale, separating this sandstone tongue from the higher (younger) Point Lookout Sandstone. Similar to the lowest Point Lookout Sandstone strata at Stop 1, the lower part of the Dalton-Hosta tongue is characterized by interbedding of sandstones, siltstones, and mudstones, representing the shallowing-upward transition from offshore (labeled OS) to the distal lower shoreface (LSF). The main ledge-forming sandstone body is 6–9 ft (2–3 m) thick and mostly massive (probably due to thorough bioturbation) with some swaly laminations. It is interpreted to have been deposited in the proximal lower shoreface (LSF). Note the paleochannels (pc) and highly scoured base of the massive sandstone, perhaps due to a forced regression. The channels trend 170–180°. The upper 1 m has well-defined beds (Fig. 2.60), ranging from horizontal-planar to hummocky cross-stratified (HCS), as well as abundant bivalve molds; it is interpreted to have been deposited in shallower water than the main sandstone ledge, probably in the lower-upper shoreface transition (LSF-USF).

(Fig. 2.60) probably indicates a slightly shallower position in the proximal lower shoreface or in the lower shoreface–upper shoreface transition. At stratigraphic sections 3 mi (4.8 km) to the southwest and 30 mi (49 km) to the south, this hummocky cross-stratified interval is disconformably overlain by deep-water, fissile shales (D.J. Koning, unpubl.), which is very likely a flooding surface. Synthesizing these observations indicates sea level shallowing associated with a forced regression, followed by a major transgression associated with the overlying Satan Tongue of the Mancos Shale.

Note the granite-rich gravel lying on the mesa top. These clasts were sourced from the Nacimiento Mountains and deposited here by the Rio Puerco several hundred thousand years ago. Subsequent incision by the Rio Puerco isolated the former valley floor from further fluvial activity, creating this mesa-top terrace (the S5 geomorphic surface of Slavin, 1991a) that stands 220–230 ft (67–70 m) above the unincised valley floor. S5 is a widespread surface that mainly consists of piedmont slopes grading to this geomorphic level of the valley floor. The S5 surface may possibly correlate to a Rio Puerco terrace deposit with the Lava Creek B ash near Interstate 40 (Cikoski et al., 2012; Koning et al., 2013), based on tentative terrace correlations between there and here (D.J. Koning, unpubl.), but that remains to be confirmed. *0.3*

6.6 Descend into Rio Puerco Valley. A >50-ft-thick (15 m) Mancos Shale sequence (upper Mulatto Tongue) is exposed in the right road cut (underlying the Dalton-Hosta sandstone tongue). *0.2*

6.8 Road bends left and goes south across middle–late Holocene, valley-floor alluvium. *0.3*

7.1 Road turns left (to southeast) and travels down Arroyo Chico valley. At 10:00 is the Rito Leche terrace. *0.2*

FIGURE 2.60. Horizontal-planar to gentle hummocky cross-stratification in the upper 1 m of the Dalton-Hosta sandstone tongue. This was probably deposited in the proximal lower shoreface or perhaps in the transitional zone of the lower to upper shoreface. A pencil 13 cm long provides scale.

7.3 Mulatto Tongue of grayish Mancos Shale on bluffs to left, capped by 3–6 ft (1–2 m) of gravelly sediment of the Rito Leche terrace (*sensu* Bryan and McCann, 1936). *0.3*

7.6 To right, ~30-ft-deep (~9 m), historic inner arroyo of Arroyo Chico. If it is relatively stable for a period of months, salt precipitation may be seen on the surface of the modern arroyo floor. *0.1*

7.7 Road bends right and crosses cattle guard. *0.1*

7.8 Bridge over modern wash of Arroyo Chico. Note the piping occurring in middle–late Holocene alluvium on the northeastern bank of the arroyo (Fig. 2.61). Refer to Optional Stop 1 for discussion of the importance of piping in arroyo widening. Arroyo Chico meets the Rio Puerco about 0.3 mi (0.5 km) to the southeast. *0.1*

7.9 Road intersection with driveway to private residence. Follow the main road as it bends right and travels west over Holocene alluvium flanked on the left by hills of Mancos Shale. *0.4*

8.3 Road bends sharply left and proceeds south. Nice view to right of sandstone-capped butte (Dalton-Hosta sandstone tongue) overlying Mancos Shale (Fig. 2.62). *0.2*

8.5 Road ascends a small ridge underlain by Mancos Shale, capped on left by thin Pleistocene gravel (~3 ft, 1 m thick). Ridge continues southward. *0.6*

9.1 **Dirt road intersection. Turn left on dirt road that heads to Guadalupe. RE-ZERO ODOMETER.**

Waypoint 18 [35.581611°, -107.207375°] *0.2*

0.2 Thin, gravelly, Pleistocene terrace deposits overlie Mancos Shale to west and east. *0.5*

FIGURE 2.61. Piping features on the north side of the recently incised wash of Arroyo Chico. View to east. Butte in background is capped by the Dalton-Hosta sandstone tongue, which overlies the Mulatto Tongue of the Mancos Shale.

FIGURE 2.62. View to west of 10–20-ft-thick (3–6 m) Hosta Sandstone overlying Mancos Shale (Mulatto Tongue) across an interfingering, transitional zone, similar to what we observed at the base of the Point Lookout Sandstone at Stop 1.

0.7 Homestake well adjoining the road. This artesian well is interpreted to draw from the Gallup Sandstone aquifer. It has good water quality, with a specific conductance of 490 µmhos/cm at 25°C, and the water chemistry is sodium bicarbonate. Inferred groundwater flow direction is to the northeast, and recharge to the aquifer probably occurs in the Mount Taylor-Chivato Mesa area (Stone, 1981; Kernodle et al., 1989). More information on this well is found in the paper by Belew et al. (2024). *0.1*

0.8 Descend gradually onto Holocene alluvium of a small tributary to the Rio Puerco. Ojo de las Yuegas (Spring of the Mares) is located 0.5 mi to the west. At a distance 1.1 mi (1.8 km) to the west in this canyon is an unnamed seep discharging from the Dalton-Hosta sandstone tongue. *0.1*

0.9 Road bends left. *0.3*

1.2 Thin, gravelly terrace deposit to right. *0.2*

1.4 Road wraps southwestward to avoid the recent gully incision occurring in this unnamed Rio Puerco tributary valley. At the mouth of this drainage, a tragedy occurred, probably early in the 20th century, as related by Eduardo Valdez in García (1987). While traveling back from Catholic mass in Guadalupe, the Ramirez family's wagon was washed away in a flash flood while crossing a deep arroyo somewhere in this drainage, and it was found the next day where the arroyo fed into the Rio Puerco. Some young men decided to excavate the wagon since it was a valuable commodity, but while doing so, the Rio Puerco arroyo sidewall collapsed and killed three of them. This is a deadly example of arroyo widening by sidewall collapse (facilitated by stream-flow undercutting), and the story serves as a warning to all field geologists who like to traipse up and down these steep-walled arroyos. *0.3*

1.7 Cross a 025°-trending dike in Mancos Shale (Fig. 2.63). The dike is locally vesicular (1–3 mm wide). *0.2*

FIGURE 2.63. Basaltic dike about 12 in. (30 cm) wide and trending 025°, oriented toward Cerro Cuates. The dike extends 1000 ft (300 m) south of and 350 ft (105 m) north of the road. This dike, like many in the Rio Puerco Valley, shows signs of lateral chill zones and vesicles along the outer 8 in. (20 cm) from initial gas exsolution as the dike neared the surface. Note the en echelon character typical of dikes ascending through shallow sedimentary sections, where stress orientations are typically rotated within the weaker sedimentary rocks.

1.9 Cross small arroyo. *0.3*

2.2 Ascend onto ridge underlain by Mancos Shale. Geomorphic surface(s) within ~1000 ft (~330 m) to left and right are relatively high-level terrace deposits sloping north-northeast toward the Rio Puerco. The gravel is composed of volcanic rocks (mainly basaltic) sourced from Mesa Chivato. *0.1*

2.3 Tight bend in road; descend into small canyon. Adjoining the road are exposures of the middle Mancos Shale (Mulatto Tongue), which here has a 20-ft-thick (6 m) interval containing abundant flaggy, laminated, very thin beds of sandstone. Such sandstone-rich intervals are relatively common in the Mulatto Tongue. *0.2*

2.5 Cross 20-ft-deep (6 m) arroyo carved into the middle–late Holocene alluvium. *0.1*

2.6 Eastern edge of valley-floor alluvium. *0.1*

2.7 Road travels across a low ridge underlain by yellowish Mancos Shale. Top of exposure has abundant sandstones. Low ridges to southeast also underlain by shale. *0.6*

3.3 Travel southeast across a wide expanse of, middle-late Holocene alluvium. Bluffs to right (southwest) are underlain by grayish Mancos Shale (Mulatto Tongue). *0.5*

3.8 Cross low ridge underlain by Mancos Shale. *0.5*

4.3 Bluff-forming, cemented sandstone of the Gallup Formation in vicinity. Cross tributary canyon of the Rio Puerco. It is not incised here, but historic and ongoing incision has occurred 0.5–2.0 mi (0.8–3.0 km) upstream (west-southwest of here). At this location, alluvial fan sedimentation is occurring at the mouth of the upstream gully, even though we are only 0.1–0.2 mi (0.2–0.3 km) from the Rio Puerco arroyo (Fig. 2.64). On this fan in the wide valley floor of the canyon, sheetflooding occurs and cascades into numerous, widespread gullies at the edge of the Rio Puerco arroyo (Fig. 2.64). *0.2*

4.5 Road bends sharply right and travels on a relatively narrow remnant of middle–late Holocene alluvium between the Gallup Sandstone–Mancos Shale on right (southwest) and the Rio Puerco on the left. The Gallup Sandstone is a late Turonian, regressive nearshore deposit. The sandstone is in very thin to thick, tabular beds; general bedding thickness increases up-section. Several Gallup Sandstone tongues are present in the Gallup area, but only one tongue is seen in the middle Rio Puerco Valley, presumably correlative to the highest tongue in the Gallup area (the A tongue). The Gallup Sandstone represents the first major regressive wedge in the Upper Cretaceous section of the San Juan Basin (Molenaar, 1983). It was named after the town of Gallup as the basal member of the Mesaverde Formation (Sears, 1925). In the area of this road log, the Gallup Sandstone crops out in the Guadalupe area and on the eastern side of Mesa Prieta, pinching out to the northeast before the main drainage of the Rio Salado. Good views of the Gallup Sandstone continue for the next 0.7 mi, and we look at it closely at Stop 3A. *0.6*

5.1 Small geomorphic alcove to right, offering nice views of the Gallup Sandstone overlying Mancos Shale. *0.1*

5.2 Abandoned buildings on right and left are the northern remnants of the town of Guadalupe. Road bends right. *0.1*

Waypoint 19 [35.539451°, -107.151532°]

5.3 **Center of Guadalupe ghost town.** This is the center of the ruins of Guadalupe, a Hispanic farming village dating from ca. 1872 through the 1950s. Several adobe buildings from this era, many of them under roof, make this a must-see for anyone interested in ghost towns and New Mexico history (Figs. 2.65–2.67). Seldom seen in ghost towns is the type of two-story, adobe building seen to the left (Fig. 2.66). This was the store (lower story) and residence (upper story) of the Juan Córdova family. About 160 inhabitants (1880 census) lived in the larger area, with about 20 residences (or residence with stores) being within ~1 mi of here. This town site was chosen because of the availability of water from Ojo del Padre spring, located 0.2 mi to the west of the Juan Córdova store (Fig. 2.65). This well is described as an artesian well in García (1994) and probably discharges from a sandstone bed in the Mancos Shale, ~40 ft (~12 m) below the bluff-forming Gallup Sandstone. Another factor that makes this ghost town so special—in addition to the plethora of abandoned buildings

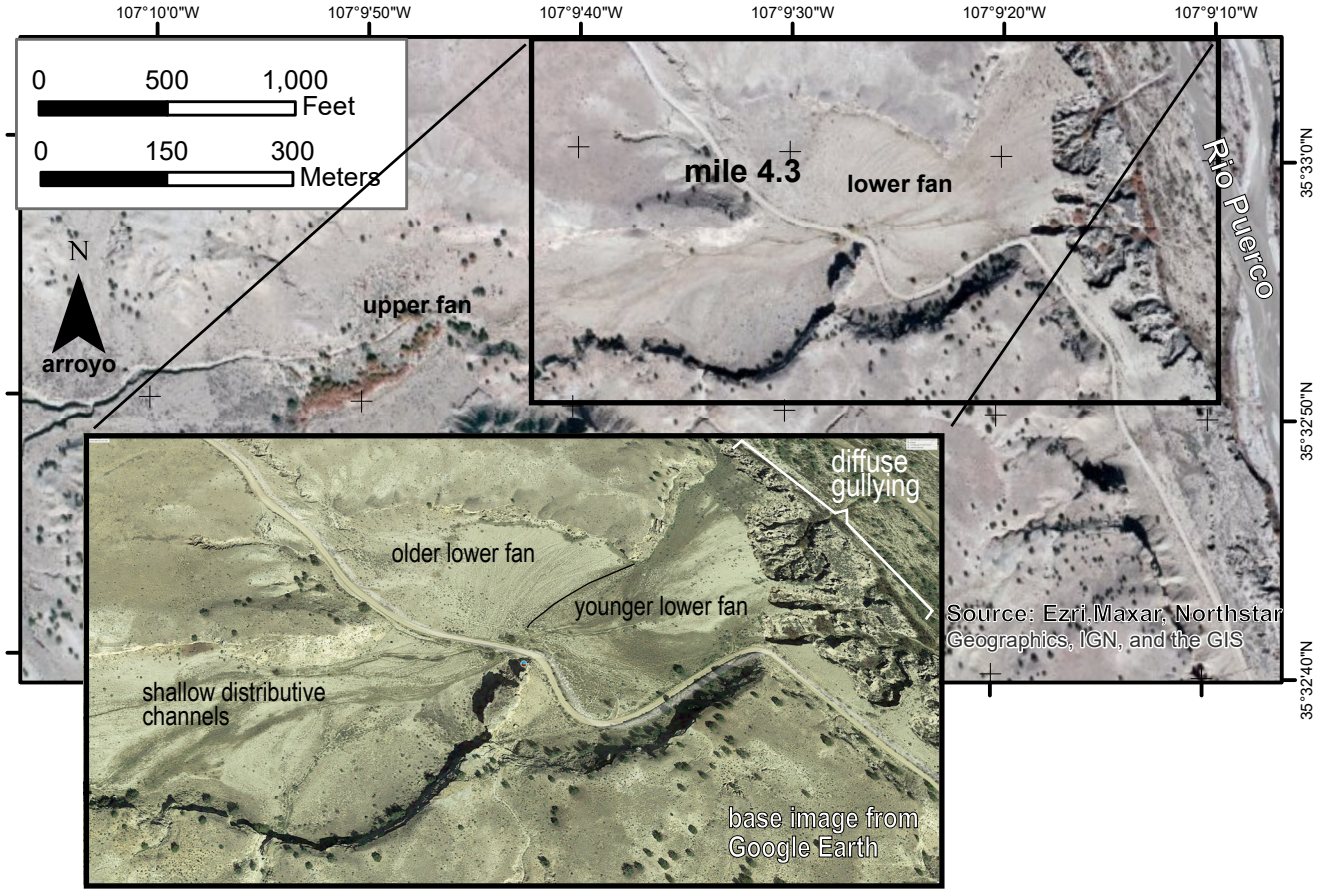

FIGURE 2.64. Aerial imagery of recent fan sedimentation at mouth of a small, east-flowing tributary drainage at mile 4.3. Two alluvial fans are noted at the mouth of the arroyo to the left (west), separated by a zone of shallow, distributary channels. The lower fan can be further subdivided into an older and younger subunit. The Rio Puerco arroyo lies on right side of photo. Cemented bluff alongside dirt road is the Gallup Sandstone. Alluvial fan sheetflooding is causing laterally extensive gullying at the downstream edge of the fan. Near Stop 3, we will observe Rio Puerco tributaries exhibiting a single, deeply incised gully at their downstream ends. However, many other tributary drainages end in a recent alluvial fan aggrading on the wider (unincised) valley floor. This illustrates that gullying is not driven solely by the base level drop of the Rio Puerco; it is a widespread phenomena involving hydraulic driving forces and resisting forces (such as vegetation density and type) that occurs in both small and large drainages.

and the beautiful, lonely landscape—is the collection of stories documenting the hard but fulfilling lives of the Hispanic farmers and ranchers who lived here. These stories are compiled in several books by author and professor Narcia García (1987, 1992, 1994, 2015). Information regarding the townsite is from García's publications, plus Harris (2003) and Mulhouse (2020). Please do not venture off the main road, as the surrounding land is all private property. *0.2*

5.5 Road gradually turns left. The cemetery of Guadalupe is located 400 ft (120 m) to the right. *0.3*

5.8 A wide terrace developed on middle–late Holocene alluvium, the pre-1885 valley floor, is to the left (northeast). A 50-ft-tall (15 m) cliff capped by Gallup Sandstone flanks the road to the right, where one can see its interfingering and transitional contact with the underlying Mancos Shale. Note how lateral retreat of the Gallup Sandstone cliff is expedited by rockfall processes, the boulders of which flank the footslope below the bluffs. *0.2*

FIGURE 2.65. View to west-southwest of three abandoned adobe structures in Guadalupe. A modern residence lies behind, near the foot of the bluffs capped by Gallup Sandstone. The blue arrow denotes the location of Ojo de Padre spring, which likely discharges from a sandstone bed in the uppermost part of the lower tongue of the Mancos Shale. The white arrow points to the Catholic church. Adobe buildings behind and to the left of the church probably included the school and dancehall (per fig. 1 of García, 1994).

FIGURE 2.66. Juan Córdova store and residence (lower and upper stories, respectively), as it looked in 1981.

FIGURE 2.67. Catholic church at Guadalupe (photo taken in 1978). Since then, the steeple has fallen (or was placed) on the ground.

6.0 Road bends sharply right (southwest). *0.1*

6.1 On right, soft-sediment deformation in the lower part of the Gallup Sandstone. *0.1*

6.2 Road descends into a ~20–30-ft-deep (~6–9 m) arroyo of Cañon Guadalupe, likely carved in the past ~100 years. On the far (southeast) side of the arroyo, two historic diversion ditches were dug, perhaps to provide water for pastures. The road continues southeast along the foot of the Gallup-capped mesa. Springs are located 0.9 mi (1.4 km) up the canyon, and associated discharge often makes it to the road crossing. *0.4*

6.6 Small butte to left capped by cemented Gallup sandstone. *0.4*

7.0 Good exposure of Gallup Sandstone underlain by Mancos Shale seen to right. On left is 0.75-mi-wide (1.2 km), relatively undissected valley-floor alluvium. Its surficial pattern (smooth with subtle, downgradient linear stripes) indicates it was once farmed, probably using runoff from canyons to the west (especially Cañon Salado). *0.2*

7.2 Cross abandoned, shallow channel of Cañon Salado. Dirt road to 2:00 once veered 0.7 mi (1.1 km) to the southwest to get around a presumably upstream-propagating, narrow, and deep arroyo developing in Cañon Salado. However, at some point in time the arroyo there became too deep, and rather than continue the 0.7-mi (1.1-km) detour it was decided to just "barrel-through" this impressive arroyo with the present-day road. Comparison of different-aged aerial imagery, combined with notes of an incised arroyo by Pippin (1979), indicates that deep arroyo incision occurred after 1954 in the lower Cañon Salado. *0.3*

7.5 Road descends steeply down and then up Cañon Salado, which is ~30 ft (~9 m) deep and only 50–80 ft (15–24 m) wide. *0.3*

7.8 Road intersection, with the right road being the former "detour" mentioned above. *0.1*

7.9 Cross topographic saddle with an impressive basaltic dike, which we view in Stop 3A. Turn left on the poor road 400 ft (120 m) beyond the saddle and drive as far as possible down this side road to allow ample parking for the caravan.

Park at Waypoint 20 [35.515756°, -107.126997°].

STOP 3. Gallup Sandstone, basaltic dike and terrace deposits, ancestral Pueblo site, and recent arroyo incision.

At this stop, we split into two groups that alternately visit Stop 3A and Stop 3B (see Fig. 2.68 map). Optional Stop 3C entails a 10-min walk from the parking area to the south, where the southeast side of the arroyo offers exposures of a pre-Chacoan, late Holocene paleoarroyo fill (Fig. 2.68).

STOP 3A. Gallup Sandstone and Guadalupe Ruin.

Waypoint 21 [35.518232°, -107.126622°]

Just east of the topographic saddle and signpost, a well-marked trail ascends the mesa to the northeast. The mesa is capped by the well-exposed, cemented Gallup Sandstone, which is ~60 ft (18 m) thick at this location (Figs. 2.69, 2.70). The main body of the formation is characterized by tabular beds (Figs. 2.70, 2.71, units 5–7) composed of lower-fine to upper-fine sand (minor lower-medium grain size). Its base is conformable and transitional with the underlying, lower tongue of the Mancos Shale, and transitional strata can be viewed closely along the middle part of the trail to the mesa top. In this transition zone, very fine– to fine-grained sandstone interfinger with silty-clayey shales (Figs. 2.70–2.72). Also note the conspicuous iron-oxide, nodular cementation, which seems to be controlled by paleoburrows (Fig. 2.72). What appears to be a 20–30-cm-thick ash is really a zone of gypsum precipitation at the base of the sandstone-dominated strata (Fig. 2.71, top of unit 3e).

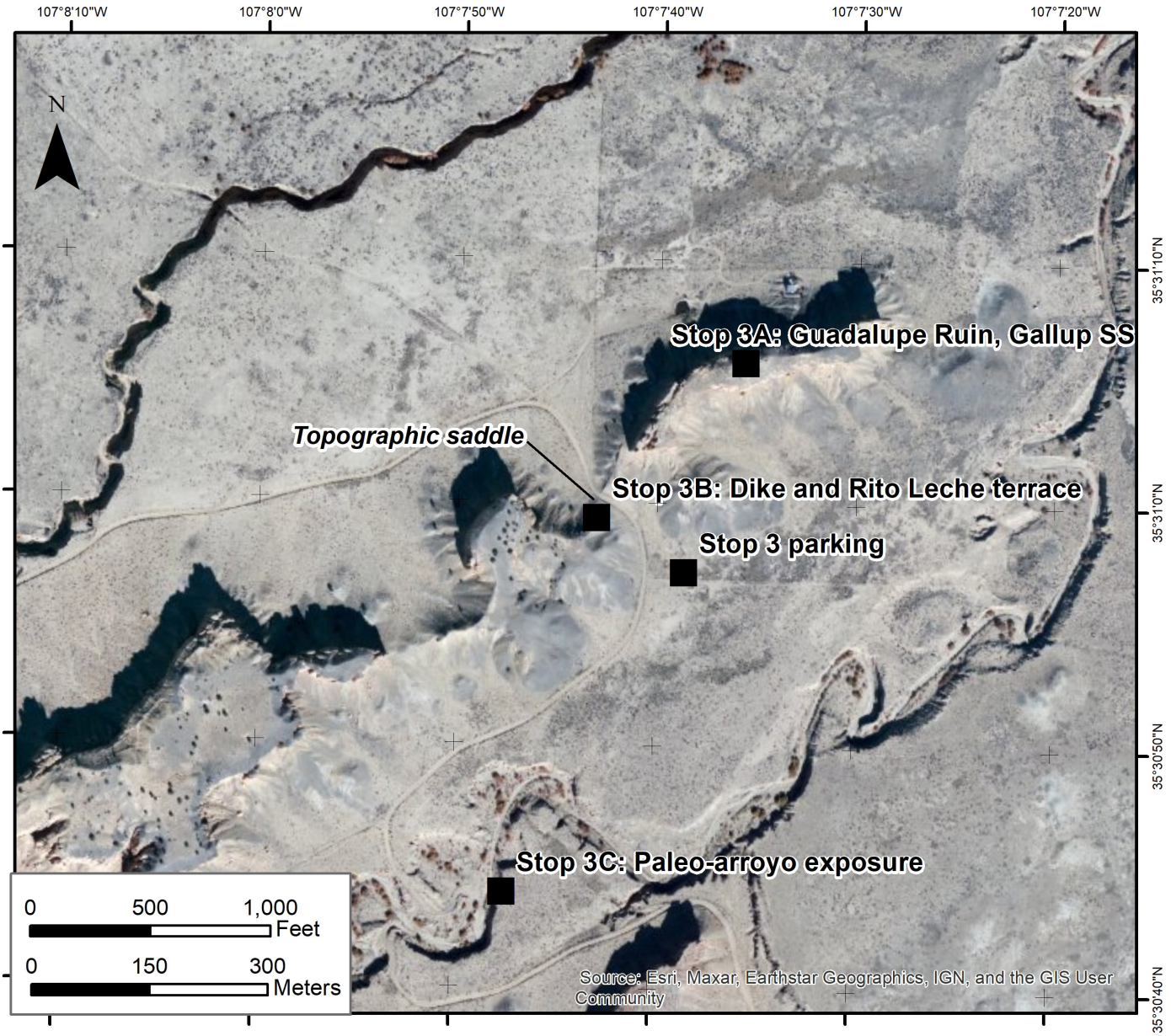

FIGURE 2.68. The geographic and cultural features of Stop 3.

The steep part of the trail just below the mesa top climbs through units 5 and 6 (Fig. 2.70); note the bulbous forms in the lower part of unit 5, coinciding with the first switchback of the trail (Fig. 2.73), likely caused by burrowing. On the mesa top, the trail turns northeast and climbs up ~30 ft (~10 m) across thick, tabular beds of sandstone (Fig. 2.70, units 8–10; Fig. 2.74). Lack of sedimentary structures and bulbous outcrop faces probably reflect thorough bioturbation. Distinctive burrows are only seen near the top (unit 10). The inferred depositional environment for the observed Gallup Sandstone is proximal lower shoreface. The middle-upper sandstone (units 7–10) appears to have been deposited in relatively similar depositional environments (Fig. 2.70), reflective of aggradation in relatively static water depths and presumably fixed shoreline position. This scenario contrasts to the relatively frequent changes in water depths (and presumably lateral shifts in shoreline) inferred

FIGURE 2.69. A 20–24-in.-wide (50–60 cm), 25°-trending basalt dike forms a black wall in the topographic saddle at Stop 3. The yellowish butte behind (to the north) is capped by Gallup Sandstone. On the northeastern end of the butte is the site of Guadalupe Ruin (not visible).

for the Point Lookout Sandstone at Stop 1 (Koning, 2024).

A high-energy, upper shoreface depositional environment would be characterized by notable cross-stratification. It is prevalent in the upper half of the Gallup Sandstone where it is mapped 20 mi (30 km) to the south (Koning and Rawling, 2017; Rawling and Koning, 2019), and its absence here reflects the more basinward position (and deeper water) at Guadalupe Ruin in the early Coniacian.

We stop at the top of the Gallup Sandstone exposures to compare and contrast the sedimentologic features seen here

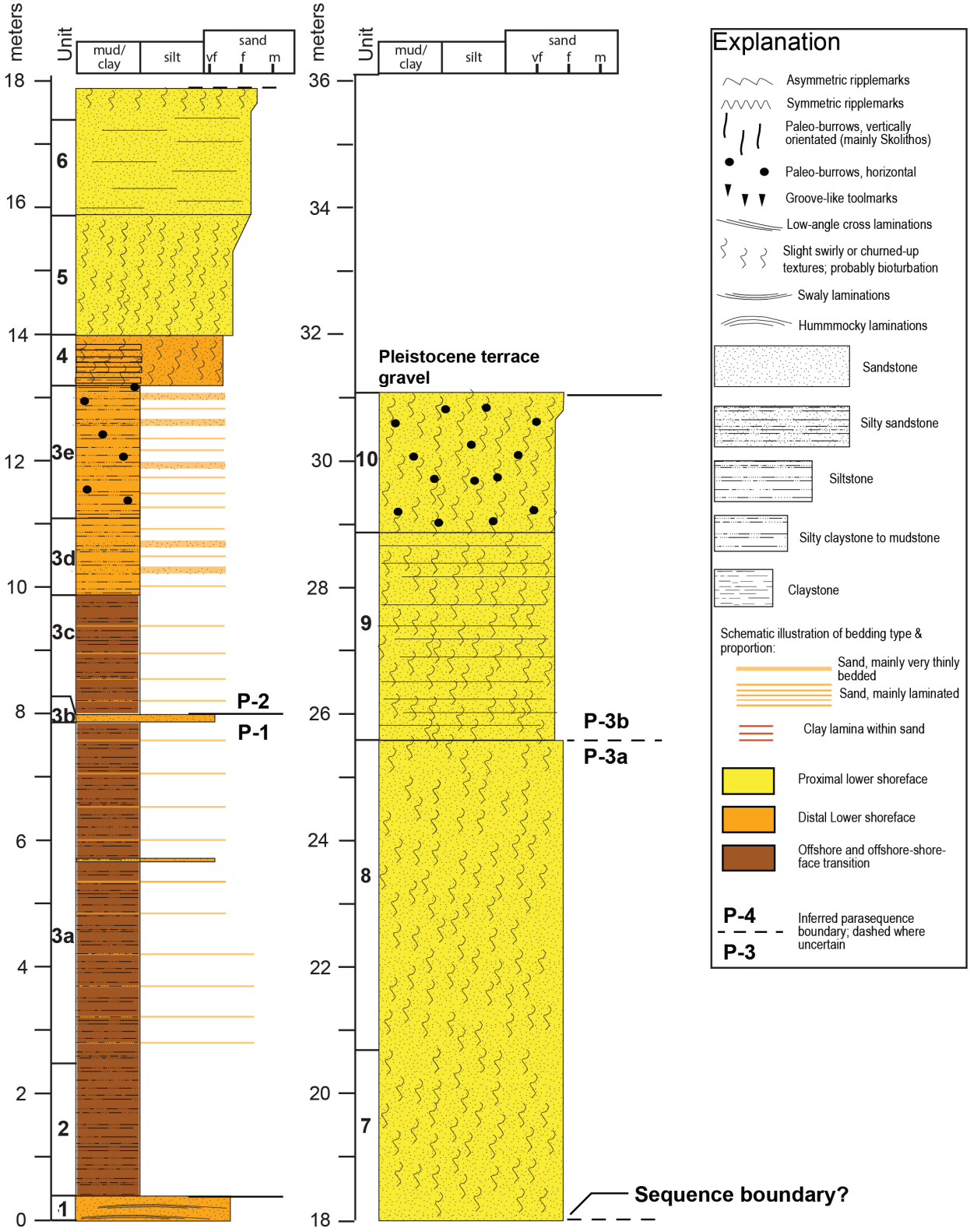

FIGURE 2.70. Stratigraphic section of the uppermost Mancos Shale and Gallup Sandstone at Stop 3A. Slightly modified from Koning (2024). The orange, horizontal lines in unit 3 are schematic representations of the relative proportion of sandstones within mudstone and siltstone.

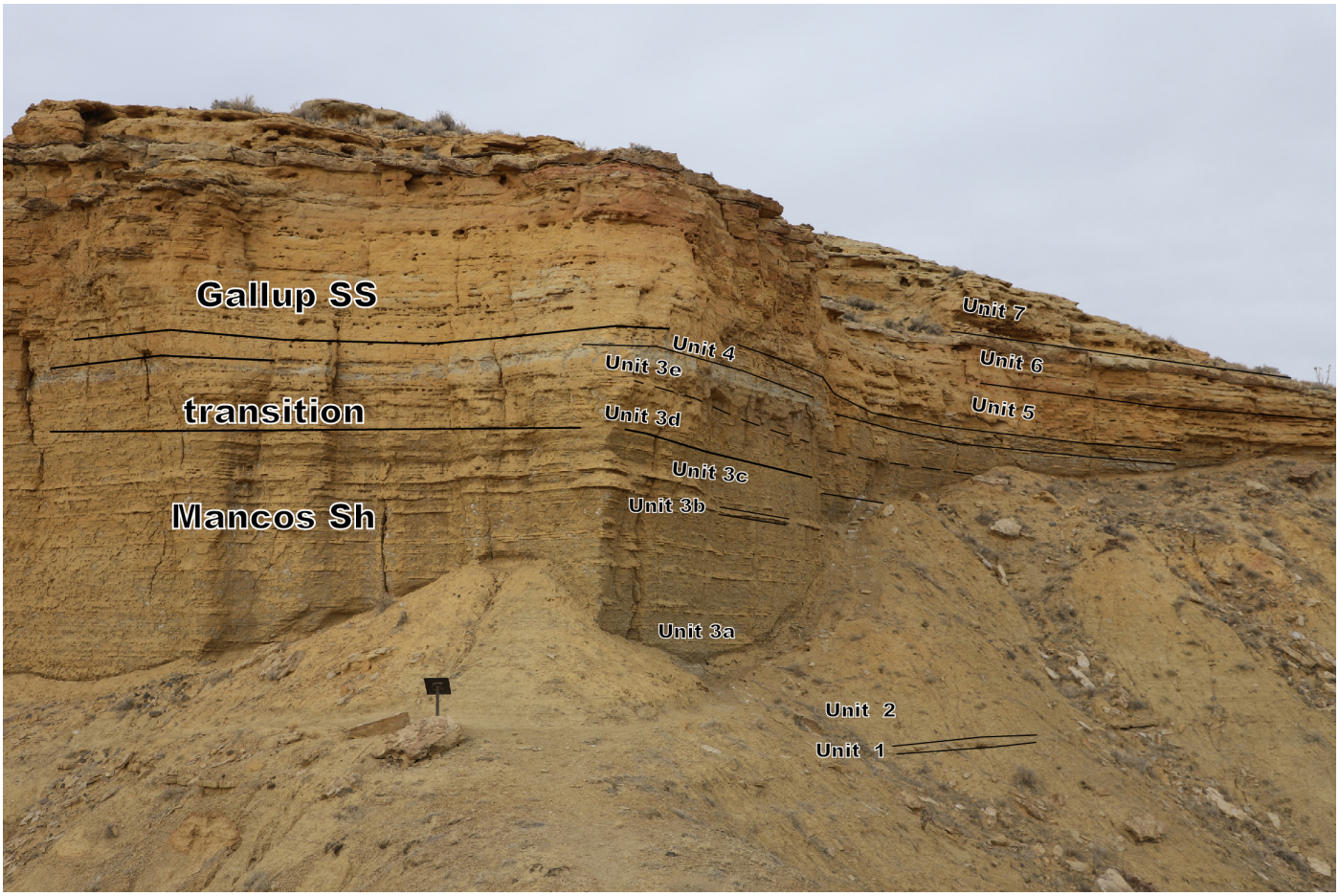

FIGURE 2.71. Photograph of the southeastern face of the butte at Guadalupe Ruin (Stop 3A). Units shown in the stratigraphic section (Fig. 2.70) are labeled. The white bed (upper part of unit 3e) is a 20–30-cm-thick zone of gypsum precipitation in interbedded sandstone-mudstone strata immediately underlying the sandier unit 4.

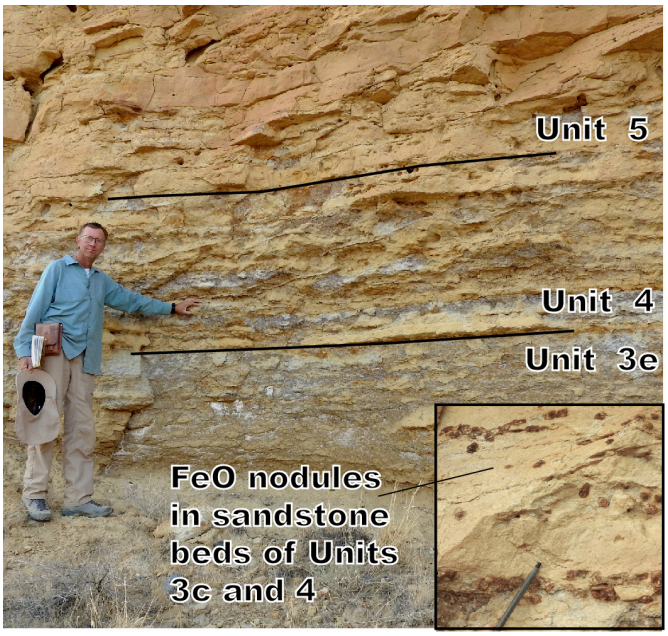

FIGURE 2.72. Interfingering mudstones and sandstones at the transitional base of the Gallup Sandstone, as observed along the trail to the mesa top. Nodular precipitation of iron-oxide (inset, lower right) may coincide with paleoburrows.

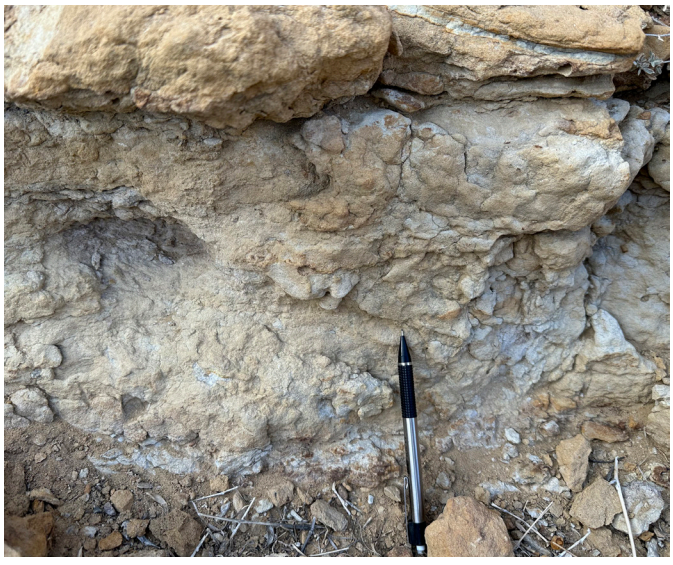

FIGURE 2.73. Bulbous outcrop texture reflective of burrowing. Found in the lower part of unit 5 at the first switchback of the trail to the mesa top.

FIGURE 2.74. Thick, tabular-bedded sandstone near the top of the bedrock exposure at Guadalupe Ruin. The massive texture, with slightly bulbous outcrop character (e.g., just above the hammer head), reflects high-intensity bioturbation. Swaly lamination is evident to the left of the hammer (below the cavities in the outcrop face).

with those seen at Stop 1, the latter being the transitional base and lower part of the Point Lookout Sandstone. The sandstones at both stops are a coarsening-upward (in terms of sandstone to mudstone proportions), regressive sequence. Two important differences between the two sites are the lack of meter-scale, transgressional mudstone beds (e.g., T2 at Stop 1) and the lack of strong current indicators (e.g., paleochannels and tool marks) at this location as compared with Stop 1. What do these differences imply about paleodepositional environments and related sedimentologic processes? Perhaps climatic conditions during the early Campanian were more conducive to strong storms, generating more storm beds in the Point Lookout Formation, than climatic conditions in the early Coniacian (upper Gallup Sandstone deposition). Or perhaps the paleogeomorphology of the coastline resulted in notably weaker storm currents in this location in the early Coniacian? What role might deposition of stratigraphic units relative to sea level changes (sequence stratigraphy) play in the lack of meter-scale mudstone beds in the Gallup Sandstone at Stop 3? These lithologic comparisons and questions are explored in a paper by Koning (2024).

At the top of the mesa, proceed southeast to the highest point of the butte and the location of a roofed kiva, where an outstanding, panoramic view awaits (Fig. 2.75). Before we delve into the human history, it is worth taking a moment to look around us, reflecting on the overall solemnity of the landscape and its integral geologic features. It is truly an interplay of "water and fire." Yellowish, bold cliffs and muted slopes of Cretaceous strata, deposited by water under an ocean 80–90 million years ago, are overlain by lava-capped mesas to the east (Mesa Prieta) and west (Mesa Chivato). Black pillars of rock appear to poke upward through the yellowish marine strata, like fists thrust up from some god of the underworld. In reality, of course, these are magma- and pyroclastic-filled throats and vents of the 3.7–2.4 Ma volcanoes of the northeastern Mount Taylor volcanic field. What the paleolandscape looked like at 3.7–2.4 Ma, and the history of Rio Puerco incision since that time, are topics explored in Stop 3B.

Here, at the top of the mesa, we compare and contrast Ancestral Puebloan settlements with Hispanic settlements, their respective land use, and how they adjusted to the climate-related limitations of this landscape. We also discuss how their respective lives were influenced by the geologic features of this landscape.

The Chacoan culture in northwest New Mexico flourished between the 9th and 12th centuries. During the 10th and 11th centuries, Chacoan influence expanded with a series of outlier settlements throughout the Four Corners region. Located 45 mi (72.4 km) east-southeast of Chaco Canyon is the easternmost of these outliers: Guadalupe Ruin, which was constructed and occupied between 900 and 1300 CE. Situated atop an isolated sandstone mesa rising 160 ft (48.8 m) above the valley floor, Guadalupe Ruin offered expansive views of the Rio Puerco Valley (Figs. 2.75, 2.76), which was an important migration and trade corridor. The ruins consist of masonry architecture

FIGURE 2.75. View to north-northwest from Guadalupe Ruin. Volcanic necks include (left to right): Cerro de Santa Clara, Cerro de Guadalupe, Cerro Chafo, and Cabezon Peak. Note the very narrow and deep arroyo in the middle ground, carved by Cañon Salado runoff after 1954.

FIGURE 2.76. View to east from Guadalupe Ruin toward Mesa Prieta. Note the well-constructed walls of the structure in the foreground; Ancestral Puebloans selected flat stones and cemented them with subordinate adobe. In contrast, Hispanic farmers chose to construct most of their buildings with adobe bricks, although stones were used locally.

with approximately 50 rooms and seven semisubterranean kivas (Fig. 2.77). The site was intensely, albeit briefly, reoccupied and remodeled by inhabitants from San Juan/Mesa Verde in the late 13th century. Evidence of occupation diminishes after the early 14th century. After the Puebloans left, the Navajos occupied the region, and the Torreon Chapter of the Navajo still consider the area around Cabezon part of their traditional homeland. See Jeffries (2024) for more information about Guadalupe Ruin.

Between 1972 and 1975, Eastern New Mexico University excavated approximately 40% of the Guadalupe Ruin site. The BLM conducted numerous stabilization efforts at the site between 1978 and 2008. Pot sherds can be found in the vicinity, and for a time an interesting collection could be seen inside the kiva (Fig. 2.78). Be sure to leave all artifacts, including pot sherds, at this protected site!

Human settlement since the mid-19th century consisted primarily of Hispanic farmers and ranchers. Looking ~300°, there are buildings at the base of the next ridge to the northwest (0.9 mi in distance). These are part of the larger settlement of Guadalupe. Earlier in the field trip, we drove through the main placita (town center) of Guadalupe (Figs. 2.65–2.67); its buildings can be vaguely seen from here 2 mi away along a 320° trend. The adobe-brick buildings in the Guadalupe area were built by Hispanic farmers, who initially came here in the 1700s but were driven out by repeated Navajo raids. After the cessation of raiding and creation of the Navajo reservation in the mid-1860s following the Navajo people's return from Bosque Redondo and Fort Sumner, Hispanic farmers from the east (primarily Albuquerque) settled here (Widdison, 1959). The wide, expansive valley floor 0.5 mi (0.8 km) west-northwest of here was farmed using local runoff or direct precipitation (evidenced by parallel stripes on Google Earth imagery). Most farming, however, took place on the northeast side of the southeast-trending Rio Puerco. There, a long acequia system, with a diversion dam located 6.2 mi (10 km) northwest of here, provided water for irrigation of crops (Widdison, 1959). Former inhabitants recall wheat, corn, pinto beans, chiles, melons, pumpkins, and peas being grown in these fields (García, 1992, 2015).

Hispanic settlers in the middle Rio Puerco Valley between 1870 and 1950 epitomize, in a human sense, the nexus theme of this field trip. Societal interactions extended in three main directions: west (Navajos on the Colorado Plateau), northeast-east (Jemez and Zia Pueblos in the southern Rock Mountain Region), and east-southeast (Albuquerque area in the Rio Grande rift). Hispanic relations with the Navajo may have been hostile initially. For example, one early settler recounted a nighttime Navajo "visit" that sent the family scurrying down the Rio Puerco arroyo for safety (García, 1987, p. 14). Relations warmed with time, however, and there are accounts of friendships between Guadalupe residents and Navajo people, visits of Navajo to Guadalupe, and tales of Navajo magic and witchcraft (like Navajos turning into coyotes) woven into the stories passed on by the Guadalupe settlers (García, 1987, 1992). In addition, Ricardo Heller of Cabezon employed Navajos to shear and haul the wool of his vast sheep herd (Sherman and Sherman, 1975). Trade was carried out with Jemez Pueblo, where wheat was milled; Guadalupe residents bartered farm produce for Jemez pots and fruit (García, 2015). A road led directly to Albuquerque over the northern Ceja del Rio Puerco and then over the Llano de Albuquerque. Guadalupe residents would travel to Albuquerque to visit relatives, obtain manufac-

FIGURE 2.77. View of the inside of the roofed kiva.

FIGURE 2.78. Pottery from the various Ancestral Puebloan groups that lived here from 900 to 1300 CE. Severe droughts in the late 13th century may have contributed to abandonment of this area, similar to the ca. 1950s droughts that marked the end of the Hispanic farmer populations in the mid-20th century.

tured goods, and for jobs when the "population exodus" occurred after WWI. From Albuquerque, various peddlers (often held in suspicion by Guadalupeans) traveled to Guadalupe to sell their wares and tonics (García, 1987).

The aforementioned irrigation infrastructure allowed relatively high-intensity farming to occur. However, an eroding Rio Puerco and a progressively drier climate spelled the end of farming and a dramatic curtailment of the population. Nasario García's father remembers the ditches having flowing water when he was a boy (ca. 1905–1920). The final failure of the dam occurred in 1936 (García, 1992; Widdison, 1959), by a flood or possibly an accidental fire, and the arroyo was too deep and too wide at that time for the people still residing in the valley to economically rebuild it. In the decade after the dam failure, farmers tried to rely on natural precipitation and natural runoff for agriculture, but with a drying climate, such water was often insufficient (García, 2015). Consequently, the former inhabitants of Guadalupe moved away (many to Albuquerque) or turned to ranching. Raising sheep, goats, and cattle went hand-in-hand with farming prior to 1930, but it became increasingly important for economic livelihood after the demise of farming (García, 1994; 2015).

The most coveted rangeland for the people of Guadalupe was the former Ojo del Espiritu land grant, located north and northeast of Cabezon Peak (García, 1987, 1992, 1994). By the mid 1930s, due to severe droughts, that rangeland became severely overgrazed and began eroding. In addition, the federal government bought the grant from the Catron family in 1935 for $2.50 an acre (Van Hart, 2013). The federal government immediately utilized the Taylor Grazing Act to enforce limitations on grazing. It also began demanding that lands once held in common be fenced into individual allotments, which completely altered the way the Hispanic farmers raised livestock and prevented their animals from "following the rain." Because there was little available forage elsewhere, cattle herds decreased to the point that ranching also became very difficult.

By the height of the 1950s drought, the Guadalupe area was practically abandoned. Human land use was curtailed by the realities of climate (i.e., amount and intensity of precipitation events) and climate-modulated geomorphic processes (i.e., arroyo incision). A landscape where green fields bordered the Rio Puerco, and where the valley floor was initially not deeply nor continuously incised, has been dramatically transformed into the landscape we see today. A soon-to-be-published work by Peter Stacey and Nasario García entitled "When the Acequias Run Dry: The Middle Rio Puerco Valley of New Mexico" uses new and old photographs and the recollections former residents to explore in detail the cultural and ecological consequences of this remarkable ecological and societal transformation.

STOP 3B. Basaltic dike and terrace deposit.

Waypoint 22 [35.516538°, -107.128544°]

At the topographic saddle, we view a 15–24-in.-wide (40–60 cm), 1180-ft-long (360 m), basaltic dike emplaced in the Mancos Shale (Figs. 2.79–2.80). It correlates to the "Gonzales dike" of Bruce Hallett's work, which returned a $^{40}Ar/^{39}Ar$ age of 2.61±0.03 Ma (Hallett, 1994; Hallett et al., 1997). The dike is vesicular, which implies it was relatively near the surface when it was emplaced. This dike trends 23–25° and appears to continue on the other (northeast) side of the Rio Puerco about 1.5 mi (2.4 km) to the northeast, but it does not project to a particular volcanic neck. Take a close look at the margins of the dike with the Mancos Shale; it is less obvious than one would think. The dike is characterized by joints oriented roughly perpendicular to the margins that are likely controlled by lateral cooling surfaces in contact with preexisting rocks. Alteration zones 4–8 in. (10–20 cm) wide are present in the sedimentary rock on both sides of the dike. Elongate vesicles occur in the outer 8 in. (20 cm) of the dike and tend to be less frequent near the core of the dike. Dikes grow by expanding perpendicular to their walls, such that the initial magma is displaced outward as the influx of new magma continues. As a result, the presence of vesicles in the outer zones may indicate the initial stages of exsolution of gases during the final stages of ascent. As the flow accelerates, such as during eruption in a fissure vent, the ascent rates may occur quickly enough that ascent outpaces vesicle growth. The result in many cases is fewer or smaller vesicles

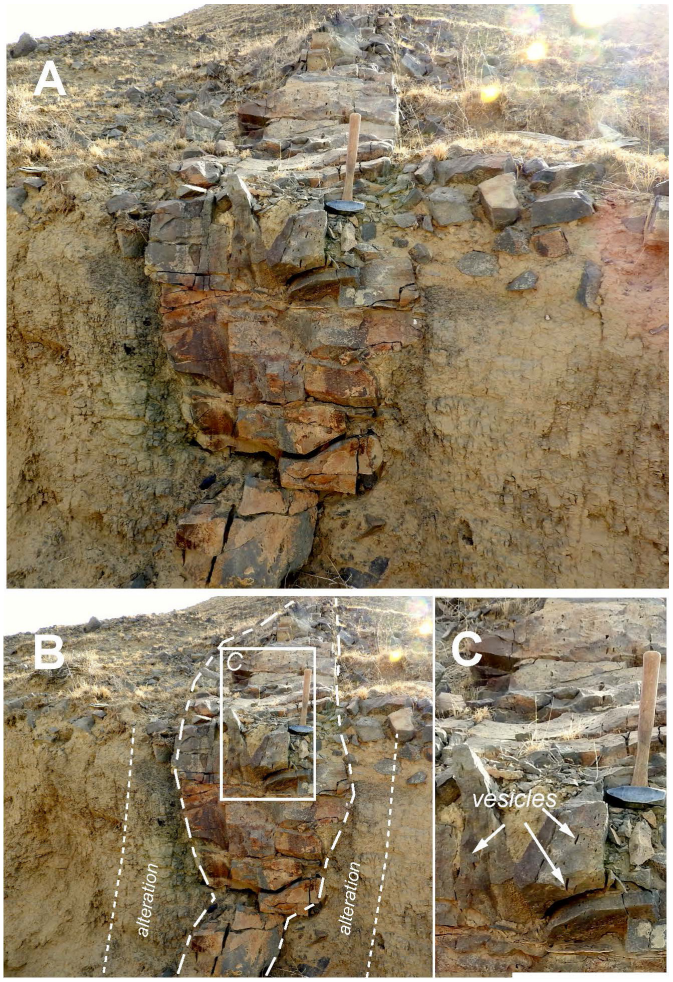

FIGURE 2.79. (A) Close-up of the 15–24-in.-wide (40–60 cm) basaltic dike on the topographic saddle with rock hammer for scale. (B) Sketch of dike margins and principal zone of alteration on either side. (C) Detail of vesicles in the dike interior.

in the interior. Because the thermal losses to the dike walls far exceed that of a cylindrical column, dikes quickly cool below the solidus, and further magma ascent takes place at an erupting vent once the basalt intercepts the surface.

On the south side of the road, the dike is truncated by a Middle Pleistocene terrace deposit (Figs. 2.68, 2.80). The tread of this deposit is ~100 ft (~30 m) above the adjoining valley floor of Cañon Tapia, comparable to the height of the gravel-capped dark, low mesa 0.5 mi to the northeast. Since it is inset on the same side of the Gallup bedrock ridge as this canyon, we can infer the terrace deposit was laid down by Cañon Tapia, probably in the middle Pleistocene (no direct age control is available). This terrace level is extensive along the middle Rio Puerco Valley and was called the Rito Leche terrace by Bryan and McCann (1936). Like most terraces, the basal stratum of the terrace deposits consists of gravel, which here is 2 ft (0.6 m) thick and comprises poorly sorted pebbles, cobbles, and boulders that are well-cemented (Fig. 2.80). Clast imbrication and the presence of copious basalts indicate it was laid down by a northeast-flowing, tributary drainage associated with Cañon Tapia. The gravel is composed of basalt and basaltic andesite with ~10% tan sandstone; only 1% red granite clasts are present, likely reworked form older (and higher) Rio Puerco terrace deposits. The gravel is overlain by very fine to fine sand (<20% medium sand) and clayey-silty fine sand that is approximately 20 ft (6 m) thick and overprinted by weak pedogenesis (e.g., stage I calcic horizons). This fine sediment occurs in very thin to thin beds and can be viewed at an exposure above the cemented terrace gravel. Within this fine sediment are minor gravel lenses composed of pebbles (minor cobbles) of subangular to subrounded basalt and sandstone with ~5% granite. Proceed to the top of the terrace deposit for a fine view to the east of the middle Rio Puerco Valley and Mesa Prieta.

Landscape evolution

Stop 3B offers an excellent opportunity to examine the long-term fluvial evolution of the Rio Puerco and its tributaries, including the Cañones Tapia and Salado. Numerous studies have been undertaken to decipher the long-term geomorphic evolution of the Rio Puerco Valley, starting with the classic work of Bryan (1928), Bryan and McCann (1936, 1938), and Wright (1946). Studies by Love (1986) focused on both the long-term and short-term storage of sediment in the Rio Puerco. Mapping of terraces and geomorphic surfaces of the Rio Puerco and its tributaries were conducted by Slavin (1991a, b), Drake et al. (1991), and Hallett (1992, 1994); these studies incorporated volcanic features and related geochronologic dates to better understand the Pliocene to Quaternary geomorphic evolution of the Rio Puerco drainage system. Slavin (1991a, b) and Hallett (1994) focused on long-term Rio Puerco incision in the Cabezon-Guadalupe area and are particularly interesting because they pose different landscape models with implications for estimating long-term erosion rates.

FIGURE 2.80. Cemented basal gravel of the Rito Leche terrace, unconformably overlying the basalt dike (the dike is also pictured in Figure 2.69). Inferred manganese imparts black color to terrace gravel.

Slavin (1991a, b) defined and mapped eight geomorphic surfaces (S1 to S8, oldest to youngest) that include basalt-capped mesas, the tops of eroded volcanic necks, terrace deposits, pediments, and alluvial fills. About a third of the tops of volcanic necks show a concordance in height above base level (Rio Puerco Valley), which were incorporated into Slavin's S3 surface (Fig. 2.81). Incorporating published K-Ar dates, heights above base level, and the relative soil development, Slavin estimated the ages of her mapped surfaces to range from Pliocene and Earliest Pleistocene (S1–S4), Early Pleistocene (S5), Mid-Pleistocene (S6), Late Pleistocene to Holocene (S7), and Present (S8). Several of those surfaces can be observed at this field stop. Combined, these surfaces along the Rio Puerco and its tributaries demonstrate a period of long-term regional incision (>1600 ft, >500 m) interpreted by periods of base-level stabilization, lateral erosion, and aggradation.

Hallett (1994) conducted the most detailed geomorphic studies of the landscape evolution of this portion of the Rio Puerco drainage. In these, he utilized morphometric analysis, geologic reconstructions, and age-dating of the volcanic necks. Hallett's model of formation of volcanic necks indicates that the top of volcanic necks do not reflect a pre-eruptive surface; rather, they approximate the height of the volcanic edifice (cone) that formed on an underlying paleotopographic surface. The paleotopography can be approximated by looking at the morphology of the neck and the top-of-bedrock at the neck site (Hallett, 1994). Therefore, by dating the lavas in the neck, Hallett (1994) postulated that he could constrain the elevation of the paleoground surface at a certain time (Fig. 2.82); however, elevational errors were not stated, and they could be at least 50 m (see discussion in Stop 2). His detailed research presents a more complicated evolutionary history of the Rio Puerco Valley from Pliocene to Early Pleistocene, indicating that highly variable topographic relief existed during neck emplacement at 3.5–2.5 Ma (Figs. 2.82, 2.83). Thus, the erosional form of the Rio Puerco Valley was "well established prior to 2.91 Ma" (Hallett, 1990), leading Hallett to challenge Slavin's interpretation that the top of the volcanic necks represented pre-eruption surfaces. Hallett's results are compelling.

However, Slavin (1991a, b) did not state that the tops of the volcanic necks represent pre-eruption surfaces; rather, she stated the top of necks represent the "former positions of the

Rio Puerco valley floors" or a fluvial (base-level) erosional surface. She based this conclusion on the fact that the tops of seven volcanic necks of differing ages are concordant (Fig. 2.81), implying that these surfaces are erosional surfaces truncating the volcanic necks by the ancestral Rio Puerco drainage system. Supporting this interpretation, Slavin reconstructed a down-valley longitudinal profile taken on the tops of the S3 volcanic necks that parallels the modern gradient of the modern Rio Puerco (Slavin, 1987, fig. 18). Thus, in Slavin's model the ancestral Rio Puerco would have a broad valley floor truncating the volcanic landscape after the eruption of the youngest volcano around 2.5 Ma.

Is it possible to rectify both landscape models which appear to show significant differences in how the Rio Puerco Valley evolved? Is the concordance of the elevations and down-valley profiles of the volcanic necks coincidental with no geologic significance? We will leave these questions for discussion on our field trip.

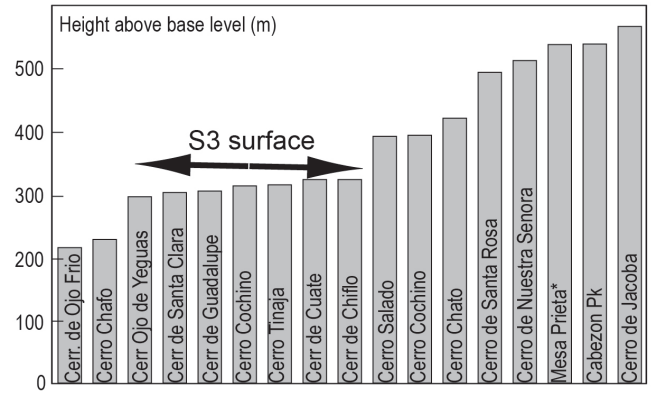

FIGURE 2.81. Plot from Slavin (1991b) illustrating the heights (tops) of various volcanic necks in the middle Rio Puerco Valley. The concordance of seven neck-tops led her to interpret a Plio-Pleistocene geomorphic surface that she called S3 (Slavin, 1991a).

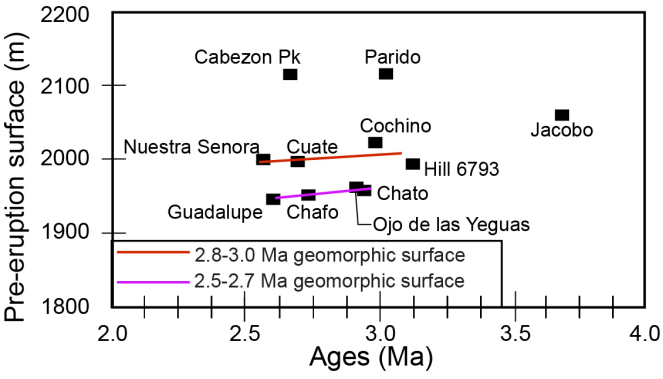

FIGURE 2.82. Plot supporting the interpretation of Hallett (1994) that notable paleotopography existed when the Rio Puerco necks were emplaced ca. 2.5–3.0 Ma. Two geomorphic surfaces were inferred (color-coded the same as the surfaces in Fig. 2.83). Note that necks of similar ages could be associated with paleosurfaces that differed by more than 100 ft (30 m) in elevation.

Pleistocene surfaces

Slavin (1987) recognized two fluvial terraces and associated pediment surfaces in this part of the Rio Puerco Valley and estimated that they are Early Pleistocene (S5) and Middle Pleistocene (S6). These two surfaces may correspond, respectively, to terraces identified by Bryan and McCann (1936), which are the La Jara surface, 60 m above base level, and the Rito Leche surface, 27–30 m above base level.

S5 is a strath terrace and pediment approximately 230 ft (70 m) above the mid-1980s Rio Puerco base level. The pediments slope toward the Rio Puerco from the western and northwestern flanks of Cabezon Peak and are mantled by subrounded basaltic cobbles and an overlying eolian deposit. Soil development in the eolian deposits is characterized by 19-in.-thick (49 cm) B horizon with strong subangular blocky structure and Stage III calcium carbonate accumulation. The terrace deposits range from 6 to 15 ft (2 to 5 m) in thickness and consist of subrounded to rounded gravels derived from the Nacimiento Mountains. The terrace remnants are deeply eroded and are mainly preserved in the La Ventana area. The soil development on S5 indicates that the soil was stripped, leaving 5–7-cm-long calcium carbonate clasts on the surface.

S6 is a terrace deposit with axial Rio Puerco deposits overlying the strath approximately 130 ft (40 m) above the entrenched Rio Puerco base level (as it was in the mid-1980s). The gravel clasts, as with S5, are derived from the Nacimiento Mountains, and the clast size is typically smaller than those on S5. Soils related to the S6 terraces are less developed than those soils on S5 and may reflect stripping of the terrace surface.

Valley fill

S7 is recognized as a broad valley floor at the top of an aggradation sequence (Slavin, 1991a). The alluvial fill spans the Rio Puerco Valley and continues up along its tributary valleys. The surface is approximately 50 ft (15 m) above the mid-1980s Rio Puerco base level, and the height of S7 above local base level in the Rio Puerco tributaries varies significantly, depending on the depth of local arroyo downcutting. The fill is typically bedded fine sands, silts, and clay layers with gravel lenses that are either reworked from higher surfaces or derived from the Nacimiento Mountains. The surface soils on S7 are weakly developed with thin Bw, Bt, and Bk horizons. In addition, buried soils are observed in the alluvial fill exposed by the incised arroyos. Radiocarbon dating of fill in the Rio Salado suggests the middle part of the valley fill unit is approximately 3100 years old, and stratigraphic observations indicate three cut-and-fill events occurred between ~1000 and 3000 years ago (Pippin, 1979; Niels, 2003).

S8 is defined as a low inset terrace below S7, ranging 1–3 m above the 1980s channel floor, and it is a result of the Rio Puerco incising the Holocene alluvial fill. Bryan (1928) interpreted that the Rio Puerco started incising rapidly after 1885, and by 1915, it was already incised 10 m in this area. S8 probably formed in the past 50–100 years during this recent down-cutting episode.

Slavin (1991): Minimal paleotography during emplacement of individual lava flows or necks; ages of top of necks or at base of lavas close to paleogeomorphic surface

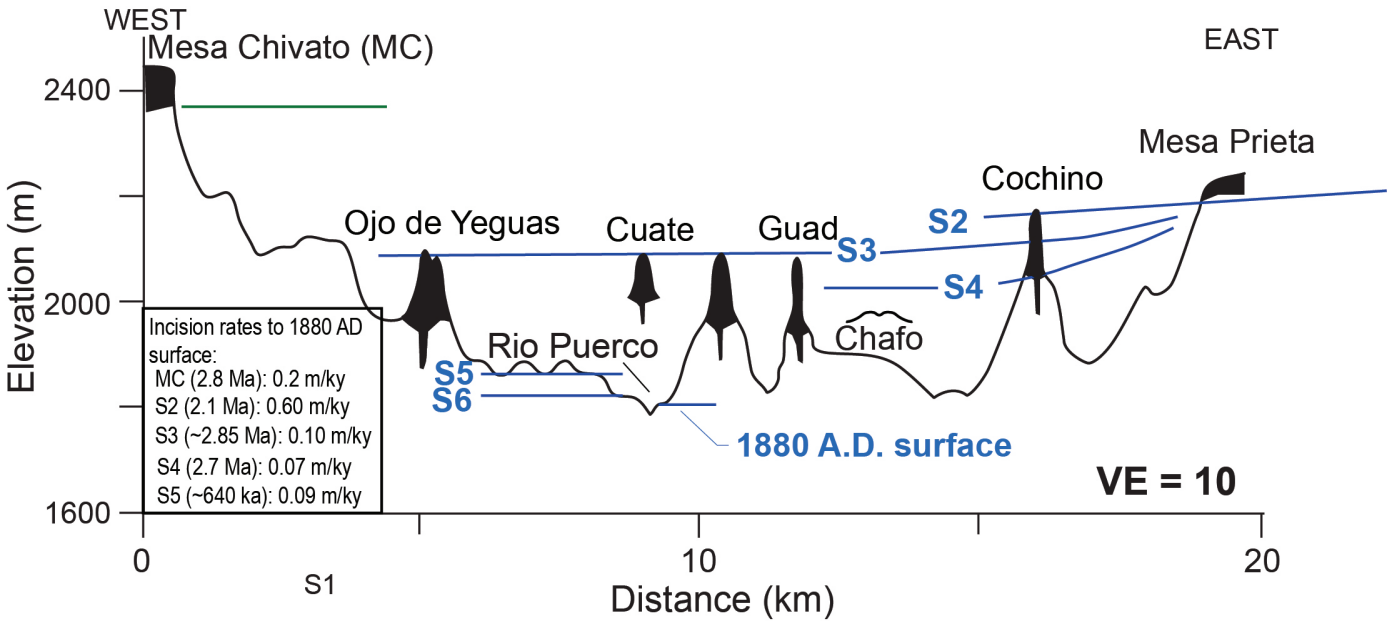

Hallett (1994): High-relief Rio Puerco valley at 2-3 Ma; Mesa Prieta and Mesa Chivato basalt flows perched on much-older, high-level geomorphic surface

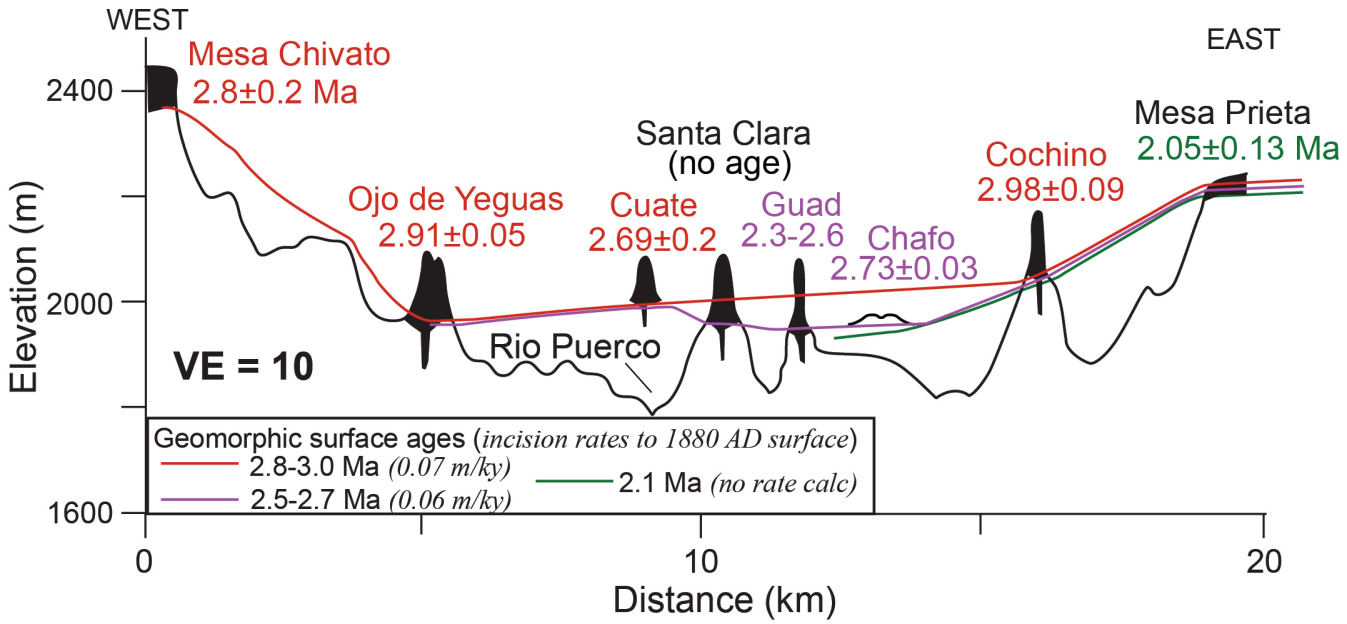

FIGURE 2.83. Comparison of the geomorphic evolution models proposed by Slavin (1991a, b) and Hallett (1994). Major differences are: (1) the existence of a Rio Puerco paleovalley in the Hallett model, and (2) the 2.1-Ma lava emplaced on Mesa Prieta was emplaced on a paleotopographic high; in other words, Mesa Prieta was already a topographic feature at 2.1 Ma. Also shown are incision rates calculated between their respective geomorphic surfaces and the 1880 valley-floor surface of the Rio Puerco. Most rate calculations yield 0.05–0.10 m/ky. However, if one just used the mesa-top lavas, the incision rates would be erroneously too high (by a factor of 2 to 6). Guad = Cerro de Guadalupe.

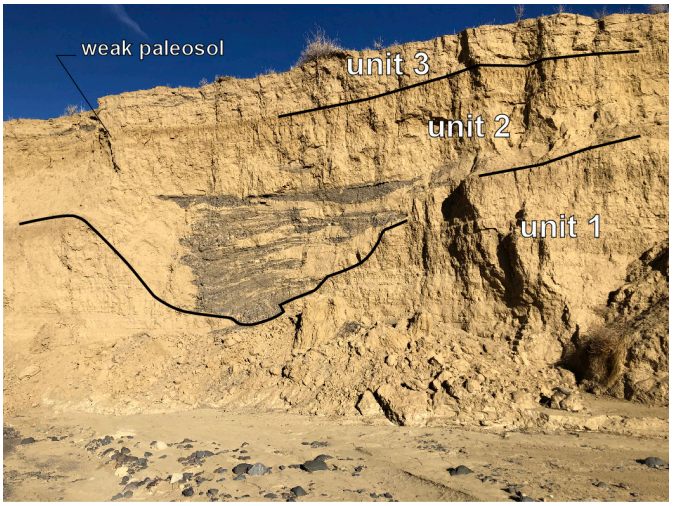

FIGURE 2.84. Illustrative outcrop located on the southern wall of Cañon Tapia, at a location 300 ft (100 m) downstream of road crossing. Estimated wall height is 25–30 ft (7–10 m). Three allostratigrpahic, middle-late Holocene units are denoted by black lines. Note the paleo-arroyo at the base of unit 2. Past study of an exposure in Cañon Salado ~1 mi to the northwest of here indicates a similar three-fold division of stratigraphic units for the middle–late Holocene alluvium. There, charcoal collected from upper strata of unit 1 returned a radiocarbon age of 3100±60 years before present (Pippin, 1979). The base of unit 3 can be traced to an archaeological "living surface" associated with pottery types tree-ring dated to between 900 and 1200 CE (Pippin, 1979). Thus, the unit 2 paleoarroyo incised and then backfilled between 1200 and 3100 years ago. What does the stacked, well-defined, zig-zagging nature of the gravel in the paleovalley of unit 2 tell one about aggradation rates? How might these rates compare with those of the fine-grained sediment of unit 1 and upper unit 2? What was the depositional environment and rate of aggradation of unit 3?. Exposures such as this, and those in many other places, for the middle-late Holocene in the Southwest indicate that arroyo incision is a natural process and has episodically occurred in the Holocene well before the intensive grazing of the late 19th century.

OPTIONAL STOP 3C. Middle-late Holocene stratigraphy of Cañon Tapia.

Waypoint 23 [35.511960°, -107.129806°]

Walk 600 ft (200 m) southwest of the vehicles to the edge of the incised arroyo of Cañon Tapia (Fig. 2.68). Here, we inspect middle–late Holocene sediment comprising the valley-floor alluvium (Fig. 2.84). The sediment consists of weakly consolidated sand and silty-clayey sand, mostly in tabular beds. Three allostratigraphic units can be recognized, bounded by weak soils or scour-related disconformities (time breaks in the geologic record). Particularly striking is a 4–5-m-deep paleoarroyo developed at the base of unit 2, backfilled by zig-zagging dark gravel (Fig. 2.84). The dark gravel is mostly mafic volcanic rocks, derived from erosion of older terrace deposits (like what we see at Stop 3B) or transported to here directly from the drainage's headwaters on the east side of Mesa Chivato. Age control indicates aggradation of units 1 and 2 occurred ca. 3500 to 1000 years before present (Pippin, 1979). Incision and back-filling of the arroyo at the base of unit 2 occurred during this time period and perhaps correlates to a 2600- to 2900-before-present cut-and-fill event interpreted in Niels (2003). This is before settlement of large numbers of Ancestral Puebloan people in the area and demonstrates that arroyo cutting and back-filling is a natural process, as is observed elsewhere in the American Southwest. Although not seen in this exposure, elsewhere in the area, Niels (2003, fig. 3.3) interpreted two cut-and-fills that overlap with Ancestral Puebloan occupation: 1000–1030 CE and 1175–1200 CE. Did land-use activities of the Ancestral Puebloans influence these latter episodes of arroyo cutting? At this stop, we discuss these possibilities along with natural geomorphic and climatic controls on aggradation versus erosion in this landscape.

The three sites at Stop 3 indicate a sensitive Holocene landscape subjected to aggradation and erosion. Past climate changes and their impact on geomorphic processes directly molded the lifestyle of the few hundred former inhabitants of Guadalupe and the several hundred (maybe >1000) Ancestral Puebloans that lived here 600–1000 years earlier. For the comparably recent Hispanic population, we have the written and physical evidence of their initially successful endeavors to farm and ranch in the Guadalupe area (García, 1987, 1992, 1994). The thought of their green farm fields flanking the Rio Puerco, in contrast to the dry and stark landscape we see today, is impressive. One cannot help but be saddened by the narrative of how their community and lifestyle were doomed by the dramatic landscape and climatic changes in the early to middle 20th century, namely deep incision of the Rio Puerco (which probably lowered the water table and made irrigation practically impossible) and a drying trend that culminated in the 1950s drought. Without irrigation, sustained farming efforts were practically impossible. Humans can influence the environment and, in turn, are dependent on the environment. With humility and efficacy, we need to use the knowledge gained by the natural sciences to guide how we are to best live on this planet.

Return to vehicles and proceed back to Bernalillo using the route on which we came.

We would like to thank Scott Aby and Peter Stacey for their reviews of this road log.

END OF SECOND-DAY ROAD LOG

Combined references for the First-Day, Second-Day, and Third-Day Road Logs are available on p. 95 and on the NMGS website at: https://nmgs.nmt.edu/publications/guidebooks/downloads/74